Design Considerations for

Low Pressure Solar Water Heating

in South Africa

December 2012

University of Cape Town

by

Oelof de Meyer

Supervisors:

Prof. P. Pillay Prof. A.B. Sebitosi Dr. R. Okou

Declaration

I know that plagiarism is wrong.

Plagiarism is to use another's work (even if it is summarized, translated or rephrased) and pretend that it is one's own. This assignment is my own work.

Each contribution to and quotation (e.g. "cut and paste") in this assignment from the work(s) of other people has been explicitly attributed, and has been cited and referenced. In addition to being explicitly attributed, all quotations are enclosed in inverted commas, and long quotations are additionally in indented paragraphs.

I have not allowed, and will not allow, anyone to use my work (in paper, graphics, electronic, verbal or any other format) with the intention of passing it off as his/her own work.

I know that a mark of zero may be awarded to assignments with plagiarism and also that no opportunity be given to submit an improved assignment.

I know that students involved in plagiarism will be reported to the Registrar and/or the Central Disciplinary Committee.

Name: ....

Student no: ....

Signature: ....

Date: ....

Abstract

This thesis investigates the application of solar water heating in South Africa. The solar water heating system investigated work on the thermosiphoning effect or natural convection. An extensive literature study has been undertaken to investigate this phenomena. The three partial differential equations (governing equations) are non-dimensionalized and a similarity solution is applied to obtain two coupled non-linear ordinary differential equations. These equations are then solved in *MATLAB* to obtain the velocity and temperature profiles. Two scenarios were considered, a vertical wall with a constant wall temperature and a vertical wall with a constant heat flux. LP SWH systems use vacuum tubes to absorb solar radiation and transfer it to the water, which is similar to the vertical wall with a constant heat flux. A simulation model has been developed for a LP SWH system which is able to simulate the system performance for a given geographical location, where the user can specify the system component attributes. Experiments on the system were conducted to validate the simulation model. The simulation model accompanies a 6-Step Design Guide developed to assist the user to design a system able to satisfy the consumer's hot water demand. The 6-Step Design Guide developed can be used in future design considerations for LP SWH systems in South Africa.

Acknowledgements

To acknowledge the people who contributed in the success of this thesis. The person who brought most value to this success is Chris Wozniak, who assisted in the experimental setup and was always available for consulting. He has a great heart and inspires many students with his attitude. I want to thank him sincerely for his contribution. To my family and friends for their support. To my Creator for giving me strength, dedication and the mind to contribute something to this life.

TABLE OF CONTENTS

Page

LIST OF FIGURES

Page

1. INTRODUCTION

In South Africa, Eskom is our main supplier of electricity. Most of its power generation capabilities arise from coal fired power stations, located in upper region of South Africa. Coal fired power stations create carbon emission as a byproduct that is harmful to the environment and contribute to the effects of Global Warming. Thus alternative power generation technologies have been investigated throughout the years to reduce the dependence on coal fired power stations. The costs involved in generating electricity from renewable energy are expensive compared to coal fired power stations. Eskom has been funding research at Universities around South Africa for this purpose to enhance the renewable energy field and create possibilities for future power generation from renewable energy resources.

Apart from the vision of using cleaner power generation technologies, Eskom is generating electricity at full capacity for the high power demand in South Africa. The current power stations are being refurbished, as some of the power stations are in the end of their expected lifetime, and equipment, control systems and components are starting to fail due to age. The new build power stations are in construction phase and commission of these plants will commence in the near future. Although these plans are in place to ensure electricity for the future, South Africa still suffers in the present time from power availability and reliability of continuous power supply to the consumers.

The initiative from Eskom to introduce a rebate on Solar Water Heating (SWH) systems to households in South Africa, encourage consumers to install these systems to reduce electricity usage for hot water, thus reducing their power consumption. The average household uses up to 44% of their electricity for heating water. If each household could reduce their power consumption by at least 30% from using these SWH systems, it would reduce the demand on the grid significantly, and consumers would save on their electricity bill.

The above mentioned scenario impress as the ideal solution for the current power crisis experienced in South Africa, but all parties involved to execute this ideal makes it only possible to some extent. The research conducted in this thesis is to assist South Africa, Eskom and the consumer to apprehend this ideal. This research elaborates on the effectiveness of renewable energy, to share insight in the nature of solar energy and in SWH applications. Considerations to be taken into account when designing, installing and using these systems. Furthermore Low Pressure (LP) SWH systems are primarily important from China or India. These systems were designed for those specific countries, but installed as is in South Africa. The geographical location, weather data, consumer hot water demand and solar radiation profile of South Africa differs from these countries, thus this research concentrates in optimizing the designs for South Africa specifically.

1.1. Global Warming

Global Warming is a term used to describe the entrapment of solar radiation by the earth's atmospheric layers. The atmospheric layers consist out of various gasses and water vapor. The amount of solar energy passing through the atmosphere remains fairly constant but due to the excessive carbon dioxide in these atmospheric layers (Figure 1), heat is trapped, introducing the greenhouse effect, leading to global warming. About 20% of this trapped heat warms the air and the remaining 80% evaporates the water. An average temperature increase of about 0.6°C has been documented worldwide over the past 50 years. In the 1980s, this decade was recorded to be the warmest. In the 1987-1997 there have been many disastrous floods from storms. Other documented evidence reveals a 10% decrease in global snow cover, a 40% thinning of Arctic Ocean ice, a 20% decrease in glacier extent and a 10% increase in rainfall in the northern hemisphere (Silberg, 2006).

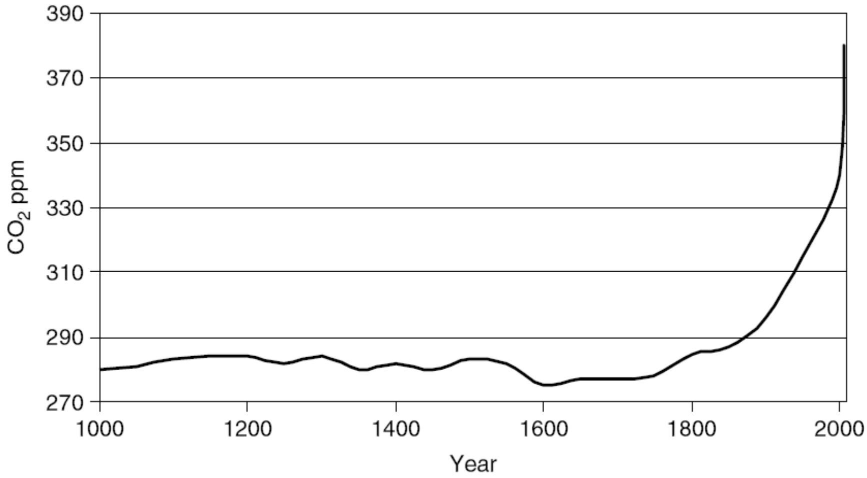

Figure 1: CO_2 levels over last 1000 years (Duffie, Beckman, 1991)

1.2. Power Generation and Renewable Energy

For years people have relied on coal and oil as the main suppliers of energy for power generation, this is due to its high availability worldwide, its abundance, low cost and easy transportation. The process in generating power from coal has been mastered over the years, the capacity factor for coal fired power stations are typically in the range of 85-95%. For this reason and the low costs involved, coal fired power stations are popular for its reliability, availability and cost effectiveness. Due to the high carbon emissions from these power stations, alternative power generation technologies have been investigated. Renewable energy surfaced from identifying the potential in alternative energy resources. To understand this concept, the process in a coal fired power station will be discussed together with Figure 2.

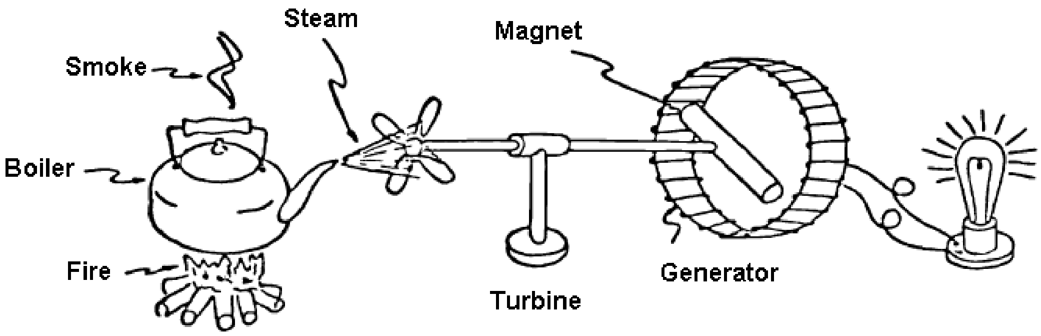

Figure 2: Power generation concept (Joyce, 2012)

From the illustration in Figure 2, coal is burned as energy source to heat up the kettle that serves as a boiler; water inside the kettle heats up and starts to boil that creates steam, the steam is used to turn a turbine blade which in effect is used in a generator to produce electricity. The energy conversion process is as follow: fossil energy – thermal energy – mechanical energy – electrical energy. From this analysis it is clear that there are four stages in the conventional power generation process in generating electricity. When alternative methods are introduced from a renewable energy perspective to replace a stage in this process, the same principle applies, and electricity is obtained. No net greenhouse gases are emitted from renewable energy technologies and can thus lower carbon emissions and conserve fossil fuels. These technologies include photovoltaic, solar thermal, biomass, wind power, geothermal and hydropower (Silberg, 2006). As illustrated in Figure 3, biomass can be burned to generate heat for the boiler application, solar energy can be used directly to generate electricity from photovoltaic panels, or heat for the production of steam and wind turbines generate electricity from harnessing the energy from the wind, see.

1.3. Generating Power using Solar Energy in South Africa

The research conducted in this thesis focus on the potential of solar energy in South Africa, and thus from this point forward, only solar energy will be considered. South Africa is endowed with good solar radiation throughout the country. For this reason solar energy as alternative energy can be effectively utilized. The Northern Cape Province has the highest total annual solar radiation. Eskom is currently in the process of constructing one of the largest Concentrated Solar Power (CSP) plants in Upington, with a minimum capacity factor of 60%. This CSP plant will generate 100 MW power using molten salt as the heat transfer fluid and storage medium. In 2011, Eskom erected two solar photovoltaic farms at Lethabo and Kendal power stations. Other smaller applications such as SWH systems and photovoltaic panels are installed around the country at households, schools, hospitals and businesses. The solar industry in South Africa has a great potential for job creation and many entrepreneurs have seized this opportunity.

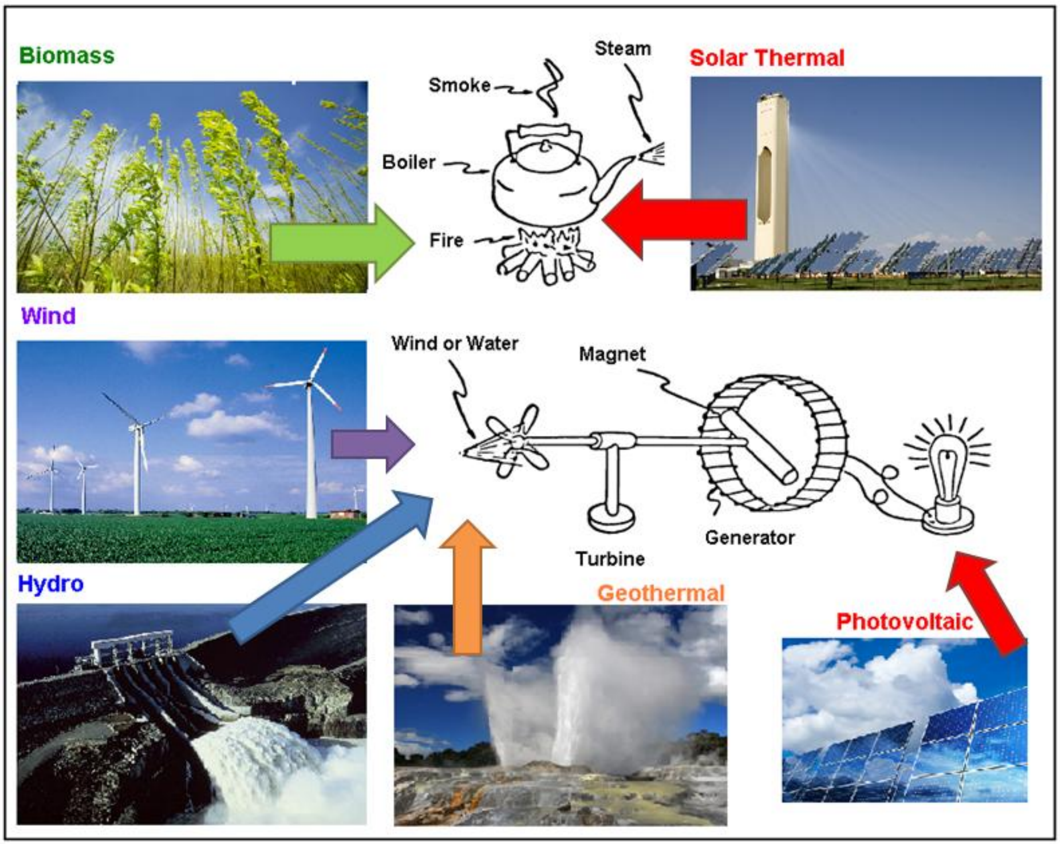

Figure 3: Renewable energy power generation concept (de Meyer, 2012)

1.4. Solar Water Heating in South Africa

Solar water heating for domestic users became very popular due to its promising results and low cost to the consumer from the rebate offered by Eskom. This rebate program was rolled out for the reason that an average household uses approximately ±44% of their power consumption for hot water. If a SWH system can deliver this energy, then in theory it will reduce the power usage of the household by ±44%. However these SWH systems are not optimized as standardized systems are installed for all the households, despite their geographical locations and annual solar radiation received. Thus these systems can be optimized based on the consumer's need, geographical location and the amount of solar radiation received during summer and winter. Various solar water heating systems are available on the market, however this research focuses on a Low Pressure (LP) Solar Water Heating (SWH) system.

2. SOLAR ENERGY

2.1. Introduction

Solar energy is heat and radiant light emitted from the sun. In this section, the sun as energy source will be discussed and how the energy reaching the earth's surface can be harnessed. For centuries humans have been developing and implementing architecture, technologies and social living to benefit from the energy supplied by the sun. Some civilizations worshipped the Sun as a supernatural phenomenon, such as Inca and Aztecs, where the Germanic paganism believed that it was a goddess. Ancient monuments, like the pyramids in Egypt, were constructed based on solar phenomena's, others such as the stone megaliths are able to indicate summer and winter solstice. (Goldstein, 1997)

2.2. Birth of the Sun

About 4.57 billion years ago, the Sun was formed from the collapse of part of a large molecular cloud consisting primarily of hydrogen and helium. The Sun was one of the many stars that formed during this phenomenon. A shock wave from a supernova occurrence in space compressed the gasses from the molecular cloud, causing selected regions to collapse under their own gravity, forming the Sun. The collapse in the cloud initiated a rotation due to the conservation of angular momentum, and heat as by-product formed due to an increase in pressure. As majority of the mass concentrated in the centre, other particles flattened out in a disk formation, becoming planets, stars and other solar systems. Gravity and pressure from the core of the compressed cloud generated excessive heat and triggered nuclear fusion. This fusion process continued, giving birth to our Sun. (Williams, 2010)

2.3. Sun Characteristics

The sun is consisting out of 73% hydrogen, 24% helium and 3% other elements including oxygen, carbon, iron, neon, nitrogen, silicon, magnesium and sulphur. Its mass is 1.9×10^{30} kg, with a volume of 1.4×10^{18} km^3 and average density of 1.4×10^{3} kg/m^3. Compromises out of various layers (Figure 4), such as the core, radiative zone, convective zone, photosphere, chromosphere and corona. The surface area is about $6 \times 10^{12} km^2$ with a temperature of 5505°C. The radiant power of the sun, ordinating from the nuclear fusion process, emits $61.1 MW/m^2$ from the sun's surface. Earth is approximately 149.6×10^{6} km away from the sun, and light travels from the sun to earth in 8 minutes and 19 seconds. The annual mean solar irradiance reaching earth's atmosphere is between 1367 W/m^2 and 1420 W/m^2. The total solar irradiance or solar constant equal to 1372 W/m^2 represents the rate at which solar energy is incident on a surface normal to the sun's rays at the outer edge of the atmosphere when the earth is at its mean distance from the sun. (Cengel, 2009)

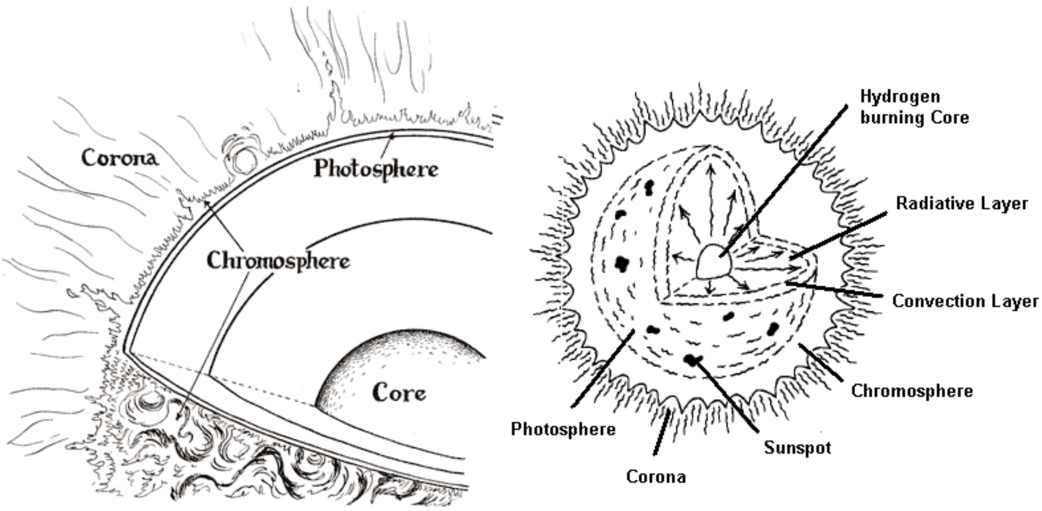

Figure 4: Layers of the Sun (Garfinkle, Gardinkle 2010)

2.4. Solar Spectrum and Energy Transfer

The sun emits various forms of electromagnetic radiation, varying in quantities. Nearly 43% of the emitted radiation is visible light, 49% near-infrared and 7% ultraviolet. The remainder 1% is in the form of x-rays, gamma and radio waves. The following graph illustrates the emitted radiation with regards to the quantity of energy and the various wavelengths (Figure 5). Energy transfer from the sun to the earth occurs across space, which is a vacuum, and is in the form of radiation. Radiation is the transfer of energy by electromagnetic wave motion. (Lightle, 2011).

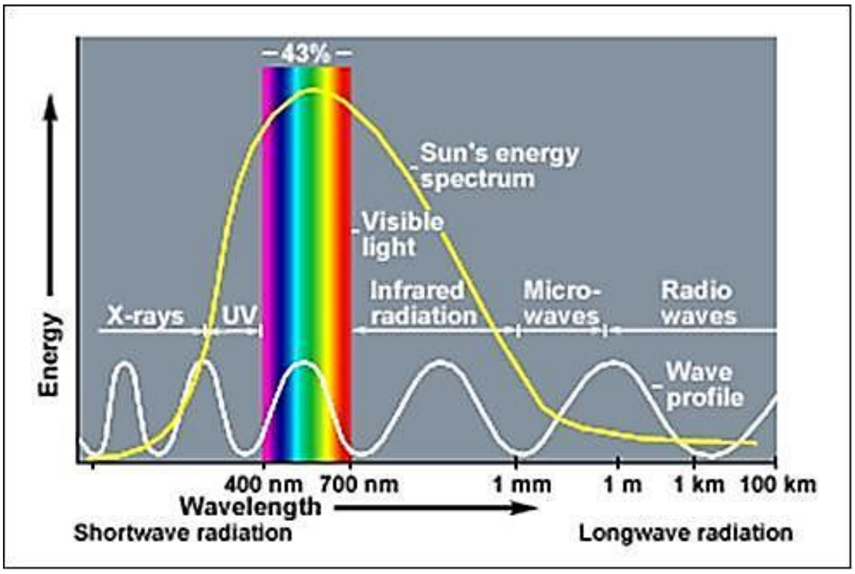

Figure 5: Solar spectrum (Lightle, 2011)

Once the radiation reached the atmosphere of the earth (between 1367 W/m^2 and 1420 W/$m^{2)}$, the ozone layer, water vapor and other gasses within the atmosphere absorbs a portion of the radiation as it penetrates through the atmospheric layers of earth. X-rays and UV rays that is harmful for humans are also absorbed. Once the radiation reached the Troposphere atmospheric layer, radiation is further absorbed, scattered and reflected by clouds, water vapor and other gasses. The radiation that finally reaches the surface of the earth is known as total radiation, and consists out of direct, diffuse and reflected solar radiation.

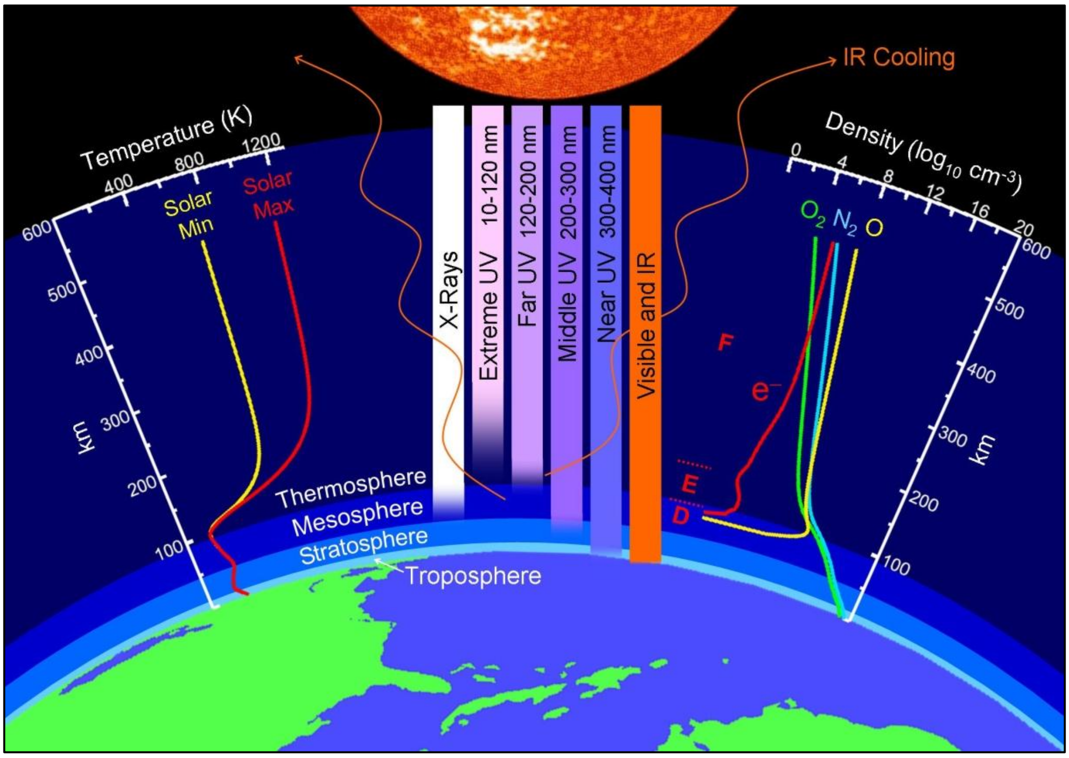

Figure 6: Radiation transfer from Sun to Earth (Emmert *et al.,* 2010*)*

2.5. Sun as Energy Source for Living Organisms

The sun is the most important source of energy to sustain life on earth. It is responsible for supplying energy for plant growth the entire ecosystem depends on the energy from the sun (Figure 7). Producers (plants) use a process called photosynthesis to produce glucoses from sunlight, which forms the basis of nutrition for consumers (herbivores and omnivores). Photosynthesis (Figure 8) takes place in the chloroplast of a plant cell. Sunlight, carbon dioxide and water are required for this process and oxygen also forms as a byproduct which is released into the atmosphere. The chloroplast contains chlorophyll which absorbs the red and blue spectrum of the light wave, green light is reflected, giving chlorophyll its green appearance. The energy from the light increases the electron state of the water to be more energetic, where these electrons then transfer to the energy poor carbon dioxide molecules to form energy rich sugar molecules. The sugar molecules are stored in molecular structures in the plant cells, and oxygen is used for respiration in living organisms. This phenomenon plays an important role in the carbon cycle of the ecosystem. When burning biomass, it is noticed that the photosynthesis process is reversed and carbon dioxide gas, water and energy is produced in the presence of oxygen.

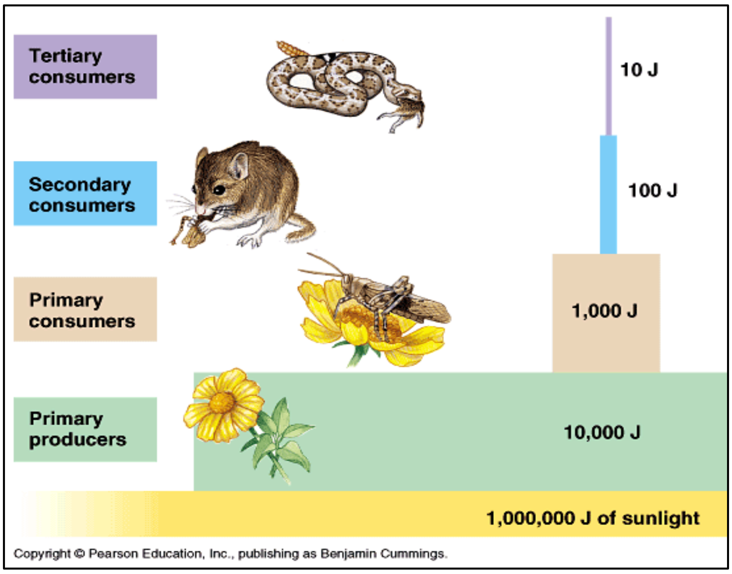

Figure 7: Energy transfer in food chain (Young, 2005)

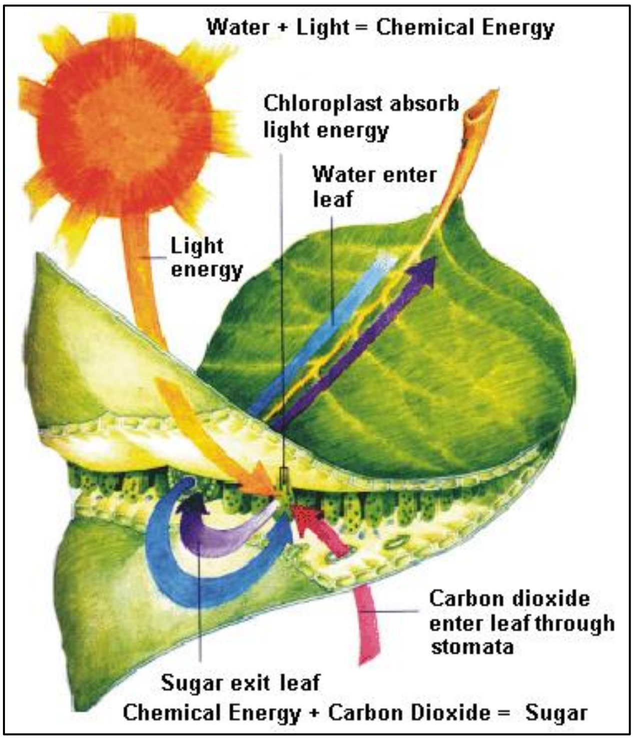

Figure 8: Photosynthesis process in a leaf (Young, 2005)

3. LITERATURE STUDY

3.1. Harnessing Energy from the Sun

To be able to harness the energy received from the sun on the earth's surface, it is important to understand the behavior of the sun in terms of seasonal changes, the specific geographical location, effect of weather conditions and cloud cover, solar angles and the surface area (shape, tilt and material) absorbing the solar radiation. The outer edge of the Earth's atmosphere receives ±1367 W/m^2 of energy from the sun. The atmosphere absorbs and reflects a fraction of this radiation, including most X-rays and ultraviolet rays. Sunlight is then distributed unevenly in different regions. Regions on the equator receive more energy than other areas. Different seasons also play a part in the amount of solar radiation received due to the tilt angle of the axis of the Earth. Other factors that also should be taken into account are the weather conditions. Some of the solar radiation is absorbed and reflected away by the clouds, thus lowering the amount of solar radiation that hits the ground. Air pollution also has a similar effect on solar energy. All these factors determine the amount of solar irradiance available for utilization.

- **Seasonal Changes**

The tilt of the earth's rotational axis and the orbit of the earth around the sun are responsible for the seasonal changes. The tilt angle of 23,5 degrees are fixed throughout the orbit, thus at certain times the Northern Hemisphere will be closer to the sun (summer), while the Southern Hemisphere will be further away from the sun (winter), and vice versa. Figure 9 illustrates these seasonal changes and fixed tilt angle of the earth. The earth completes one orbit around the sun in 365.25 days. (Duffie, Beckham, 1991)

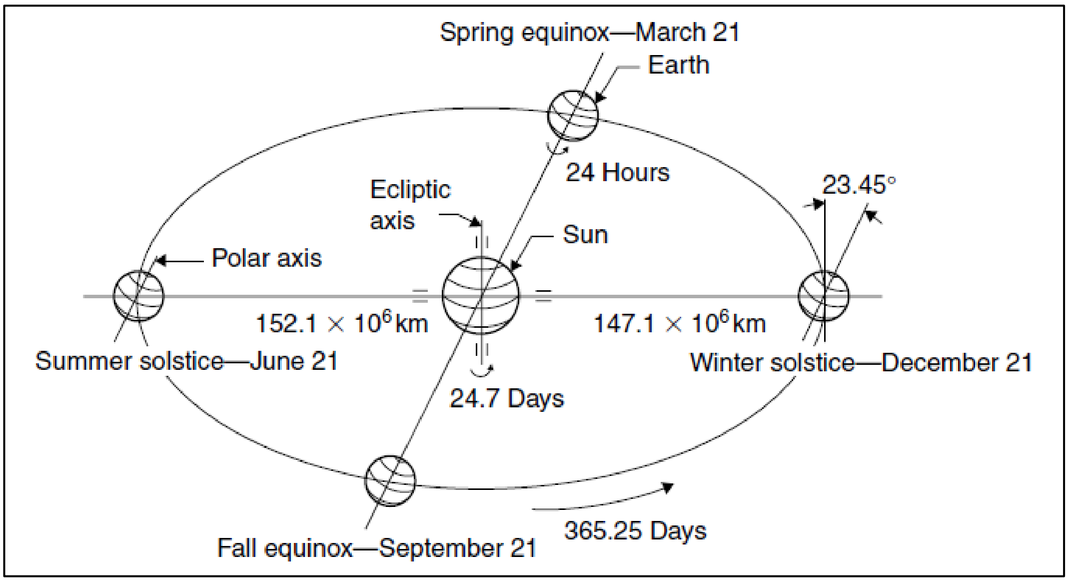

Figure 9: Seasonal changes (Duffie, Beckham, 1991)

- **Geographical Location and Solar Angles**

Each geographical location on the earth's surface has a different solar radiation profile for solar energy available to utilize. There are many factors that influence this solar radiation profile, but the most important factor is the latitude angle of the specific location. The latitude angle indicates how far the area is from the equator. Areas on or close to the equator have a higher solar radiation profiles than areas further away. It is difficult to model or take into account all the factors that play a role in the solar radiation profile for a specific geographical location, such as air pollution, weather conditions, inland or coastal and nearby surroundings. Thus it is advised to use a database that captured the solar radiation readings over a period of time, Typical Metrological Year (TMY) data, for a specific geographical location to conclude over its solar radiation profile. For simulation purposes this data is available, from a mathematical point of view, simple calculations can give an indication of an expected solar radiation profile for the specific geographical location.

Mathematical Model to Determine Solar Radiation Profile

The following equations (Kalogirou, 2005) can be used or adapted to determine the solar radiation received on a horizontal surface on a given time and day of the year. Later in this section, the amount of solar radiation on a tilted surface will be investigated, and derives from this fundamental understanding. First the extraterrestrial solar radiation on a plane normal to the intercepting solar radiation on a specific day of the year must be calculated. The following equation and graph can be used for this purpose.

$$G_{on} = \mathrm{G_{SC}} \;\; 1 + 0.033\cos\;\frac{360N}{365} \tag{3.1}$$

Where, $\mathrm{G_{SC}}$ represents the solar constant, with the value of 1367 W/m^2.

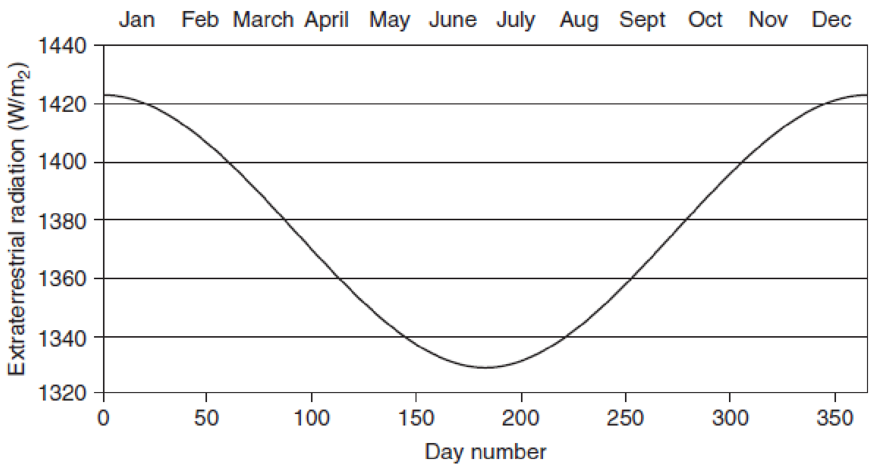

Figure 10: Extraterrestrial solar radiation variation (Kalogirou, 2005)

The solar radiation on a plane parallel to the ground, thus the extraterrestrial horizontal surface, can be expressed as follows.

$$G_{oH} = \mathrm{G}_{on} \cos\ \Phi \tag{3.2}$$

Where Φ represents the solar altitude angle with

$$\cos\ \Phi\ \ = \sin\ L\ \ \sin\ \delta\ \ + \cos\ L\ \ \cos\ \delta\ \ \cos\ h \tag{3.3}$$

As illustrated in Figure 11; L, δ and h represents latitude, solar declination and hour angle respectively. Point P on the figure represents the specific geographical location with latitude (L), and the angles of the sun respectively to this point are indicated on the figure.

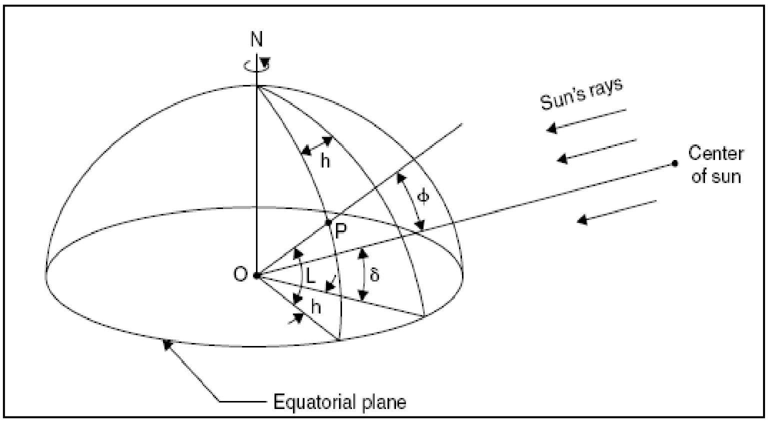

Figure 11: Solar angles and positions (Kalogirou, 2005)

The local latitude of geographical location is represented by L and is positive for the northern hemisphere, and negative for the southern hemisphere. As δ represents the solar declination throughout the year, which defines the angular distance of the sun's rays north/south of the equator, and can be calculated from the following equation with N being any day of the year. (Kalogirou, 2005)

$$\delta = 23.45 \sin\ \frac{360}{365}\ \ 284 + N \tag{3.4}$$

The hour angle is represented by h and defines the point on the earth's surface through which the earth would turn to bring the meridian of the point directly under the sun. At noon (Apparent Solar Time, AST=12), when the sun is at its highest position over the point and solar irradiation is at its peak.

$$h = (\mathrm{AST} - 12)15 \tag{3.5}$$

When calculations using solar geometry are applied, it is considered that the earth is fixed, for simplicity, since all motion is relative. With respect to the view from the earth to the sun (Figure 12) two astronomical angles are considered, the solar altitude (Φ) and solar azimuth (z).

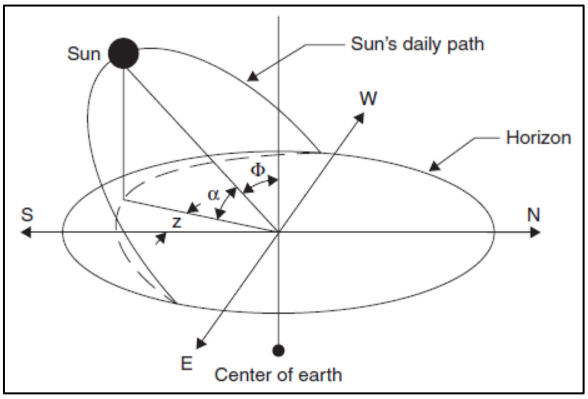

Figure 12: Sun path across the sky during the day (Kalogirou, 2005)

The solar azimuth angle is defined as the angle of the sun's rays measured in the horizontal plane from true south for the Northern Hemisphere or true north for the Southern Hemisphere, where westward is designated as positive.

$$\sin z = \frac{\cos \delta \ \sin h}{\cos \alpha} \qquad (3.6)$$

Where α represents the solar altitude measured from the horizon

- **Solar Tracking and Absorption Surfaces**

The intensity of solar radiation at which the sun's rays strike the surface, is essentially a function of the angle of incidence (θ). When the sun's position is overhead, 90 degrees from the horizon, incoming rays are most intense. The intensity decreases as the angle decreases because the sun rays spread over a larger surface area. Thus to receive the same amount of solar radiation intensity on the same horizontal area (Figure 13 and Figure 14), a larger surface area is required. During summer the horizontal surface is closer to perpendicular to the sun rays, receiving more concentrated solar energy. In winter, the sun rays hit the horizontal surface at a glancing angle, spreading out the energy. (Lightle, 2011)

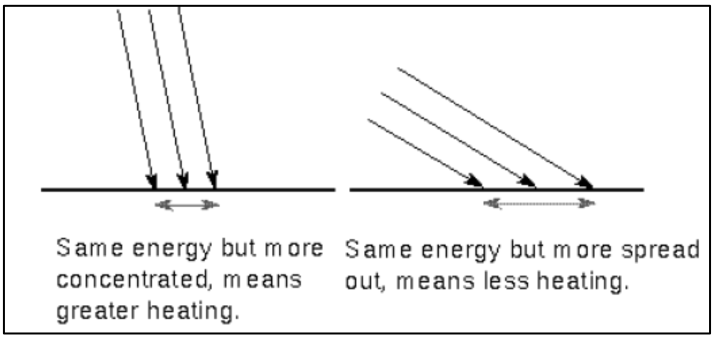

Figure 13: Solar energy distribution on surface (Lightle, 2011)

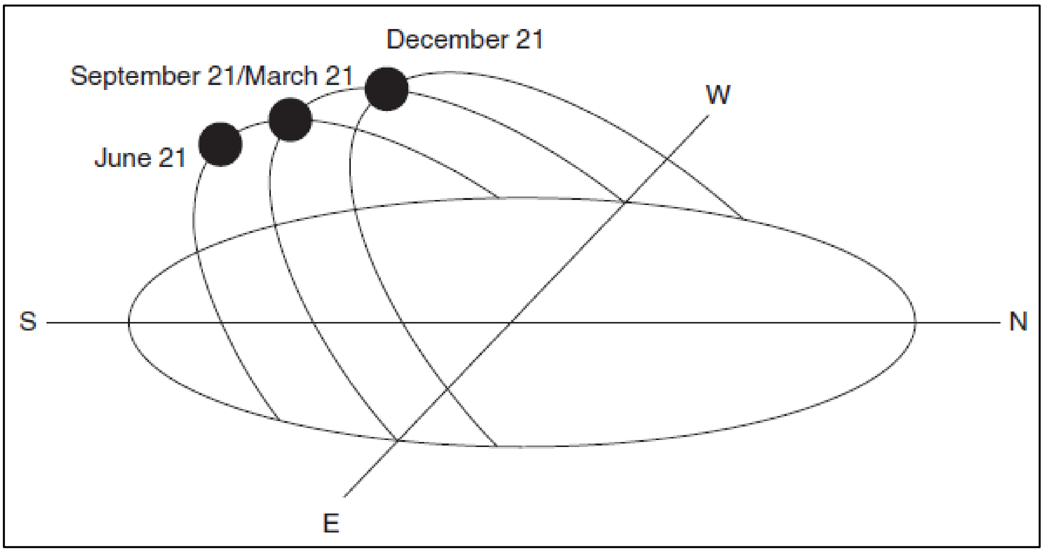

Figure 14: Annual changes in the sun's position in the sky (Kalogirou, 2005)

In order to expose the surface area to the maximum amount of energy, the surface area should be positioned to intercept the incoming rays of the sun perpendicular. All radiation that strikes the surface area, this includes direct, diffused and reflected sunlight, can be absorbed/utilized (this is not applicable for concentrating collectors as concentrating collectors only utilizes direct radiation). Different tracking mechanisms are available to ensure that the absorption/intercepting surface is exposed primarily to perpendicular direct solar radiation for the duration of the day. As discussed earlier two astronomical solar angles are defined to describe the position of sun relative to earth, the solar altitude and azimuth angles. These two angles should be tracked by the absorbing surface area. Figure 15 shows a tilted absorber surface with respected solar angles (indicating the position of the sun).

There are three basic mechanisms of tracking; two-axis tracking (full tracking), fixed surface (no-tracking), one-axis tracking (E-W tracking and N-S tracking), illustrated in Figure 16. The full-tracking mechanism refers to a two-axis tracking mechanism, ensuring that the absorbing surface area is continuously facing the sun. Thus the angle of incidence for this type of tracking is always 0°. One-axis tracking either follows the altitude or azimuth angle of the sun. The last mechanism of tracking is the fixed tilted surface, in this instance there is no tracking involved, and most solar systems have a fixed tilted surface exposed to the sun. The reasoning for this is due to the cost implications, calibration and maintenance for tracking devices. Flat plate collectors normally don't have tracking devices, some photovoltaic panels and concentrating collectors have one axis tracking devices and other concentrating collectors, photovoltaic systems and heliostat mirror fields (solar power plants) make use of two-axis tracking systems. Systems using vacuum tubes (low pressure and high pressure) have a "built-in" one axis tracking device, due to the round geometry of the absorber surface, tubular shape, thus passively tracking the sun.

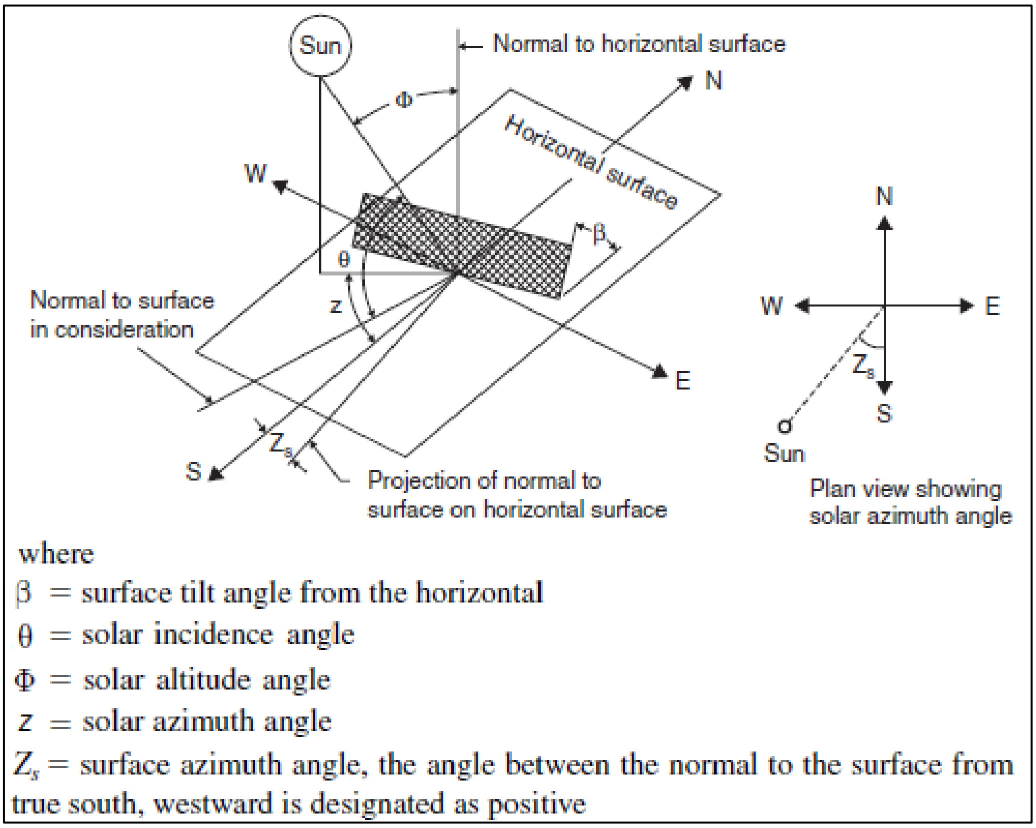

Figure 15: Tilted absorber surface and solar angles (Kalogirou, 2005)

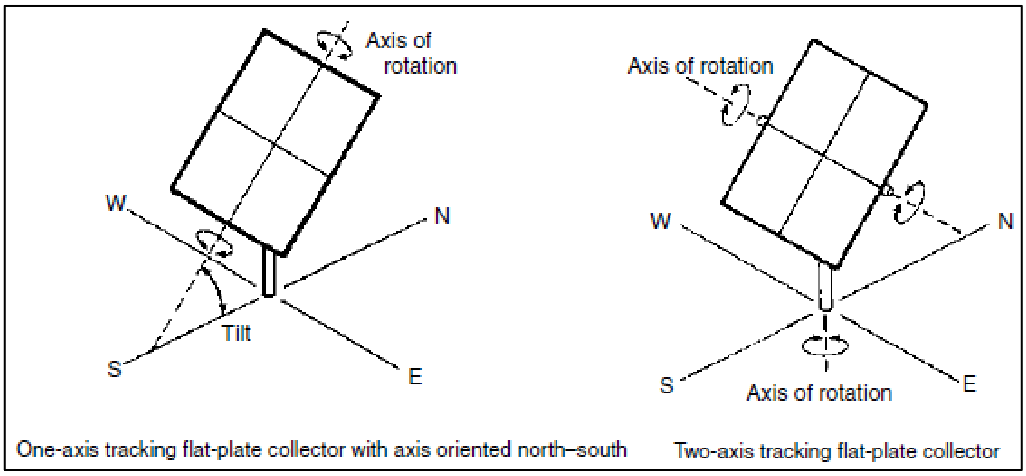

Figure 16: One-axis and Two-axis tracking (Kreith, Goswami, 2007)

3.2. Low Pressure Solar Water Heating

These systems use natural convection as means of heat transfer. The system consists of a storage tank and vacuum tubes as the main components. The vacuum tubes are connected directly into the storage tank allowing the water to fill the tubes. The vacuum tube consists of two concentric glass tube, sealed at the one end with an annular vacuum space to reduce heat loss. The inner glass tube has a selective absorber coating on the outside. Thus solar radiation is absorbed by the tube and transferred to the water inside the tube. Due to increase in temperature a density difference drive the hot water upwards into the storage tank; this phenomenon is known as natural convection. The fluid flow is induced by the buoyancy effect.

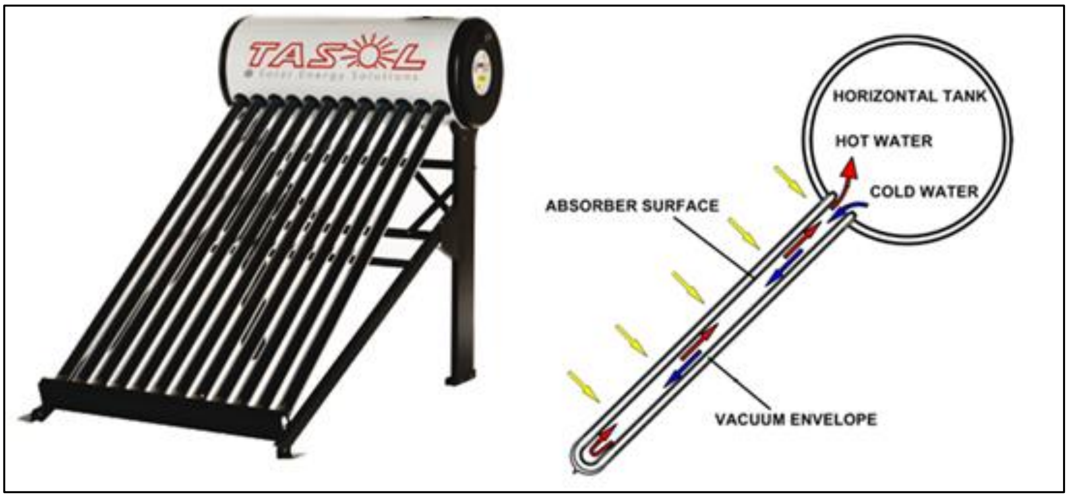

Figure 17: LP SWH system (Budihardjo, 2005)

3.3. Optical Efficiency and Heat Transfer for Vacuum Tubes

The optical efficiency of the tube plays the most important role in successfully absorbing the solar radiation, and thus transferring the energy to the water inside the tube. When sun light strikes the tube, some light is reflected and absorbed by the outer glass tube. The optical properties of glass is as follows, reflectance – the inherent ability of the glass to reflect incoming rays, absorptance – how much of the incoming ray the glass will absorb, and transmittance – the amount of incoming rays successfully passing through the glass without being absorbed or reflected. The inner tube (absorber tube) absorbs the solar radiation that passed through the outer tube; a portion of this radiation is reflected away from the absorber tube where another fraction of the radiation is emitted. The following Figure illustrates this clearly. Due to the nature of the absorber tube, the water inside the tube experience a constant heat input along the wall of the absorber tube, which induce the natural convection phenomenon by transferring the solar energy to the water. The following Section explains this phenomenon in extensive detail.

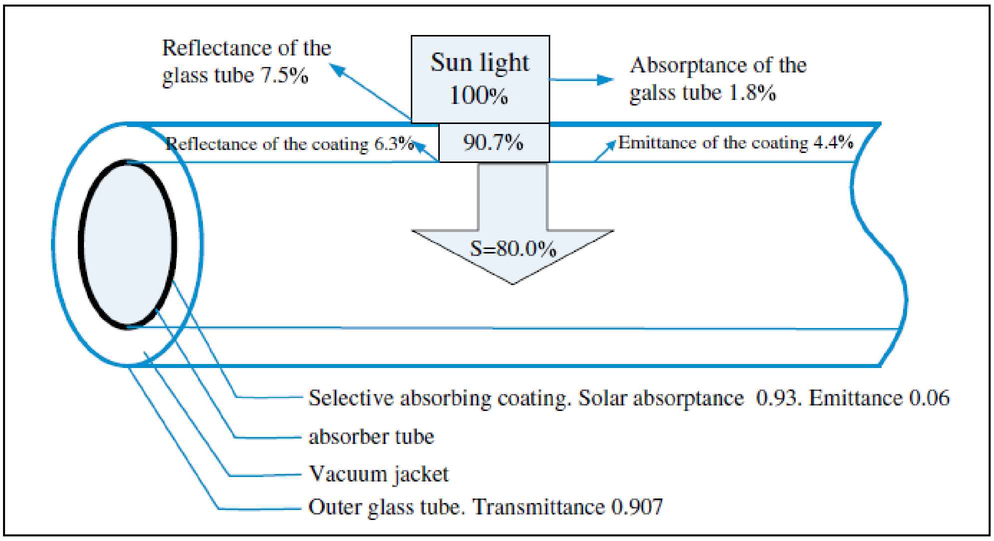

Figure 18: Optical properties of vacuum tube (Apricus, 2012)

3.4. Natural Convection

Convection is the mechanism by which heat is transferred through a fluid in the presence of a bulk fluid motion. This manner of heat transfer can be divided into two groups, forced and natural convection. The manner in which the fluid motion is initiated determines the type of convection. In forced convection, the fluid flow is initiated by an external force, such as a fan or pump. In natural convection, the fluid flow is induced by the buoyancy effect. Natural convection is normally used in cooling applications, such as electronic equipment, refrigeration coils, power transmission lines and from bodies of animals or humans. The use of natural convection as means of cooling became very popular due to its natural occurrence, eliminating the installation of cooling equipment. In many solar water heating applications, natural convection is used for heating purposes. Low pressure solar water heaters are the latest technology in solar water heating that use natural convection in an efficient and effective manner. (Cengel, 2009)

3.4.1. History

Natural convection ensures a very effective method of heat transfer when the acceleration force is large. In mechanical engineering there are various applications that produce high centrifugal accelerations such as rotary machinery. E. Schmidt (1930) proposed to use natural convection in the cooling of turbine blades. The blades contained a number of thin cylindrical cavities pointing radially outwards from a reservoir with a cool fluid in the hub. During operation heat transfer at the circumferences to the fluid and the effect of the centrifugal force field cause the heated fluid to move towards the hub and be replaced by the cool fluid. Turbine blades were constructed in Germany during the war using the cooling method proposed by E. Schmidt.

In 1952 M.J. Lighthill first explored the theoretical considerations on natural convection in tubes. Lighthill developed methods to predict the flow and heat transfer caused by natural convection in vertical heated tubes. The tubes where closed at the bottom and opened at the top into a reservoir. From these methods a prediction can be made whether the flow is laminar or turbulent and if the boundary layer of heated fluid fills the tube or fills the tube with a stagnant region near the end. Lighthill founded that the flow depends on a modified Grashof number and on the length-radius ratio.

3.4.2. Basic Theory

Heat transfer can occur either by radiation, conduction or convection. In this section a brief understanding in the physical mechanism of natural convection is discussed. As a hot object enters a colder fluid (gas or liquid), the outer temperature layer of the object will drop while the surrounding fluid temperature rise. A density difference between the hot and cold fluid cause the hotter fluid to rise creating a natural convection current (Figure 19). Heat transfer is enhanced as a result of the natural convection current. The same phenomenon occurs when a cold medium enters a warmer fluid however the natural convection currents are reversed. (Cengel, 2009)

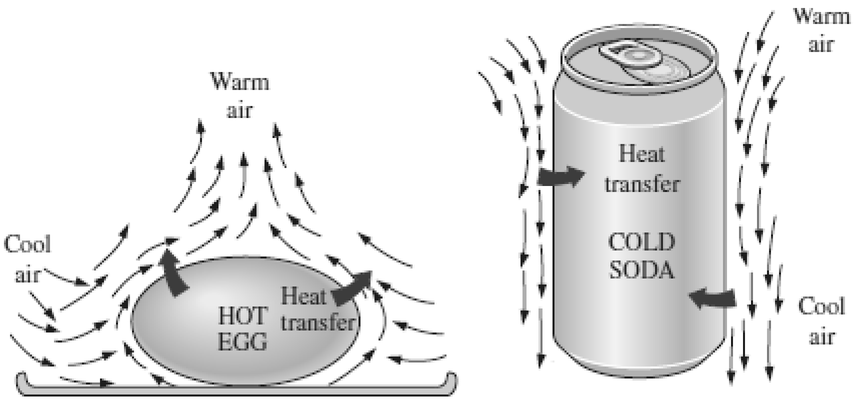

Figure 19: Natural convection currents and heat transfer (Cengel, 2009)

3.4.3. Buoyancy Effect

The gravitational field is a vital component in the natural convection phenomenon, and without it, heat transfer would only occur by means of conduction. A net force pushes a light fluid placed in a heavier fluid upwards in the presence of a gravitational field. This force is known as the buoyancy force and has a magnitude equal to the weight of the fluid displaced by the body. In natural convection the lighter fluid is an effect of the temperature rise within the fluid, and thus a relationship between the density and temperature of the fluid exists. The volume expansion coefficient β is used to express this relationship under constant pressure, see the follow Equation: (Cengel, 2009)

$$\beta = -\frac{1}{\rho}\frac{\rho_\infty - \rho}{T_\infty - T} \tag{3.7}$$

Where T and ρ the temperature and density of the fluid close to surface respectively represents, and subscript ∞ denotes away from surface. The net buoyancy force thus increase with an increase in the density difference within the fluid due to an increase in temperature, see Equation 3.8-3.9.

$$F_{\text{net}} = \mathrm{W} - F_{\text{buoyancy}} = \rho_{body}\mathrm{g}V - \rho\mathrm{g}V \tag{3.8}$$

Where g and V the gravitational acceleration and the volume of body respectively represents as in Figure 20. Furthermore Equation 3.7 can be rewritten as

$$\rho_\infty - \rho = \rho\beta(T - T_\infty) \tag{3.9}$$

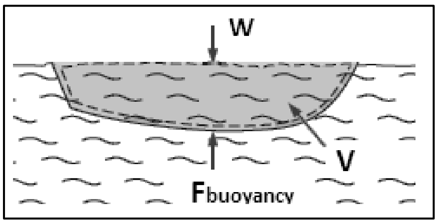

Figure 20: Buoyancy effect (Cengel, 2009)

It is clear from Equation 3.10, that an increase in temperature within the fluid will result in a positive net buoyancy force per unit volume, pushing the less dense fluid upwards. See Table 1 for various conditions in the buoyancy effect.

$$F_{\text{net}} = \ \rho_\infty - \rho\ \ \mathrm{g} = \rho\beta(T - T_\infty)\mathrm{g} \tag{3.10}$$

Condition	Effect	Result
$T > T_\infty$	$\rho_\infty - \rho > 0$	$F_{\text{net}} > 0$, Less dense fluid rises
$T = T_\infty$	$\rho_\infty - \rho = 0$	$F_{\text{net}} = 0$, No natural convection
$T < T_\infty$	$\rho_\infty - \rho < 0$	$F_{\text{net}} < 0$, More dense fluid descend

Table 1: Buoyancy effects (Cengel, 2009)

A higher buoyancy force creates stronger natural convection currents which result in a higher heat transfer rate. Thus the flow rate of the fluid determines the magnitude of the heat transfer, as in forced convection, a high flow rate result in a high heat transfer rate. In natural convection, the flow rate is determined by the balance between buoyancy and friction force. (Cengel, 2009)

3.4.4. Governing Equations

There are three fundamental laws that a fluid element conform to. In order to understand the behaviour of fluid flow these three fundamental laws are investigated. This analysis is from first principles where governing equations are formulated to predict the fluid flow and temperature gradient in boundary layers. The flow is assumed to be steady and two-dimensional and the fluid Newtonian with constant properties. In Figure 21, the flow direction is parallel to the surface and denoted by x, whereas y denote flow normal to the surface. The velocity in the x-direction and y-direction is denoted by u and v respectively. Where u(x,y) and v(x,y) the velocity in a two-dimensional fluid element represents.

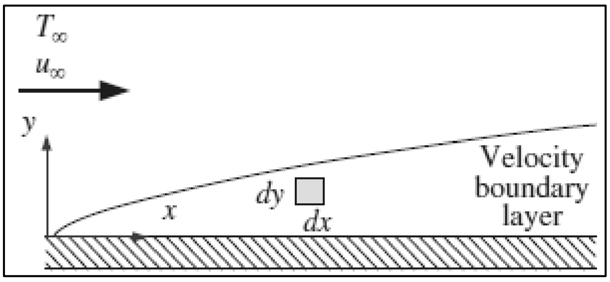

Figure 21: Velocity boundary layer (Cengel, 2009)

The following section discusses these three fundamental laws which are; the *Conservation of Mass*, *Conservation of Momentum* and *Conservation of Energy*. From this investigation the continuity, momentum and energy equations are obtained for laminar flow with boundary conditions. These equations will be used to obtain the velocity and temperature profiles for a wall with either a constant wall temperature, or constant heat flux along the wall. (Cengel, 2009)

- **<u>Conservation of Mass (Continuity Equation):</u>**

The conservation of mass principle states that no mass can be created or destroyed during a process. Thus a mass balance should be satisfied where all the mass be accounted for, see Equation 3.11.

$$\begin{matrix}\text{Rate of mass flow} \\ \text{into the control volume}\end{matrix} = \begin{matrix}\text{Rate of mass flow} \\ \text{out of the control volume}\end{matrix} \tag{3.11}$$

Where the magnitude of the mass flow rate (m) the product of the density (*ρ)*, mean velocity (*u)* and cross-sectional area (*dy)* normal to flow is. From the fluid element (Figure 22), the fluids enters the control volume at a mass flow rate, see Equation 3.12, and leaves the control volume at mass flow rate, see Equation 3.13.

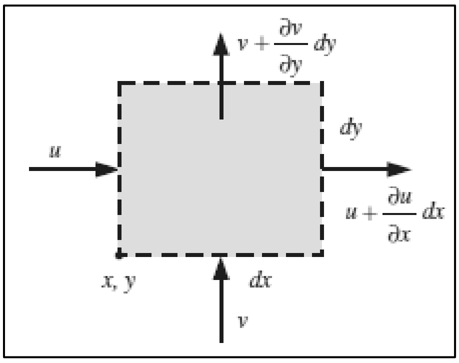

Figure 22: Fluid element for conservation of mass (Cengel, 2009)

$$m_{in} = \rho u(dy.1) \tag{3.12}$$

$$m_{out} = \rho \quad u + \frac{\delta u}{\delta x} dx \quad dy.1 \tag{3.13}$$

The same method is applied for the mass flow rate in the y-direction, and the resulting equations together with Equation 3.12 and Equation 3.13 are substituted in Equation 3.11.

$$\rho u \ \ dy.1 \ \ + \rho v \ \ dx.1 \ \ = \rho \quad u + \frac{\delta u}{\delta x} dx \quad dy.1 \ \ + \rho \quad v + \frac{\delta v}{\delta y} dy \quad dx.1 \tag{3.14}$$

The continuity equation can be obtained by dividing Equation 3.14 by $dx.dy.1$, see Equation 3.15.

$$\frac{\delta u}{\delta x} + \frac{\delta v}{\delta y} = 0 \tag{3.15}$$

- **<u>Conservation of Energy (Energy Equation):</u>**

The change in energy content of a system undergoing any process is equal to the difference between the energy input and output. In a steady-flow process this energy content stays constant, thus the energy entering the control volume equal the energy leaving the control volume, see Equation 3.16. Similarly for the rate of energy, see Equation 3.17.

$$E_{in} - E_{out} = \Delta E_{system} = 0 \tag{3.16}$$

$$E_{in} - E_{out} = \Delta E_{system} = 0 \tag{3.17}$$

Equation 3.17 can also be expressed as the energy transferred by heat, work and mass, see Equation 3.18 and Figure 23.

$$E_{in} - E_{out} \ {}_{heat} + \ \ E_{in} - E_{out} \ {}_{work} + \ \ E_{in} - E_{out} \ {}_{mass} = 0 \tag{3.18}$$

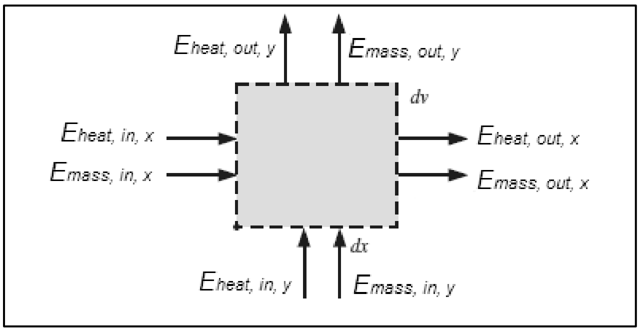

Figure 23: Fluid element for conservation in energy (Cengel, 2009)

In Equation 3.19 the energy transfer rate of mass entering and leaving the control volume in the x-direction is expressed as:

$$E_{in} - E_{out} \;\; _{mass,x} = \;\; me_{stream} \;\; _x - \quad me_{stream} \;\; _x + \frac{\partial \;\; me_{stream} \;\; _x}{\partial x} dx \tag{3.19}$$

Where e_{stream} the total energy of a flowing fluid stream per unit mass represents and its magnitude is equal to the sum of the enthalpy (h), kinetic energy and potential energy. The kinetic and potential energy is relatively small compared to the enthalpy and thus neglected in the analysis (Cengel, 2009). Thus the energy of the fluid per unit mass is:

$$e_{stream} = h = C_p T \tag{3.20}$$

Where C_p and T the specific heat and temperature respectively represents. When Equation 3.20 is substituted in Equation 3.19 with $m = \rho \;\; dy.1$, the following expression is obtained, see Equation 3.21

$$E_{in} - E_{out} \;\; _{mass,x} = -\frac{\partial \;\; \rho \;\; dy.1 \;\; C_p T}{\partial x} dx = -\rho C_p \;\; u\frac{\partial T}{\partial x} + T\frac{\partial u}{\partial x} \;\; dxdy \tag{3.21}$$

The net energy transfer to the control volume by mass is obtained by adding the result of the energy transfer rate of mass in the y-direction to Equation 3.21, see Equation 3.22.

$$E_{in} - E_{out} \;\; _{mass} = -\rho C_p \;\; u\frac{\partial T}{\partial x} + T\frac{\partial u}{\partial x} \;\; dxdy - \rho C_p \;\; v\frac{\partial T}{\partial y} + T\frac{\partial v}{\partial y} \;\; dxdy \tag{3.22}$$

If the continuity equation $\delta u \;\; \delta x + \delta v \;\; \delta y = 0$ is substituted in Equation 3.22, the following expression is obtained for the net rate of energy transfer to the control volume by mass:

$$\left(E_{in} - E_{out}\right)_{mass} = -\rho C_p \left(u\frac{\partial T}{\partial x} + v\frac{\partial T}{\partial y}\right) dxdy \tag{3.23}$$

Similarly, the same procedure is followed to obtain the net rate of heat conduction to the volume element, see Equations 3.24-3.26.

$$\left(E_{in} - E_{out}\right)_{heat,x} = Q_x - \left(Q_x + \frac{\partial Q_x}{\partial x} dx\right) \tag{3.24}$$

$$\left(E_{in} - E_{out}\right)_{heat,x} = -\frac{\partial}{\partial x}\left(-k\left(dy.1\right)\frac{\partial T}{\partial x}\right) dx = k\frac{\partial^2 T}{\partial x^2} dxdy \tag{3.25}$$

$$\left(E_{in} - E_{out}\right)_{heat} = k\frac{\partial^2 T}{\partial x^2} dxdy + k\frac{\partial^2 T}{\partial y^2} dxdy = k\left(\frac{\partial^2 T}{\partial x^2} + \frac{\partial^2 T}{\partial y^2}\right) dxdy \tag{3.26}$$

Work done by the body and surface forces is the last mechanism of energy transfer associated with the fluid in the control volume. The work done by the body force is only considered when the gravitational force is very large. The surface forces are due to fluid pressure and viscous shear stresses. The surface forces due to the fluid pressure are already taken into account in the analysis by using the enthalpy instead of the internal energy. The shear stresses can be neglected as it is only considered when the viscous effects are very large. In this analysis the velocities involved are low or moderate, resulting in small viscous effects. By substituting Equation 3.23 and Equation 3.26 into Equation 3.18 the energy equation for steady two-dimensional flow is obtained, when shear stresses are negligible and fluid properties constant. (Cengel, 2009)

$$\rho C_p \left(u\frac{\partial T}{\partial x} + v\frac{\partial T}{\partial y}\right) = k\left(\frac{\partial^2 T}{\partial x^2} + \frac{\partial^2 T}{\partial y^2}\right) \tag{3.27}$$

- **<u>Conservation of Momentum (Momentum Equation):</u>**

By applying Newton's second law of motion to a differential control volume element in the boundary layer, the differential equation of motion in the velocity boundary layer is obtained. Newton's second law states *the net force acting on the control volume is equal to the mass times the acceleration of the fluid element within the control volume, which is also equal to the net rate of momentum outflow from the control volume* (Cengel, 2009), see Equation 3.28.

$$(\text{Mass})\begin{pmatrix}\text{Acceleration}\\ \text{in a specified direction}\end{pmatrix} = \begin{pmatrix}\text{Net force (body and surface)}\\ \text{acting in that direction}\end{pmatrix} \qquad (3.28)$$

The forces acting on the control volume consists out of body and surface forces. The body forces act throughout the entire body of the control volume and are proportional to the volume of the body. These forces include gravity, electric or magnetic forces. Surface forces on the other hand act on the control surface and are proportional to the surface area. Thus Equation 3.28 can also be expressed as:

$$\delta m \cdot a_x = F_{surface,x} + F_{body,x} \qquad (3.29)$$

Where $\delta m = \rho(dx \cdot dy \cdot 1)$ and representing the mass of the fluid element. The acceleration a_x in the x-direction is

$$a_x = \frac{du}{dt} = \frac{\partial u}{\partial x}\frac{dx}{dt} + \frac{\partial u}{\partial y}\frac{dy}{dt} = u\frac{\partial u}{\partial x} + v\frac{\partial u}{\partial y} \qquad (3.30)$$

With $u = u(x,y)$ and its differential $du = (\partial u \quad \partial x)dx + (\partial u/\partial y)dy$. If the fluid element in Figure 24 is considered, the net surface force acting in the x-direction can be expressed as in Equation 3.31.

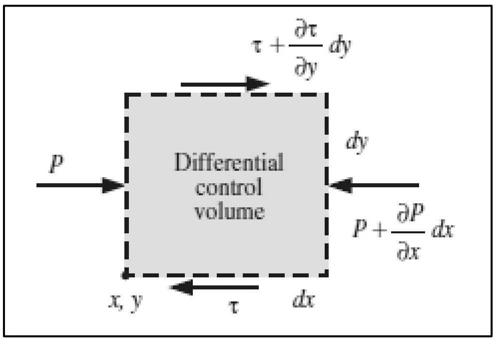

Figure 24: Fluid element for conservation in momentum (Cengel, 2009)

$$F_{surface,x} = \quad \frac{\partial \tau}{\partial y}dy \quad dx.1 \; - \; \frac{\partial P}{\partial x}dy \quad dy.1 \; = \; \frac{\partial \tau}{\partial y} - \frac{\partial P}{\partial x} \quad dx.dy.1 \qquad (3.31)$$

With $\tau = \mu(\partial u/\partial y)$ representing the viscous stress, Equation 3.31 can be expressed as:

$$F_{surface,x} = \quad \mu\frac{\partial^2 u}{\partial y^2} - \frac{\partial P}{\partial x} \quad dx.dy.1 \qquad (3.32)$$

The surface forces are due to pressure and viscous effects. Viscous stresses consist out of two perpendicular components, a normal stress which is normal to the surface, and a shear stress along the surface. Normal stresses are very small compared to shear stress due to their velocity gradient components and thus neglected in Equation 3.31 and Figure 24. The x-momentum equation is obtained by substituting Equations 3.30 and 3.32 in Equation 3.29 and dividing the result by $dx \cdot dy \cdot 1$, see Equation 3.33. The body force acting in the x-direction can be added to right side of the equation with units expressed per unit volume of fluid.

$$\rho \quad u\frac{\partial u}{\partial x} + v\frac{\partial u}{\partial y} \quad = \mu\frac{\partial^2 u}{\partial y^2} - \frac{\partial P}{\partial x} \tag{3.33}$$

The following boundary layer approximations are considered (Figure 25). In a boundary layer, the velocity component in the flow direction is much larger than that in the normal direction, thus $u \gg v$ with negligible $\partial v/\partial x$ and $\partial v/\partial y$. Furthermore, u varies significantly with y in the normal direction, while the variation of u with x along the flow is usually small, thus $\partial u/\partial y \gg \partial u/\partial x$. The same approximation applies to the temperature gradient, with $\partial T/\partial y \gg \partial T/\partial x$. Thus the velocity and temperature gradients normal to the surface are larger than along the surface. (Cengel, 2009)

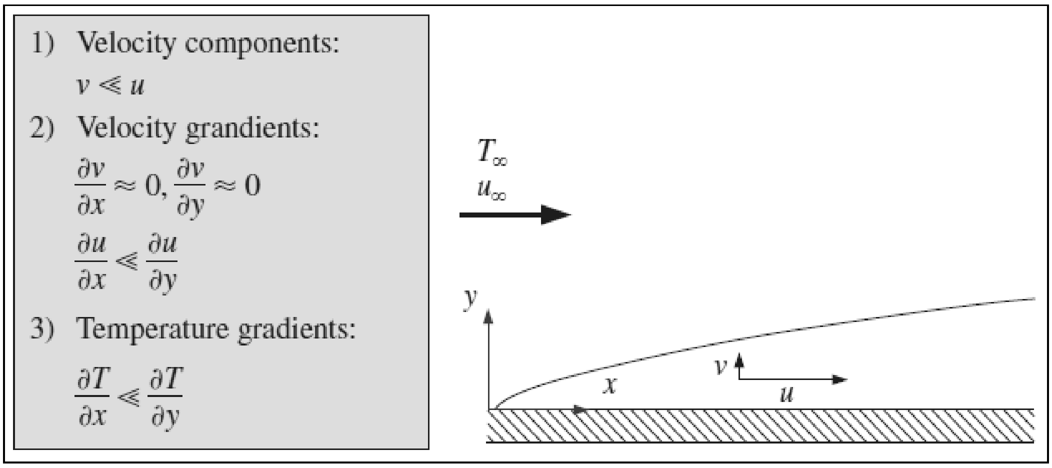

Figure 25: Boundary layer approximations (Cengel, 2009)

The governing equations derived are applicable for forced convection, though for natural convection the mass and energy equations are also applicable. Due to the buoyance effect in natural convection, the momentum equation needs to be modified.

Continuity Equation

$$\frac{\delta u}{\delta x} + \frac{\delta v}{\delta y} = 0 \tag{3.15}$$

Energy Equation

$$\rho C_p \quad u\frac{\partial T}{\partial x} + v\frac{\partial T}{\partial y} \quad = k \quad \frac{\partial^2 T}{\partial x^2} + \frac{\partial^2 T}{\partial y^2} \tag{3.27}$$

Momentum Equation

$$\rho \quad u\frac{\partial u}{\partial x} + v\frac{\partial u}{\partial y} \quad = \mu\frac{\partial^2 u}{\partial y^2} - \frac{\partial P}{\partial x} \tag{3.33}$$

- **Modified Momentum Equation for Natural Convection:**

For this analysis the flow is assumed to be steady and laminar. The fluid is assumed to be Newtonian with constant properties, but due to the buoyance effect, the density difference $\rho - \rho_\infty$ is excluded as the density difference between the inside and outside of the boundary layer result in the rise of the buoyance force, sustaining flow. This is known as the *Boussinesq Approximation.* (Cengel, 2009) The differential volume element in natural convection (Figure 26), is considered. The forces acting on the differential volume element are pressure forces, acting on the top and bottom surfaces, the force of gravity on the whole volume element and shear stresses acting on the side surfaces. The normal stresses are very small compared to the shear stresses and thus neglected in the analysis.

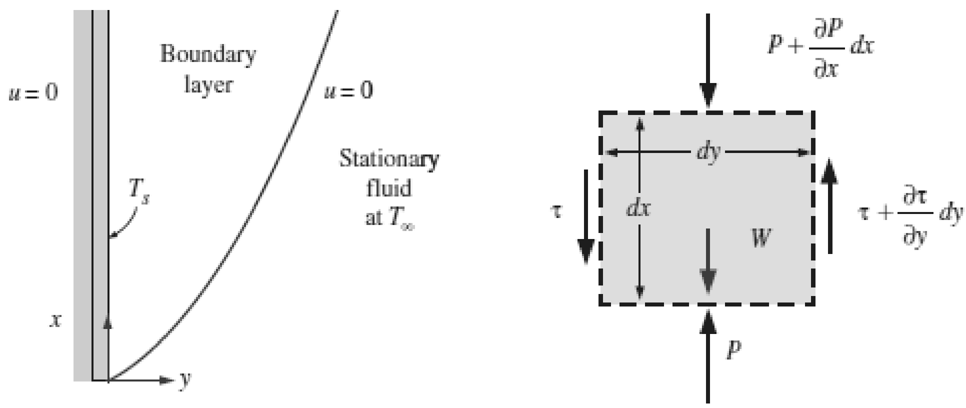

Figure 26: Free convection boundary layer and fluid element (Cengel, 2009)

The conservation of momentum in the x-direction is the same as in forced convection but with the effect of the gravitational force added, see Equation 3.34.

$$\rho\left(u\frac{\partial u}{\partial x}+v\frac{\partial u}{\partial y}\right)=\mu\frac{\partial^2 u}{\partial y^2}-\frac{\partial P}{\partial x}-\rho g \tag{3.34}$$

With reference to Figure 26 and Equation 3.34, the x-momentum equation for stationary fluid outside the boundary layer can be obtained, since u=0, see Equation 3.35.

$$\frac{\partial P_\infty}{\partial x}=-\rho_\infty g \tag{3.35}$$

With $u \gg v$ in the boundary layer, it result that $\partial v/\partial x \approx \partial v/\partial y \approx 0$, and with no other body forces in the y-direction the force balance in the y-direction result in $\partial P/\partial y = 0$. Thus there is no pressure difference in the y-direction and therefore $P = P(x) = P_\infty(x)$ and $\partial P/\partial x = \partial P_\infty/\partial x = -\rho_\infty g$. Equation 3.34 can now be expressed as Equation 3.36 with $(\rho_\infty - \rho)g$ representing the net upward force per unit volume of the fluid, or the difference between the fluid weight and buoyance force. The net upward force ensures initiation and sustaining the convection currents.

$$\rho\left(u\frac{\partial u}{\partial x}+v\frac{\partial u}{\partial y}\right)=\mu\frac{\partial^2 u}{\partial y^2}+(\rho_\infty-\rho)g \tag{3.36}$$

From the previous sections it is clear there is a relationship between the density and temperature difference denoted by Equation 3.9, $\rho_\infty - \rho = \rho\beta(T - T_\infty)$. When this equation is substituted into Equation 3.36 and the result divided by ρ, the momentum equation for natural convection is obtained, see Equation 3.37.

$$u\frac{\partial u}{\partial x}+v\frac{\partial u}{\partial y}=\nu\frac{\partial^2 u}{\partial y^2}+g\beta(T-T_\infty) \tag{3.37}$$

Where $\nu = \mu/\rho$ and the kinematic viscosity of the fluid represents.

3.4.5. Non-Dimensionalize Governing Equations

The governing equations obtained in Section 3.4.4 are very complex due to their coupled, elliptic, partial differential characteristics. Thus approximations are made to simplify these equations. The Boussinesq and boundary layer approximation is already applied in Section 3.4.4. The flow is assumed to be laminar, steady and two-dimensional, whereas the fluid incompressible with constant properties, except density. By non-dimensionalizing the governing equations and applying a similarity solution the three complex partial differential equations can be reduced to two ordinary differential equations.

Continuity Equation

$$\frac{\delta u}{\delta x} + \frac{\delta v}{\delta y} = 0 \qquad (3.15)$$

Energy Equation

$$\rho C_p \quad u\frac{\partial T}{\partial x} + v\frac{\partial T}{\partial y} \quad = k \quad \frac{\partial^2 T}{\partial x^2} + \frac{\partial^2 T}{\partial y^2} \qquad (3.27)$$

Momentum Equation

$$u\frac{\partial u}{\partial x} + v\frac{\partial u}{\partial y} = \nu\frac{\partial^2 u}{\partial y^2} + g\beta(T - T_\infty) \qquad (3.37)$$

The governing equations are non-dimensionalized introducing the non-dimensional quantities, where $X = \frac{x}{L}$, $Y = \frac{y}{L}$, $U = \frac{u}{u_0}$, $V = \frac{v}{u_0}$ and $\theta = \frac{T - T_\infty}{T_w - T_\infty}$. Equations 3.15, 3.27 and 3.37 are non-dimensionalized to 3.15a, 3.27a and 3.37a as shown below. Where *Gr*, *Re* and *Pr* the Grashof, Reynolds and Prandtl number respectively represents. The significance of these numbers is discussed in the following Section.

Continuity Equation

$$\frac{\delta U}{\delta X} + \frac{\delta V}{\delta Y} = 0 \qquad (3.15a)$$

Energy Equation

$$U\frac{\partial \theta}{\partial X} + V\frac{\partial \theta}{\partial Y} = \frac{1}{RePr}\frac{\partial^2 \theta}{\partial Y^2} \qquad (3.27a)$$

Momentum Equation

$$U\frac{\partial U}{\partial X} + V\frac{\partial U}{\partial Y} = \frac{Gr}{Re^2}\theta + \frac{1}{Re}\frac{\partial^2 U}{\partial Y^2} \qquad (3.37a)$$

3.4.6. Non-Dimensionalized Numbers (Gr, Nu, Re, Pr)

- **Grashof Number (Gr)**

The modified Grashof number plays an important role in heat transfer by natural convection and represents the natural convection effects (flow regime) which are the ratio between the buoyance force and the viscous force acting on the fluid, see Equation 3.38. The higher the Grashof number, the higher the heat transfer rate. The Grashof number also determines if the flow is laminar or turbulent, in the scenario of a vertical plate, flow is become turbulent at Grashof numbers great than 10^9 (Cengel, 2009)

$$G_r = \frac{\propto \ T_0 - T_1 \ fL^3}{\nu\kappa} \tag{3.38}$$

Where $\propto$, ν and κ the coefficient of cubic expansion, kinematic viscosity and thermal diffusivity respectively represents. The typical length is represented by L where $(T_0 - T_1)$ the temperature difference represents. To maximise the Grashof number (maximum heat transfer), the acceleration should be large and the pressure and temperature of fluid should be close to the critical condition. This will ensure that the viscosity is at a minimum and the coefficient of expansion is very large.

- **Nusselt Number (Nu)**

Another important parameter in heat transfer is the Nusselt number, the dimensionless convection heat transfer coefficient, representing the enhancement of heat transfer through a fluid layer as a result of convection relative to conduction across the same fluid layer, see Equation 3.39. The higher the Nusselt number, the more effective the convection, where a Nu=1 indicates that the heat transfer across the layer are purely by conduction, thus no fluid motion present. (Cengel, 2009)

$$N_u = \frac{Q}{kA(T_0 - T_1)/L} \tag{3.39}$$

Where Q, A and k the rate of heat transfer, area and thermal conductivity respectively represents.

- **Reynolds Number (Re)**

The Reynolds number represents the ratio between the inertia forces and the viscous forces, see Equation 3.40. Large Reynolds numbers indicate that inertia forces are larger than the viscous forces, thus the viscous forces are not able to prevent rapid fluctuations within the fluid, and flow becomes turbulent. Small Reynolds numbers indicate that the viscous forces are large enough to overcome the inertia forces, keeping the fluid stable, thus laminar flow. (Cengel, 2009)

$$Re = \frac{VL_c}{v} \tag{3.40}$$

Where V, L_c and v the upstream velocity, length and kinematic viscosity represents respectively.

- **Prandtl Number (Pr)**

The Prandtl Number describe the relative thickness of the thermal and velocity boundary layers and is the ratio between the molecular diffusivity of momentum and the molecular diffusivity of heat. Prandtl numbers range from 0.01 (liquid metals) to >100 000 (heavy oils). The Prandtl number for water is in the range of 10. The lower the Prantl number, the faster the heat diffuses in the medium relative to momentum. Thus the thermal boundary for low Prandtl numbers is wider than at high Prantl numbers. (Cengel, 2009)

$$Pr = \frac{v}{\alpha} = \frac{\mu C_p}{k} \tag{3.41}$$

Where v, α, μ, C_p and k the kinematic viscosity, thermal diffusivity, dynamic viscosity, specific heat constant and thermal conductivity respectively represents.

3.4.7. Similarity Solution:

In this section a similarity solution, introduced by Ostrach in 1953, is applied to the non-dimensional governing equations from the previous sections, to obtain ordinary differential equations. These ordinary differential equations are solved using a simulation model in *Matlab*, creating temperature and velocity profiles as illustrated in Figure 27, for flow over a vertical wall with a constant wall temperature (isothermal) or a constant heat flux (isoflux).

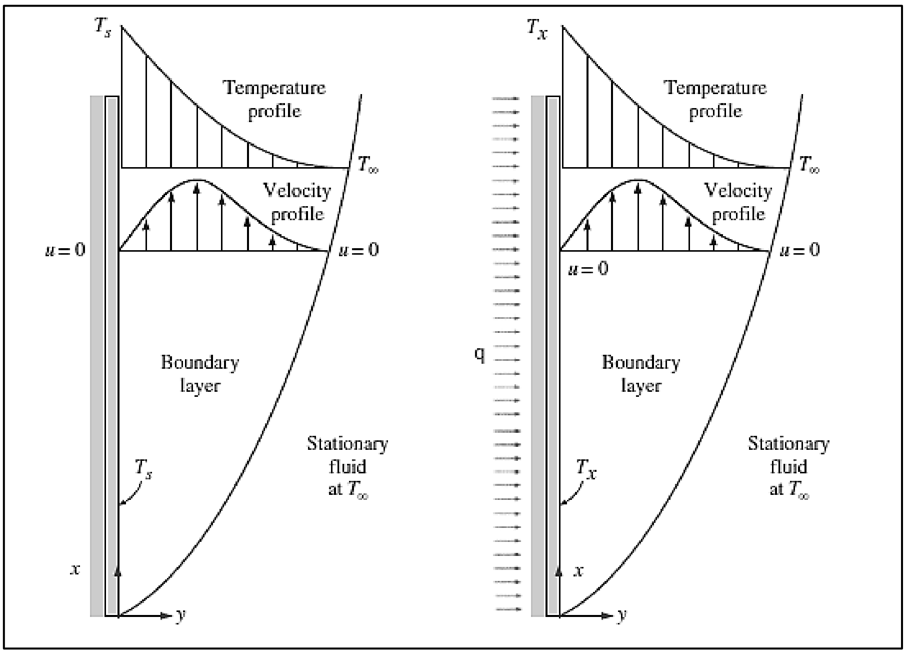

Figure 27: Vertical wall: Isothermal (left) and Isoflux (right) (Cengel, 2009)

- **<u>Vertical Wall with Constant Wall Temperature:</u>**

In this scenario, a vertical wall with a constant wall temperature is in the presence of a bulk fluid (gas or liquid). Natural convection currents are initiated up the wall due to the wall temperature being greater than that of the fluid. The following boundary conditions in Table 2 are applicable for fluid flow over an isothermal vertical wall. The dimensionless governing equations are recalled for analysis.

<u>Location</u>	**<u>Velocity</u>**	**<u>Temperature</u>**
$y = 0$	$u = v = 0$	$T = T_s$
$y \to \infty$	$u \to 0$	$T \to T_\infty$

Table 2: Boundary conditions: Isothermal vertical wall

<u>Continuity Equation</u>

$$\frac{\delta U}{\delta X} + \frac{\delta V}{\delta Y} = 0 \qquad (3.15a)$$

<u>Energy Equation</u>

$$U\frac{\partial \theta}{\partial X} + V\frac{\partial \theta}{\partial Y} = \frac{1}{RePr}\frac{\partial^2 \theta}{\partial Y^2} \qquad (3.27a)$$

<u>Momentum Equation</u>

$$U\frac{\partial U}{\partial X} + V\frac{\partial U}{\partial Y} = \frac{Gr}{Re^2}\theta + \frac{1}{Re}\frac{\partial^2 U}{\partial Y^2} \qquad (3.37a)$$

When a stream function is introduced and applied to the continuity equation the continuity equation is satisfied, see Equation 3.42. The momentum and energy equations still remain.

$$U = \frac{\partial \psi}{\partial Y} \qquad\qquad V = -\frac{\partial \psi}{\partial X} \qquad (3.42)$$

A similarity variable η and dimensionless stream function f are defined to convert the governing partial differential equations into ordinary differential equations. Gebhart in 1988 have presented a general approach to determine the conditions for similarity in a variety of flow circumstances. In the scenario where flow is over a vertical isothermal surface, the similarity variables are, see Equation 3.43. (Jaluria, 1980)

$$\eta = \frac{y}{x}\;\frac{Gr_x}{4}^{0.25} \qquad\qquad \psi(x,y) = 4\nu f\;\;\eta\;\;\frac{Gr_x}{4}^{0.25} \qquad (3.43)$$

Where ν the kinematic viscosity represents. From Equation 3.42, the x-velocity component (U) can be further be expressed in terms of the stream function, see Equation 3.44.

$$U = \frac{\partial \psi}{\partial Y} = \frac{\partial \psi}{\partial \eta}\frac{\partial \eta}{\partial Y} = 4\nu f'(\eta)\left(\frac{Gr_x}{4}\right)^{0.25}\frac{1}{x}\left(\frac{Gr_x}{4}\right)^{0.25} = \frac{2\nu}{x}Gr_x^{0.5}f'(\eta) \qquad (3.44)$$

The three partial differential equations are transformed with the similarity variables to two ordinary differential equations, see Equation 3.45 and 3.46. The primes indicate the differentiation of $f(\eta)$ and $\theta(\eta)$ with respect to the similarity variable η. The first derivative is represented by one prime, second derivative by two and third derivative by three. The function $f(\eta)$ and $\theta(\eta)$ takes on the role of the dependant variable for the velocity and temperature boundary layer respectively.

$$f''' + 3ff'' - 2(f')^2 + \theta = 0 \qquad (3.45)$$

$$\theta'' + 3Prf\theta' = 0 \qquad (3.46)$$

The boundary conditions in Table 3 are transformed to solve the momentum and energy equations. For conditions close to the wall $\eta = 0$, the velocity profile is zero and the temperature the same as the wall temperature. For conditions far away from the wall $\eta \rightarrow \infty$, the stream function strives to be stagnant and the temperature strives to be the same temperature as the bulk fluid. These conditions correspond with the assumptions in Figure 27.

Location	**Velocity**	**Temperature**
$\eta = 0$	$f = f' = 0$	$\theta = 1$
$\eta \rightarrow \infty$	$f \rightarrow 0$	$\theta \rightarrow 0$

Table 3: Transformed boundary conditions: Isothermal vertical wall

In order to solve Equations 3.45 and 3.46 numerically, these equations are first reduced to first order differential equations by defining new dependant variables, $\mathrm{F}^0, \mathrm{F}^1, \mathrm{F}^2, \Theta^0$ and Θ^1, see Equations 3.47-3.51. (Goldstein, 2004)

$$\frac{d\mathrm{F}^0}{d\eta} = \mathrm{F}^1 \qquad (3.47)$$

$$\frac{d\mathrm{F}^1}{d\eta} = \mathrm{F}^2 \qquad (3.48)$$

$$\frac{d\mathrm{F}^2}{d\eta} = -3\mathrm{F}^0\mathrm{F}^2 + 2\ {\mathrm{F}^1}^{\ 2} - \Theta^0 \qquad (3.49)$$

$$\frac{d\Theta^0}{d\eta} = \Theta^1 \qquad (3.50)$$

$$\frac{d\Theta^1}{d\eta} = -3Pr\mathrm{F}^0\Theta^1 \qquad (3.51)$$

Where F^0 and Θ^0 equivalent to f and θ is. . This five coupled first order ordinary differential equations can be solved in *Matlab* using the built-in ODE45 solver, see Section 3.4.8.

- **Vertical Wall with Constant Heat Flux:**

In this scenario, a vertical wall with a constant heat flux is in the presence of a bulk fluid (gas or liquid). Natural convection currents are initiated up the wall due to the constant energy to the wall, thus the temperature of the fluid increase as it moves up the wall. The following boundary conditions in Table 4 are applicable for fluid flow over an isoflux vertical wall.

Location	**Velocity**	**Temperature**
$y = 0$ $y \to \infty$	$u = v = 0$ $u \to 0$	$T = T_s$ $T \to T_\infty$

Table 4: Boundary conditions: Isoflux vertical wall

As in the isothermal scenario, a stream function is introduced and applied to the continuity equation, the continuity equation is satisfied, see Equation 3.52. The momentum and energy equations still remain.

$$U = \frac{\partial\psi}{\partial Y} \qquad\qquad V = -\frac{\partial\psi}{\partial X} \qquad (3.52)$$

There is no constant wall temperature in the isoflux scenario and thus a different set of similarity variables are applied, see Equation 3.53. Sparrow and Gregg, (1958) obtained the similarity solution for a vertical plate with a uniform heat flux boundary condition. They investigated Prandtl numbers in the range 0.1 to 100. (Wong, 2003)

$$\eta = D_1 y x^{-1/5} \qquad\qquad D_1 = \left(\frac{g\beta q_w}{5k\upsilon^2}\right)^{1/5} \tag{3.53}$$

$$\psi(x,y) = D_2 x^{\frac{4}{5}} f(\eta) \qquad\qquad D_2 = \left(\frac{5^4 g\beta q_w v^3}{k}\right)^{1/5} \tag{3.54}$$

Where q_w and k the heat flux at the wall and thermal conductivity respectively represents. The similarity variable for temperature is represented in Equation 3.55.

$$\theta(\eta) = \frac{D_1(T_\infty - T)}{x^{\frac{1}{5}} q_w / k} \tag{3.55}$$

From Equation 3.52, the velocity components can be further be expressed in terms of the stream function, see Equation 3.56.

$$U = D_1 D_2 x^{\frac{3}{5}} f'(\eta) \qquad\qquad V = \frac{D_2}{5x^{\frac{1}{5}}}\left(\eta f'(\eta) - 4f(\eta)\right) \tag{3.56}$$

As in the isothermal scenario, the three partial differential equations, are reduced to two ordinary differential equations, see Equations 3.57 and 3.58.

$$f''' - 3(f')^2 + 4ff'' - \theta = 0 \tag{3.57}$$

$$\theta'' + \mathrm{Pr}(4f\theta' - \theta f') = 0 \tag{3.58}$$

The boundary conditions in Table 4 are transformed to solve the momentum and energy equations.

Location	**Velocity**	**Temperature**
$\eta = 0$	$f = f' = 0$	$\theta' = 1$
$\eta \to \infty$	$f' \to 0$	$\theta \to 0$

Table 5: Transformed boundary conditions: Isoflux vertical wall

In order to solve Equations 3.57 and 3.58 numerically, these equations are first reduced to first order differential equations by defining new dependant variables, $\mathrm{F}^0, \mathrm{F}^1, \mathrm{F}^2, \Theta^0$ and Θ^1, see Equations 3.59-3.63. (Goldstein, 2004)

$$\frac{d\mathrm{F}^0}{d\eta} = \mathrm{F}^1 \tag{3.59}$$

$$\frac{d\mathrm{F}^1}{d\eta} = \mathrm{F}^2 \tag{3.60}$$

$$\frac{d\mathrm{F}^2}{d\eta} = 3\ \mathrm{F}^1\ {}^2 - 4\mathrm{F}^0\mathrm{F}^2 + \Theta^0 \tag{3.61}$$

$$\frac{d\Theta^0}{d\eta} = \Theta^1 \tag{3.62}$$

$$\frac{d\Theta^1}{d\eta} = -Pr\ \ 4F^0\Theta^1 - \Theta^0 F^1 \tag{3.63}$$

Where F^0 and Θ^0 equivalent to f and θ is. The first derivative is represented by one prime, second derivative by two and third derivative by three. This five coupled first order ordinary differential equations are used in the can be solved in *Matlab* using the built-in ODE45 solver. Results for the velocity and temperature profiles of this scenario can be seen in Section 3.4.8.

3.4.8. Velocity and Temperature Profiles (2D)

In Section 3.4.7 two coupled two ordinary differential equations are obtained for flow induced by a vertical wall with either a constant wall temperature or constant heat flux. These equations are solved numerically to obtain the velocity and temperature profiles for these scenarios. In 1911, Pohlhausen was the first to solve these equations for a vertical wall with constant wall temperature. By 1930, Schmidt and Beckmann solved these equations for Pr = 0.733. In 1953, Ostrach increased the solution to Prandtl numbers ranging from 0.01 to 1000. Sparrow and Gregg (1958) obtained a similarity solution for a vertical wall with a constant heat flux and investigated Prandtl number ranging from 0.1 to 100.

- **Vertical Wall with Constant Wall Temperature:**

The dimensionless velocity and temperature distribution developed by Ostrach in 1953 can be seen in Figure 28 and Figure 29. Values for $f''\ 0$ and $\theta'\ 0$ are obtained from solutions provided by Ostrach. A *Matlab* model has been developed to solve these solutions and compare it to solutions obtained by Ostrach. The model can also provide the velocity and temperature profile for a vertical wall with any wall temperature and length. The model can be adapted for various fluids if the fluid properties are available. These figures will give valuable insight for a basic understanding in fluid flow where a vertical isothermal wall is considered.

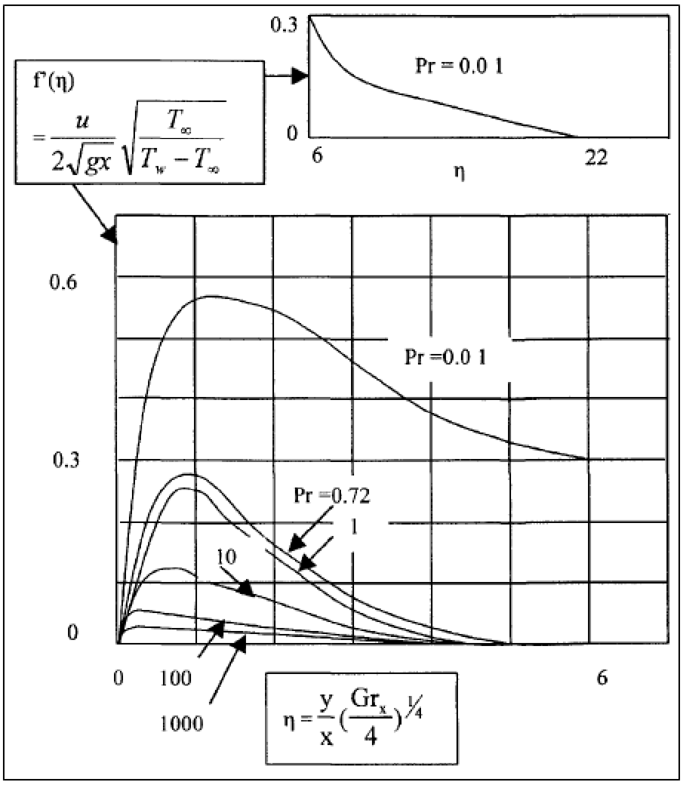

Figure 28: Dimensionless velocity distribution (Ostrach, 1953)

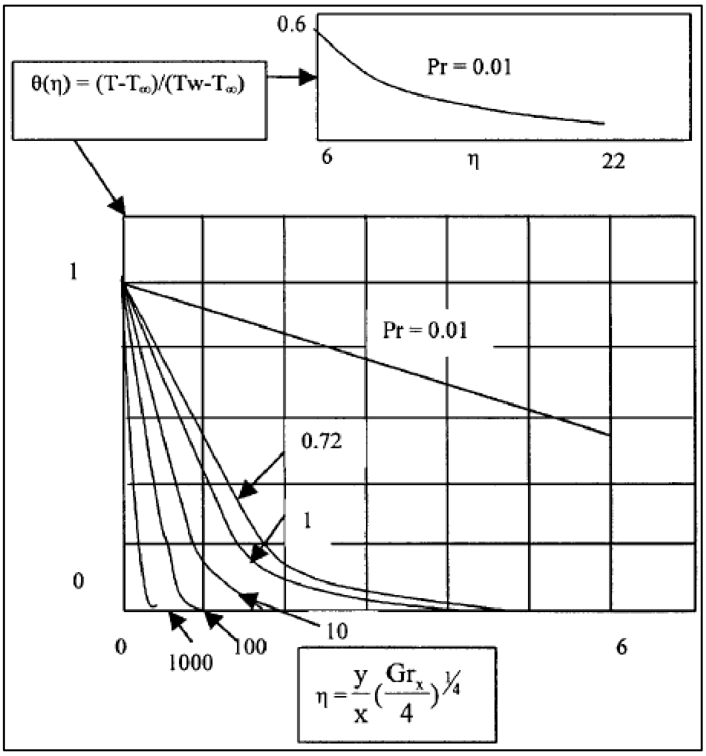

Figure 29: Dimensionless temperature distribution (Ostrach, 1953)

The dimensionless temperature and velocity distribution graphs are simulated in the *Matlab* model, see Figure 30 and Figure 31. When these results from the model are compared to those from Ostrach, a clear resemblance is observed, see Table 6. The model is thus accurate in solving the ordinary differential equations with boundary conditions. These dimensionless distribution graphs, see Figure 32 and Figure 33, are used to obtain the velocity and temperature profiles for a given wall temperature and length, see Figure 34 and Figure 35. The wall has a length of 10cm and temperature of 50 °C. The fluid medium is water with a temperature of 15 °C.

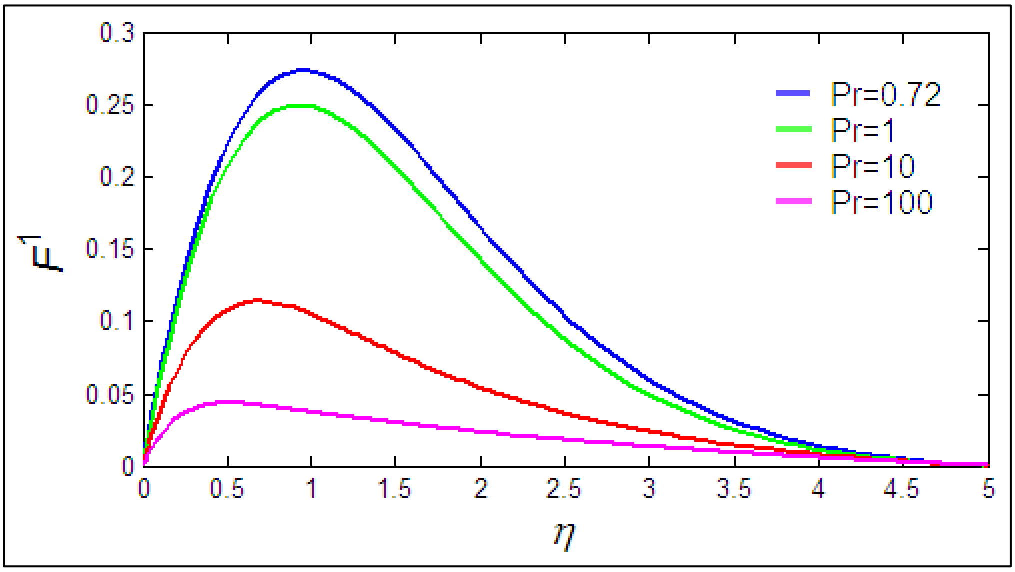

Figure 30: Dimensionless velocity distribution with various Prandtl numbers

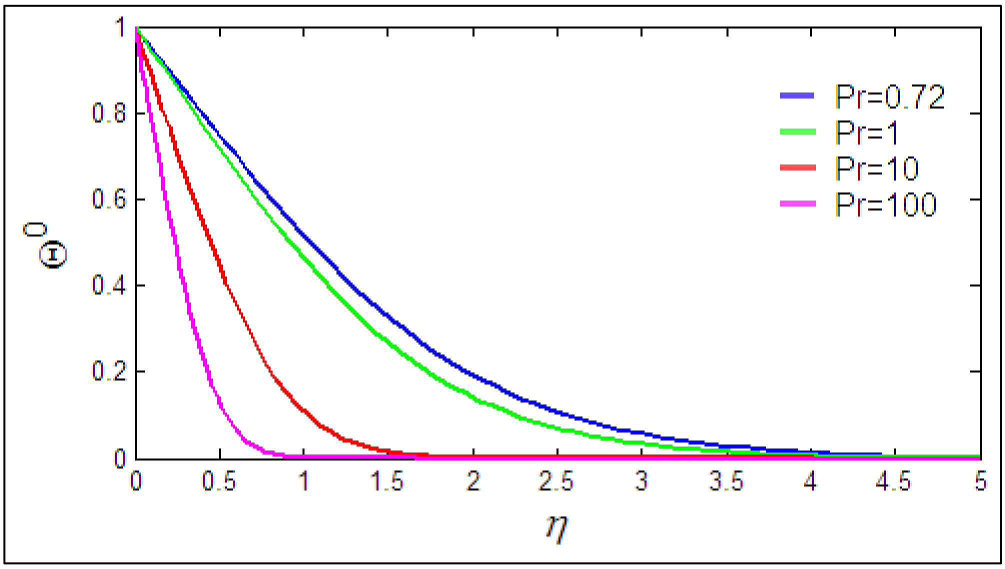

Figure 31: Dimensionless temperature distribution with various Prandtl numbers

	Ostrach (1953)		***Matlab* Model**	
Pr	$\boldsymbol{f''}$ **0**	$\boldsymbol{\theta'}$ **0**	$\boldsymbol{f''}$ **0**	$\boldsymbol{\theta'}$ **0**
0.733	0.6741	0.5078	0.6742	0.5048
1	0.6421	0.5671	0.6414	0.5669
10	0.4192	1.1680	0.4186	1.1677
100	0.2517	2.1914	0.2509	2.1857

Table 6: Calculated values for various values of Pr using *Matlab*

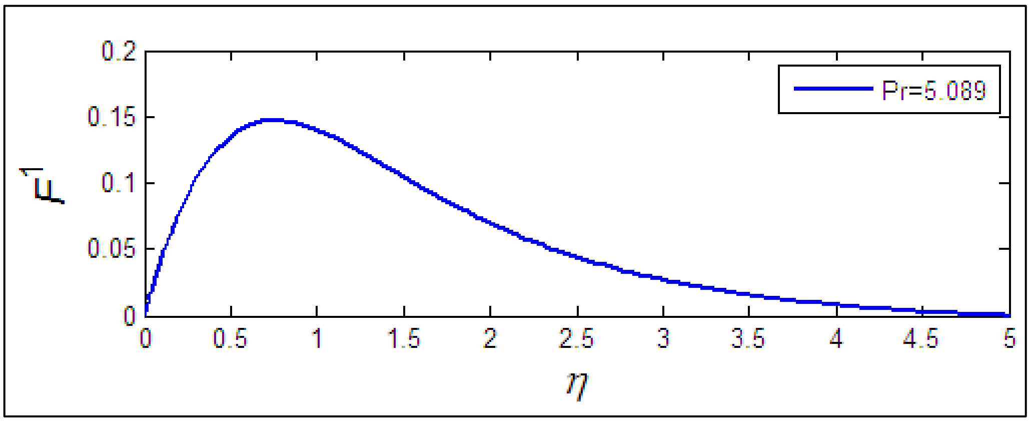

Figure 32: Dimensionless velocity distribution

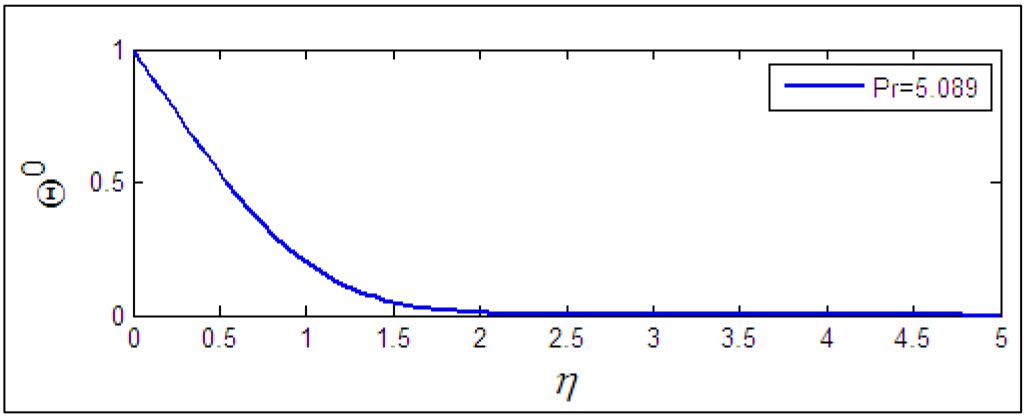

Figure 33: Dimensionless temperature distribution

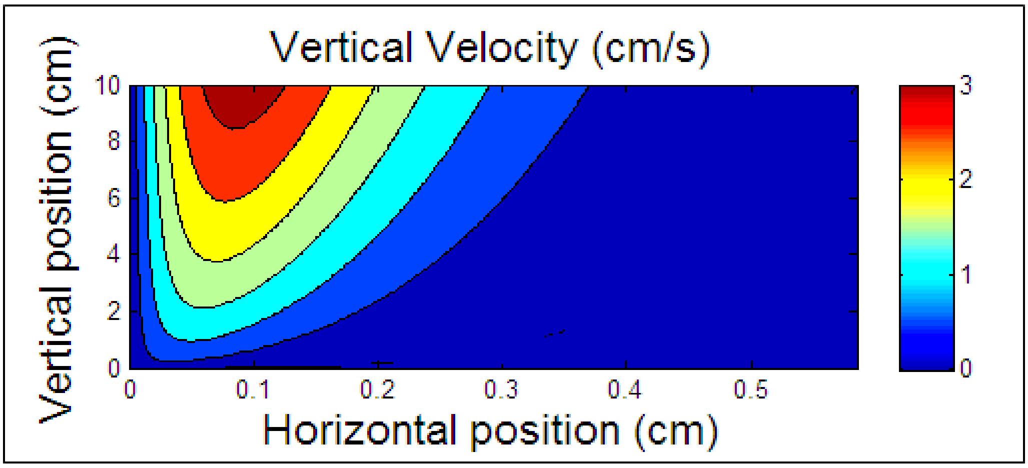

Figure 34: Velocity profile created in *Matlab*

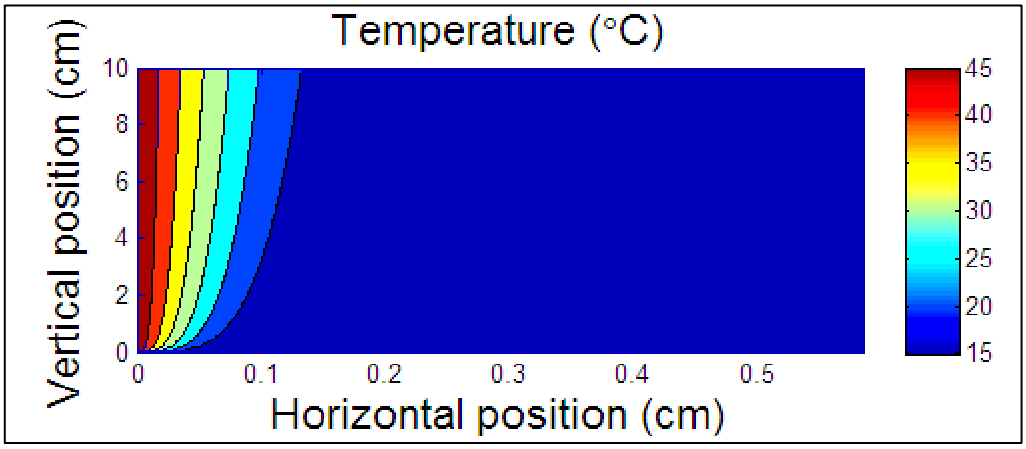

Figure 35: Temperature profile created in *Matlab*

- **<u>Vertical Wall with Constant Heat Flux:</u>**

Values for $f''\ 0$ and $\theta\ 0$ are obtained from solutions provided by Sparrow and Gregg (1958), see Table 7. A *Matlab* model has been developed to obtain the velocity and temperature profile for a vertical wall with a certain length and constant heat flux. The model can be adapted for various fluids if the fluid properties are available. These figures will give valuable insight for a basic understanding in fluid flow where a vertical isoflux wall is considered. The dimensionless temperature and velocity distribution graphs are simulated by the *Matlab* model (Figure 36 and Figure 37). When these results from the model are compared to those from Sparrow and Gregg, a clear resemblance is observed. The model is thus accurate in solving the ordinary differential equations with boundary conditions. These dimensionless distribution graphs (Figure 38 and Figure 39), are used to obtain the velocity and temperature profiles for a given heat flux and wall length (Figure 40 and Figure 41). The wall has a length of 10cm and the heat flux applied is 800 W/m^2. The fluid medium is water with a temperature of 15 °C.

Pr	f'' 0	θ 0
0.1	1.64340	-2.7507
1	0.72196	-1.3574
10	0.30639	-0.76746
100	0.12620	-0.46566

Table 7: Calculated values for various values of Pr (Sparrow, Gregg, 1958)

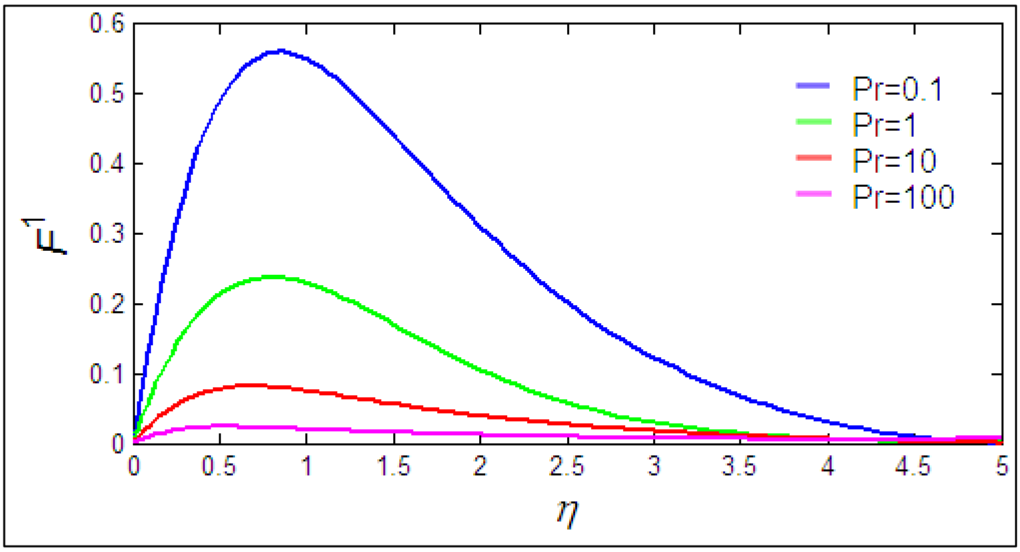

Figure 36: Dimensionless velocity distribution with various Prandtl numbers

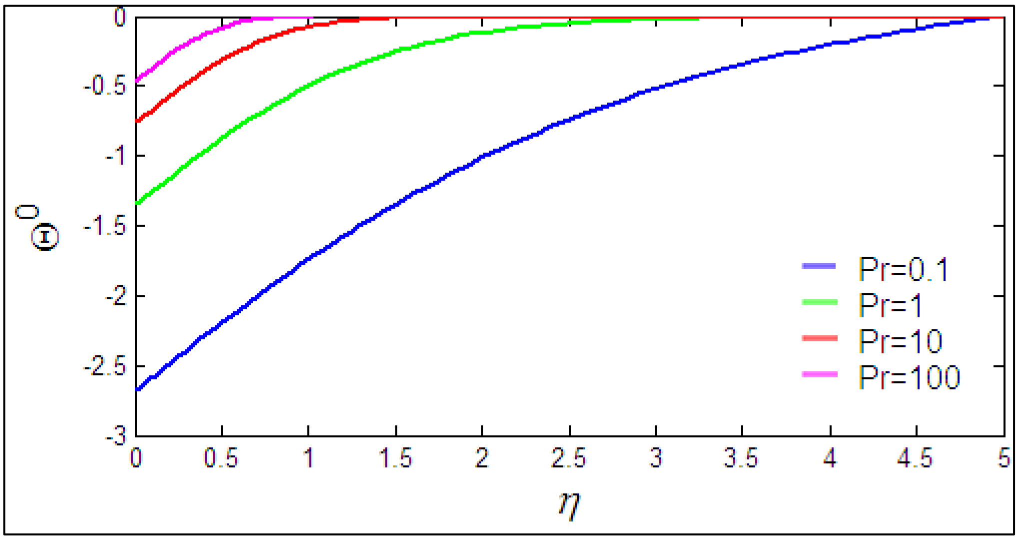

Figure 37: Dimensionless temperature distribution with various Prandtl numbers

	Sparrow (1958)		*Matlab* Model	
Pr	f'' **0**	θ **0**	f'' **0**	θ **0**
0.1	1.6434	-2.7507	1.5896	-2.6860
1	0.7219	-1.3574	0.7218	-1.3577
10	0.3063	-0.7674	0.3062	-0.7684
100	0.1262	-0.4656	0.1249	-0.4689

Table 8: Calculated values for various values of Pr (Sparrow, Gregg, 1958)

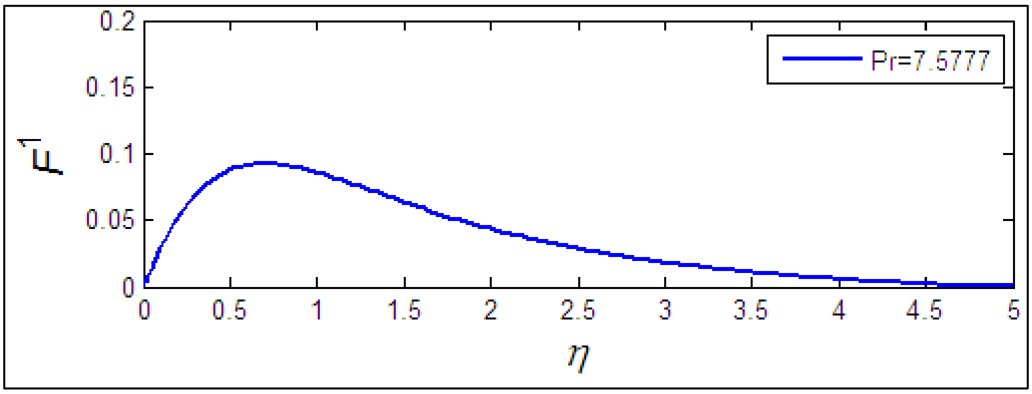

Figure 38: Dimensionless velocity distribution

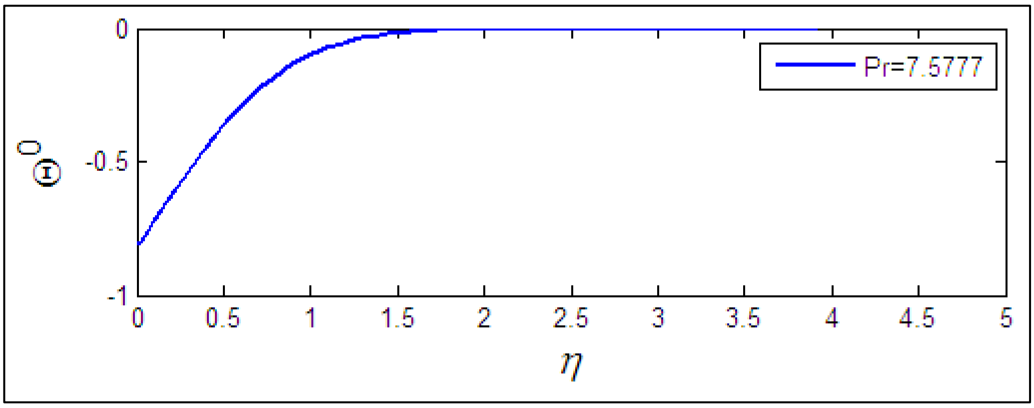

Figure 39: Dimensionless temperature distribution

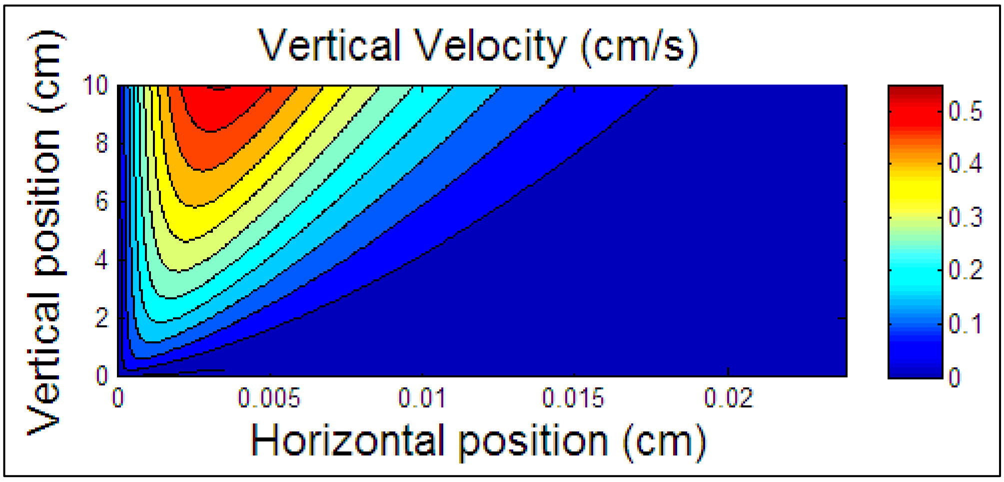

Figure 40: Velocity profile created in *Matlab*

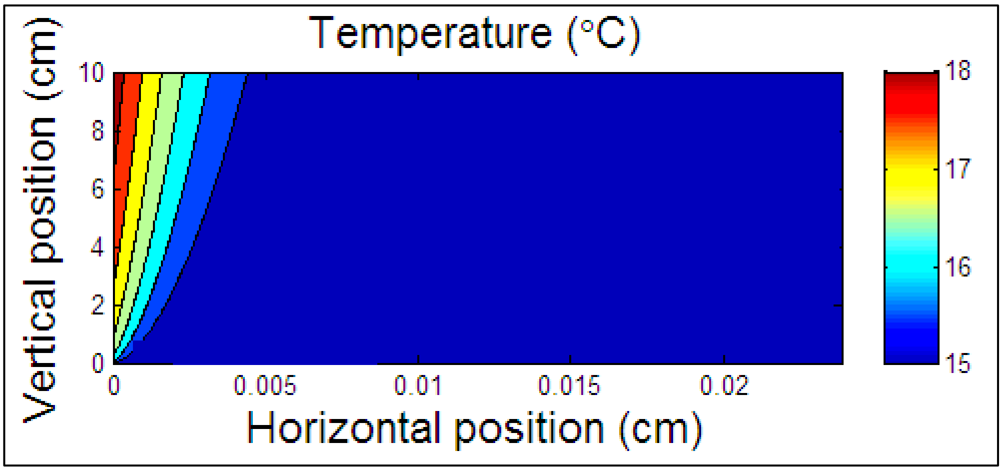

Figure 41: Temperature profile created in *Matlab*

There is a clear difference between the velocity and temperature graphs from the simulations for an isothermal and isoflux vertical wall. In both simulations, the Prandtl number was 7.5. To obtain the same Prandtl number, the wall temperature and heat flux were adjusted, to be able to make a comparison between the two scenarios. In the isothermal case the temperature distribution reduces gradually further away from the wall with almost uniform layers. In the isoflux case, the temperature distribution grows along the wall and reduces gradually away from the wall. It is also clear from the simulations that a higher velocity is achieved in the isothermal case. However if the length of the wall is increased significantly, the velocity and temperature of the isoflux scenario will be greater for the same given wall length in the isothermal case. This is due to an increase in energy per unit length from the constant heat flux. In LP SWHs, the isoflux scenario can be applied to the vacuum tubes. The vacuum tubes are exposed to the solar radiation throughout the day and for any given instance, a constant heat flux is observed on the tube wall with a flux distribution around the circumference as in Figure 42.

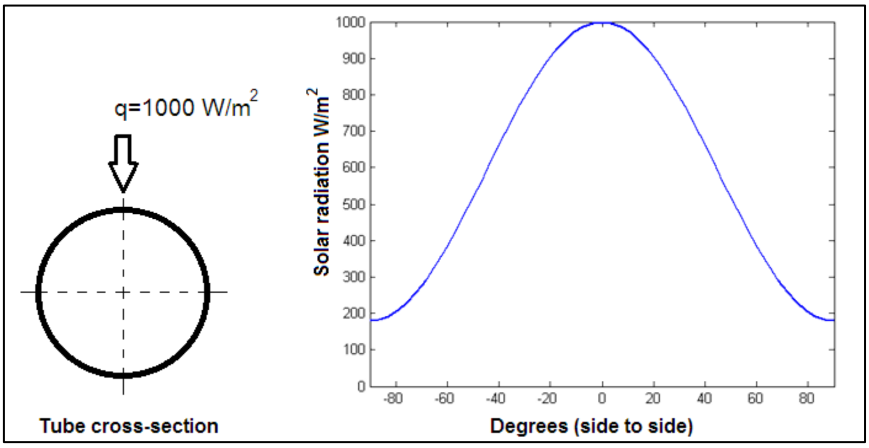

Figure 42: Solar flux distribution on a tube (Matlab simulation)

3.4.9. Velocity and Temperature Profiles (3D)

The geometrical shape of the vacuum tubes found in the low pressure solar water heaters are three dimensional and the model obtained in Section 3.4.8 only account for flow in the second dimension. However, the model is a good representation of the flow that occurs in the tubes. When the diameter is very large compared to the length of the tube, natural convection flow currents over a flat plate can be considered (Lighthill, 1952), and thus the model can be applied. The main purpose of the model is to validate the theory found in literature and provides a visual understanding of the flow found in natural convection. In the three dimensional realm the governing equations and boundary conditions are adapted to account for the extra added dimension and geographical shape of the object, see Figure 43, Figure 44 and Figure 45. Shahi, 2010, developed the temperature and velocity profiles, illustrated in Figure 43, for these equations. It is noticed that the velocity and temperature profiles are similar to those in 2D.

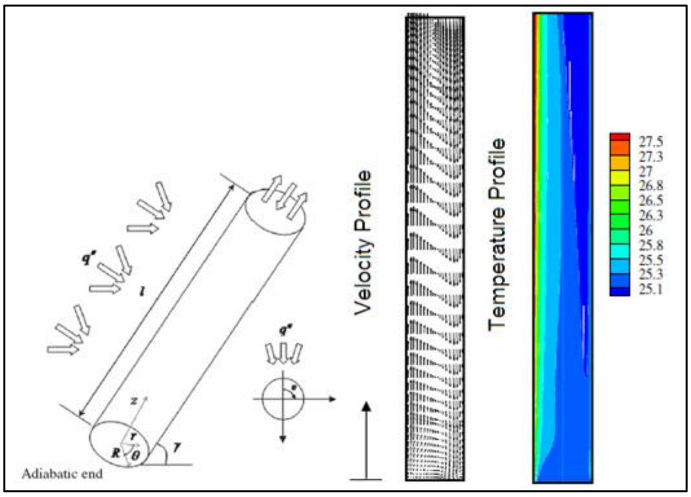

Figure 43: Tube with constant heat flux (Shahi, 2010)

The boundary conditions are in the following forms:

at the walls: $v_r, v_\theta, v_z = 0$

$$\text{at}\quad (r = Rz) : (0,l)\ \theta : (0,\pi) : k_{eff}\frac{\partial T(R,\theta,z)}{\partial r} = q''(\theta)$$

$$\text{at}\quad (r : (0,R) z : (0,l)\ \theta = 0,\pi) : \frac{\partial v_z}{\partial \theta} = \frac{\partial v_r}{\partial \theta} = 0 \ , \quad v_\theta = 0 \ ,$$

$$\frac{\partial T_z}{\partial \theta} = \frac{\partial T_r}{\partial \theta} = 0$$

$$\text{at}\quad (z = 0\ \ \theta : (0,\pi)\ r : (0,R)) : \frac{\partial T(r,\theta,0)}{\partial z} = 0$$

$$\text{at the inlet boundary} : \begin{cases} \dfrac{\partial v}{\partial z} = \dfrac{\partial u}{\partial z} = 0 \\ T = T_{in} \end{cases}$$

$$\text{at the outlet boundary} : \begin{cases} \dfrac{\partial w}{\partial z} = -\left(\dfrac{\partial v}{\partial r} + \dfrac{\partial u}{\partial \theta}\right) \\ \dfrac{\partial T}{\partial z} = 0 \end{cases}$$

Figure 44: Boundary conditions (Shahi, 2010)

The momentum equations (for r, θ and z directions)are as follows:

$$\rho_{nf}\left(\frac{1}{r}\frac{\partial(rv_r v_r)}{\partial r} + \frac{1}{r}\frac{\partial(v_\theta v_r)}{\partial \theta} - \frac{v_\theta^2}{r} + \frac{\partial(v_z v_r)}{\partial z}\right)$$
$$= -\frac{\partial P_d}{\partial r} + \mu_{nf}\left[\frac{\partial^2 v_r}{\partial r^2} + \frac{1}{r}\frac{\partial v_r}{\partial r} - \frac{v_r}{r^2} + \frac{1}{r^2}\frac{\partial^2 v_r}{\partial \theta^2} - \frac{2}{r^2}\frac{\partial v_\theta}{\partial \theta} + \frac{\partial^2 v_r}{\partial z^2}\right]$$
$$-\rho_{nf} g_r \beta_{nf}\left(T - T_{ref}\right)$$

$$\rho_{nf}\left(\frac{1}{r}\frac{\partial(rv_r v_\theta)}{\partial r} + \frac{1}{r}\frac{\partial(v_\theta v_\theta)}{\partial \theta} + \frac{v_r v_\theta}{r} + \frac{\partial(v_z v_\theta)}{\partial z}\right)$$
$$= -\frac{1}{r}\frac{\partial P_d}{\partial \theta} + \mu_{nf}\left[\frac{\partial^2 v_\theta}{\partial r^2} + \frac{1}{r}\frac{\partial v_\theta}{\partial r} - \frac{v_\theta}{r^2} + \frac{1}{r^2}\frac{\partial^2 v_\theta}{\partial \theta^2} + \frac{2}{r^2}\frac{\partial v_r}{\partial \theta} + \frac{\partial^2 v_\theta}{\partial z^2}\right]$$
$$-\rho_{nf} g_\theta \beta_{nf}\left(T - T_{ref}\right)$$

$$\rho_{nf}\left(\frac{1}{r}\frac{\partial(rv_r v_z)}{\partial r} + \frac{1}{r}\frac{\partial(v_\theta v_z)}{\partial \theta} + \frac{\partial(v_z v_z)}{\partial z}\right)$$
$$= -\frac{\partial P_d}{\partial z} + \mu_{nf}\left[\frac{\partial^2 v_z}{\partial r^2} + \frac{1}{r}\frac{\partial v_z}{\partial r} + \frac{1}{r^2}\frac{\partial^2 v_z}{\partial \theta^2} + \frac{\partial^2 v_z}{\partial z^2}\right]$$
$$-\rho_{nf} g_z \beta_{nf}\left(T - T_{ref}\right)$$

The continuity equation:

$$\frac{1}{r}\frac{\partial(rv_r)}{\partial r} + \frac{1}{r}\frac{\partial v_\theta}{\partial \theta} + \frac{\partial v_z}{\partial z} = 0$$

The energy equation:

$$\frac{1}{r}\frac{\partial(rv_r T)}{\partial r} + \frac{1}{r}\frac{\partial(v_\theta T)}{\partial \theta} + \frac{\partial(v_z T)}{\partial z} = \frac{k_{eff}}{(\rho c_p)_{nf}}\left[\frac{1}{r}\frac{\partial}{\partial r}\left(r\frac{\partial T}{\partial r}\right) + \frac{1}{r^2}\frac{\partial^2 T}{\partial \theta^2} + \frac{\partial^2 T}{\partial z^2}\right]$$

Figure 45: Governing equations (3D), (Shahi, 2010)

3.4.10. Mass Flow Rate

In 2005, I. Budihardjo developed a correlation for the natural circulation flow rate through single-ended tubes (at the tube opening). The flow rate correlation is based on the solar input the tube receives, the tank temperature, the collector's tilt angle and tube aspect ratio.

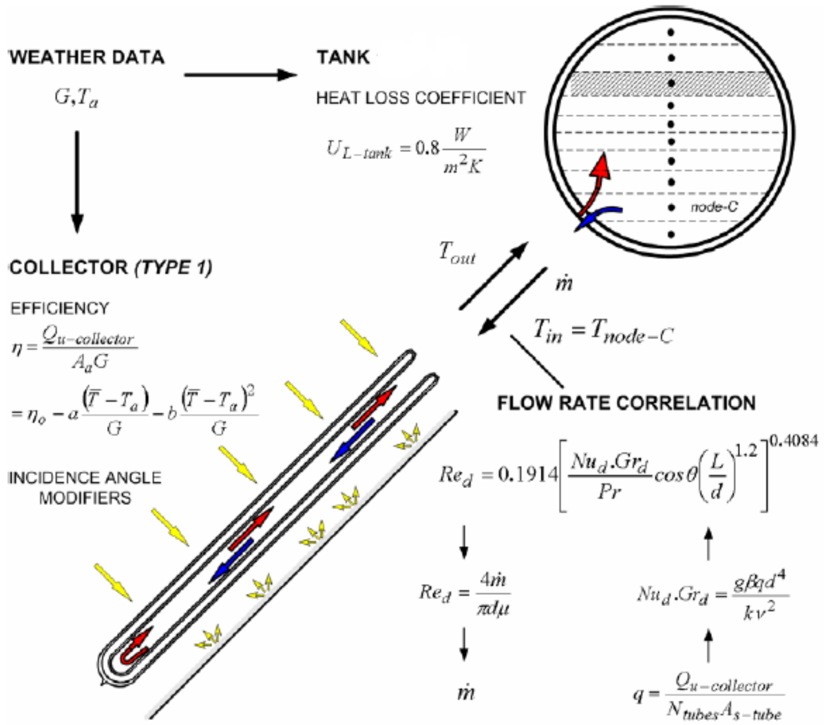

Figure 46: Mass flow rate correlation developed by Budihardjo in 2005

3.5. Collector Features

3.5.1. Tilt Angle

To maximise the annual energy collection from the collector, the tilt angle of the collector should be mounted at an optimal tilt angle. In 2009, R. Tang investigated the optimal tilt angles of all-glass evacuated tube solar collectors and developed a detailed mathematical procedure for calculating the collected radiation on a tube for any given tilt and azimuth angle. It was found that south facing collectors only rely on the optimal tilt angle for maximum annual energy collection. The optimal tilt angle for these collectors are generally less than the site latitude, and the optimal tilt angle decreases with an increase in the central distance (B) between adjacent tubes, see Table 9. Where D_1 and D_2 the inside and outside diameter respectively represents.

	Optimal Tilt Angles (Degrees)					Optimal Tilt Angles (Degrees)			
Latitude	B=80	B=90	B=100	B=110	B=120	B=70	B=80	B=90	B=100
45.75°N	34.8	34.0	33.4	32.8	32.3	34.3	33.5	32.7	32.1
43.78°N	31.6	30.9	30.3	29.8	29.3	31.2	30.4	29.7	29.1
39.95°N	30.5	29.8	29.3	28.8	28.4	30.1	29.4	28.8	28.2
36.02°N	26.9	26.4	25.9	25.4	25.0	26.6	25.9	25.4	25.0
34.25°N	21.9	21.4	20.9	20.5	20.1	21.6	21.0	20.5	20.1
31.20°N	20.2	19.7	19.3	19.0	18.6	19.9	19.4	19.0	18.5
30.67°N	15.4	14.9	14.5	14.1	13.9	15.0	14.5	14.1	13.8
25.01°N	21.0	20.7	20.3	20.1	19.8	20.8	20.4	20.1	19.7
Tubes	$D_1 = 47, D_2 = 58$					$D_1 = 37, D_2 = 47$			

Table 9: Optimal tilt angles for south facing collectors (Tang *et al.*, 2009)

According to Tang 2009, for areas with a high solar radiation index, the optimal tilt angle is close to the site latitude, whereas areas with a low solar radiation index, the optimal tilt angle is lower than the site latitude. If the site latitude is larger than 30°, the optimal tilt angle is 10° lower than that of the site latitude. Vacuum tube collectors are different than flat-plate collectors which are generally installed with the same tilt angle as the site latitude. South facing tube collectors should thus be installed with a tilt angle lower than the site latitude to ensure maximum annual collectable radiation. If two cities in South Africa are considered, Johannesburg (26.12°S 28.4°E) and Cape Town (33.55°S 18.22°E), the total annual energy collection for these cities will vary according this study, thus an optimal tilt angle is required for these cities respectively. The fixed tilt angle of 45° that's used for most low pressure solar water heaters should be reconsidered if these systems are to be optimized.

3.5.2. Length-Radius Ratio

Lighthill (1951) developed methods to predict the flow and heat transfer caused by natural convection in vertical heated tubes. From these methods a prediction can be made whether the flow is laminar or turbulent and if the boundary layer of heated fluid fills the tube or fills the tube with a stagnant region near the end. Lighthill founded that the flow depends on a modified Grashof number and on the length-radius ratio. When stagnant region develop in the vacuum tube, this section will become inactive, resulting in lower heat transfer in the tube (Budihardjo, 2005). The parameter defining the existence of a stagnant region as developed by Lighthill is:

$$T = R_a \cos\theta \frac{r}{L} \tag{3.64}$$

Where R_a, θ and L/r the Rayleigh number (based on the radius of the tube), tilt angle from the vertical and length-radius ratio respectively represents. When T<350 a stagnant region forms.

4. THERMAL ENERGY ANALYSIS

4.1. Three Basic Mechanisms of Heat Transfer

In this section the basic mechanisms within heat transfer are investigated. It is important to understand how solar radiation is transferred to storage tank to obtain heated water as the end product and where heat is lost through design. In this section the efficiency of the system will be discussed, factors in heat transfer that play a role in the efficiency of the system, is the heat loss through conduction, convection and radiation. Conduction is the transfer of energy from more energetic particles of a substance to the adjacent, less energetic ones as a result of interactions between particles. Convection is the mode of heat transfer between a solid surface and the adjacent liquid or gas that is in motion. Radiation is the energy emitted by matter in the form of electromagnetic waves (or photons) as a result of the changes in the electronic configurations of the atoms or molecules. (Cengel, 2009)

4.2. Energy Flow Analysis of LP SWH System

From the literature study done in Section 3, it was clear that the collector tilt angle played an important role in successfully absorbing the incoming solar radiation. For flat plate collectors, the maximum value the IAM can take on is 1; this is when solar incidence is perpendicular to the absorber surface, thus when optical efficiency of both angles for tubular collector are the same, the IAM=1, see Equation 4.1 and Figure 47. Due to the round geometry of the tubes, the tubes passively track the sun, thus absorbing more solar radiation than a fixed flat plate collector with the same absorber surface area as illustrated in Figure 48.

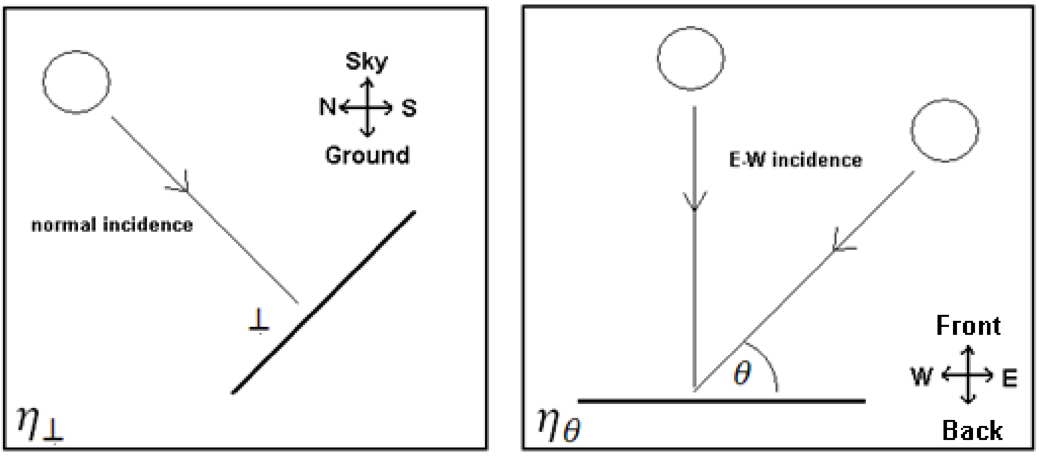

Figure 47: Optical efficiency on different solar angles

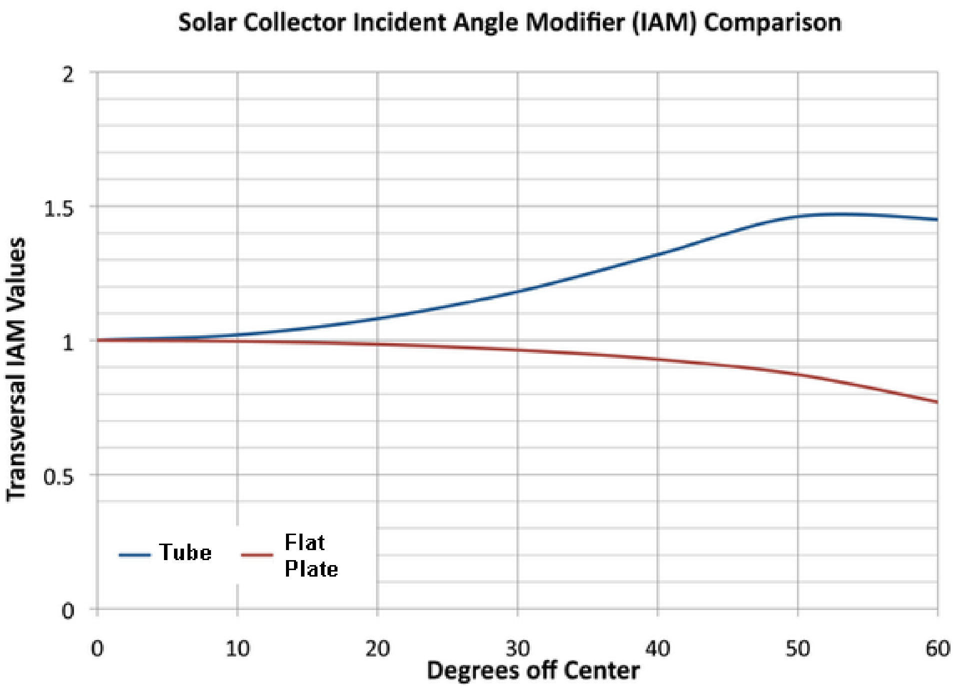

Figure 48: IAM between tubular and flat plate collector (Apricus, 2012)

$$IAM = \frac{\eta_\theta}{\eta_\perp} \tag{4. 1}$$

Where η_θ and $\eta_\perp$ represents the instantaneous collector efficiency for E-W incidence angle, and collector efficiency for normal incidence radiation respectively. The following figure illustrates the reflectance and transmittance of solar radiation intercepted by the tube. The absorbed radiation by inner tube (absorber tube) is transferred to the water present in the tube.

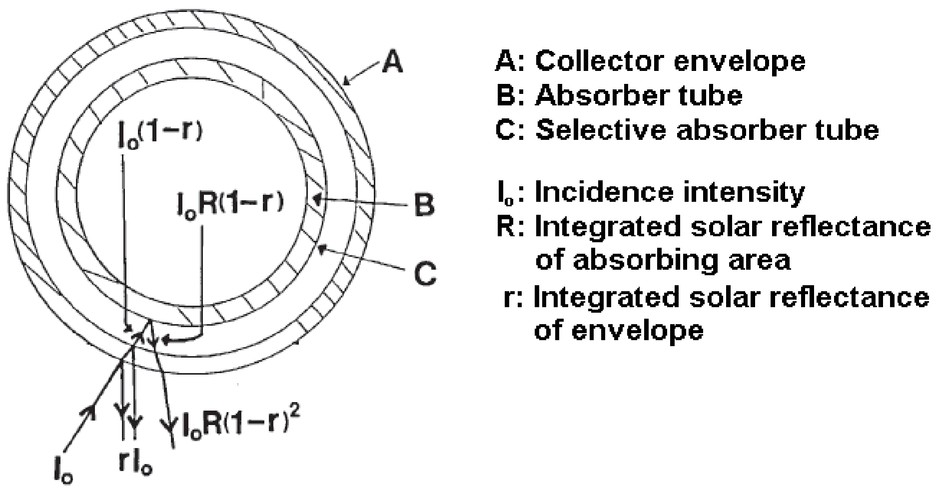

Figure 49: Solar radiation reflectance within the tube (Window *et al.*, 1983)

From the simulation results, based on the theory covered in Section 3, the tube wall represents a wall with a constant heat flux input. Thus energy (heat) is transferred to the fluid (water) by means of natural convection. Hot water rises up in the tube and entering the storage tank. As illustrated in Figure 50, cold water inside the storage tank replaces the hot water due to a density difference, and enters the tube at its opening. The cycle continues until no more solar radiation is absorbed from the tubes and tank stratification reaches equilibrium.

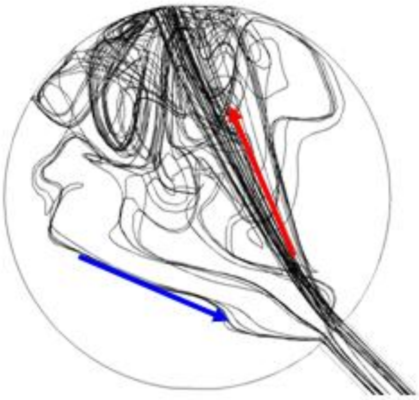

Figure 50: Flow structure from tube into tank (Budihardjo, 2005)

4.2.1. System Efficiency

The efficiency of a system indicates how successful the system utilizes the energy it receives. The efficiency of the LP SWH system dependants on the component properties. The biggest challenge in any hot water system is to prevent heat loss either through conduction, convection or radiation.

$$\eta = \frac{Energy\ Absorbed}{Energy\ Received} = \frac{Q_u}{GA} \qquad (4.\ 2)$$

Where Q_u, G and A represents energy absorbed, total solar radiation on collector and collector area respectively. Furthermore, the energy absorbed can be described as follows, see Equation 4.3-4.4 and Figure 51:

$$Q_{u-collector} = dE_{system} + Q_{loss-tank} \qquad (4.\ 3)$$

$$Q_{u-collector} = mC_p\ T_2 - T_1\ + \int_{t1}^{t2} U_{loss-tank}A_{tank}\ T - T_a \qquad (4.\ 4)$$

In the following sections, the thermal loss of the tubes and tank will be investigated.

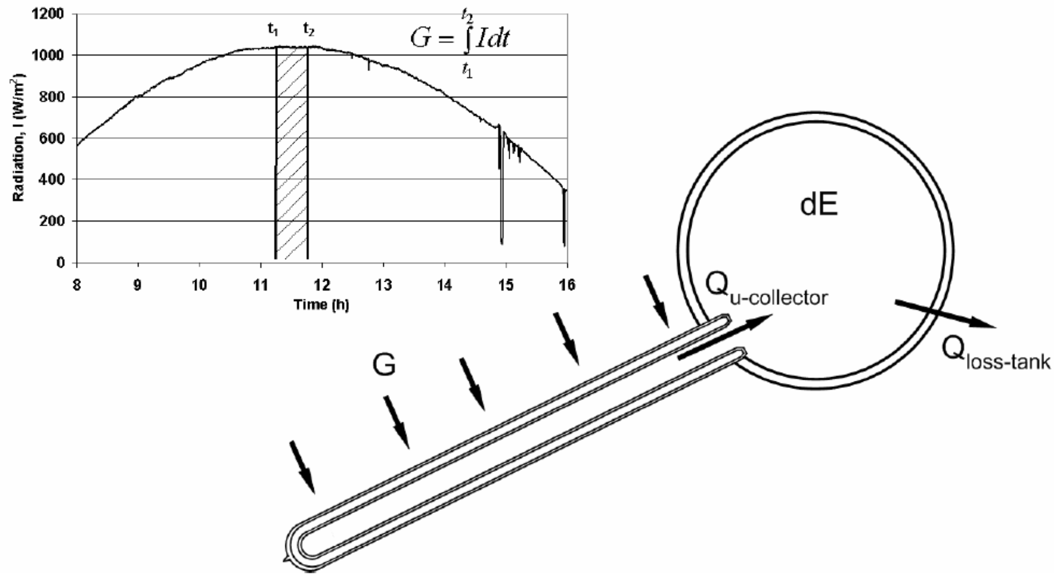

Figure 51: Energy absorbed and loss in LP SWH system (Budihardjo, 2005)

4.2.2. Energy Loss (Vacuum Tubes)

One of the biggest advantages of using vacuum tubes, as to flat plate collectors, apart from tracking the sun passively due to its geometry, is the fact that the tubes have a vacuum between the outer and inner cylinder. Heat can only be transferred in a vacuum by means of radiation. This gradually reduces heat loss by the tubes. Heat is lost through conduction by the tube joints at the tube opening (which is inside the storage tank, thus heat is lost to the water inside the tank. Another small amount of heat is conducted away from the collector by the tube support. The outer tubes lose heat by means of convection to the atmosphere. The water inside the tubes serves as "cooling medium", heat is transferred to the water by means of natural convection, cooling the inner tube. Figure 52 illustrates the different types of heat loss within the tube.

- **Conduction through tube support**

$$Q_{cond} = \frac{k_{ts}A_{c-ts}\ T_{abs} - T_g}{L_{ts}} \tag{4. 5}$$

Where k_{ts}, A_{c-ts} and L_{ts} represents thermal conductivity of tube support, tube support area and length of tube support respectively. Where T_{abs} and T_g represents the temperature of the absorber tube and outer tube respectively.

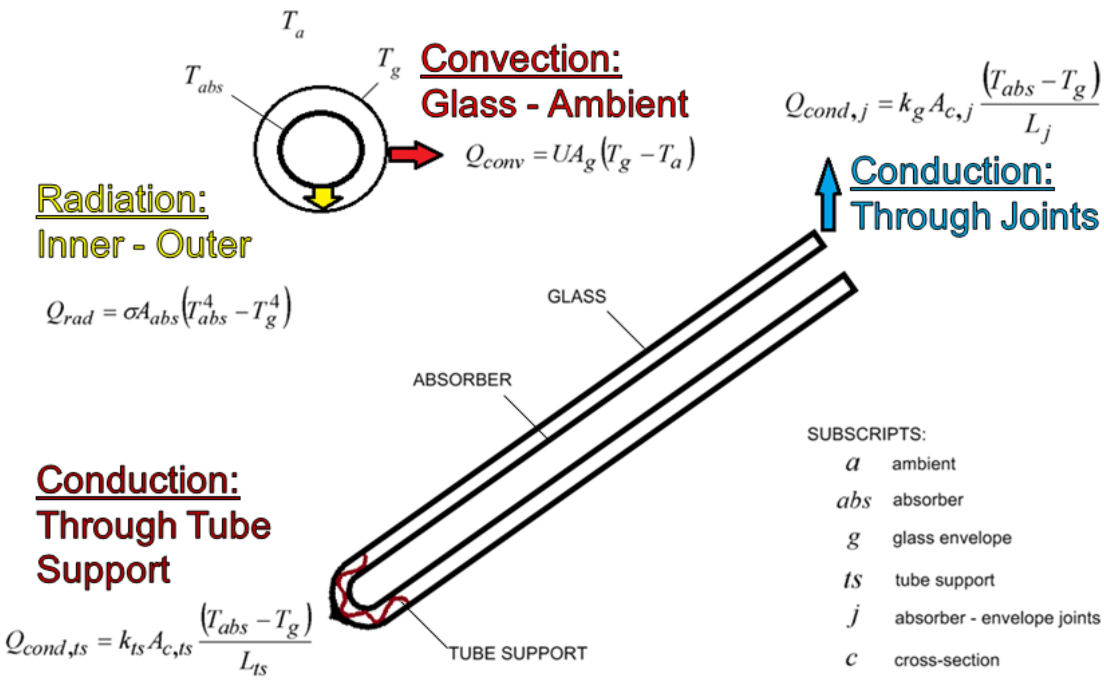

Figure 52: Energy loss from vacuum tubes

- **Conduction through tube joints**

$$Q_{cond} = \frac{k_g A_{c-j}\ T_{abs} - T_g}{L_j} \tag{4. 6}$$

Where k_g, A_{c-j} and L_j represents thermal conductivity of the tube glass, tube joint area and length of tube joint respectively. Where T_{abs} and T_g represents the temperature of the absorber tube and outer tube respectively.

- **Convection through outer tube**

$$Q_{conv} = UA_g\ T_{abs} - T_g \tag{4. 7}$$

Where U and A_g represents the thermal loss coefficient of the tube and tube area respectively. Where T_{abs} and T_g represents the temperature of the absorber tube and outer tube respectively.

- **Radiation between inner and outer tube**

$$Q_{rad} = \sigma A_{abs}\ T_{abs}^4 - T_g^4 \tag{4. 8}$$

Where σ and A_{abs} represents the Stefan-Boltzmann constant and inner tube area respectively. Where T_{abs} and T_g represents the temperature of the absorber tube and outer tube respectively. The outer tube furthermore radiate heat out to the atmosphere.

4.2.3. Energy Loss (Tank)

The storage tank stores the hot water for utilization. The higher the water temperature compared to the ambient temperature, the higher the heat loss rate. A hot water storage tank consists out of an inner layer (where hot water is stored), a very thick insulation layer, and the outer casing. The thick insulation reduces the amount of heat loss to the environment. The efficiency of a storage tank depends on how successful the insulation layer prevents heat loss. Once heat is conducted through the insulation layer to the outer casing, heat is further distributed to the environment through convection and radiation.

$$Q_{loss-tank} = \int_{t1}^{t2} U_{loss-tank} A_{tank}\ T - T_a \tag{4. 9}$$

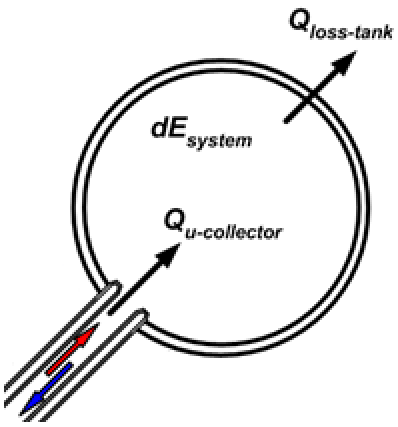

Figure 53: Heat loss through storage tank (Budihardjo, 2005)

5. EXPERIMENTAL SETUP

5.1. Aim of Experiments

The aim of the following experiments is to validate the literature study done in the previous sections. The results would be used in simulation programs (TRNSYS and MATLAB) to simulate the LP SWH with accurate component attributes to be as precise as possible, thus reducing the probability of uncertainty in system performance. The main aim of the experiments is to determine the system's performance over a period of time; the system's performance would then be compared to the simulation model results under similar weather conditions. These results would be compared between the experiment and simulation and a valuable conclusion can then be made with regards to system optimization and areas for improvement, thus design considerations to take into account.

5.2. Measurements Required

The following tests are required in order to successfully simulate the system in MATLAB or TRNSYS.

TEST1: Determine heat loss coefficient of storage tank

TEST2: Determine coefficients (a, b) for collector efficiency formula

TEST3: Determine optical efficiency of the collector over solar noon

TEST4: Determine system performance over given time frame

5.2.1. TEST1: Heat Loss Coefficient of Tank (V=100L)

The following formula (correlation specified in the ISO 9459-2 (1995)) is used to determine the heat loss coefficient of a tank.

$$UA = \frac{\rho C_p V}{\Delta t} \ln \frac{T_i - T_a}{T_f - T_a} \tag{5.1}$$

Where ρ and C_p represents the density and capicity of heat for the water and storage tank respectivily. The volume of the tank filled with water is represented by V. The average initial, final and ambient temperatures over a period of time are represented by T_i, T_f and T_a respectively with time as t. The storage tank is filled with water and heated with an element to a desired temperature. The tank is left to cool down over a period of time and tube holes closed-up with insulation material (stoppers). The logged data is used in the above mentioned formula to determine the heat loss coefficient. The following section shows these results, and the average heat loss coeffient for the tank calculated to be U=0.70 W/m^2.

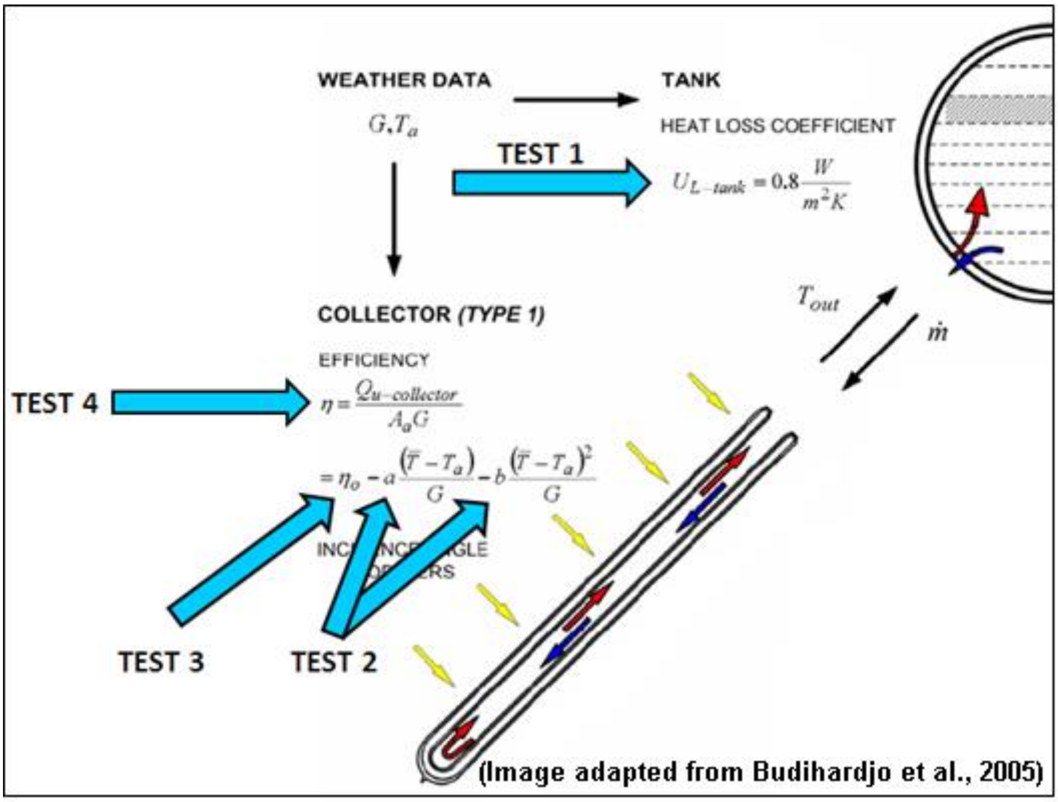

Figure 54: Tests required on LP SWH system for simulation

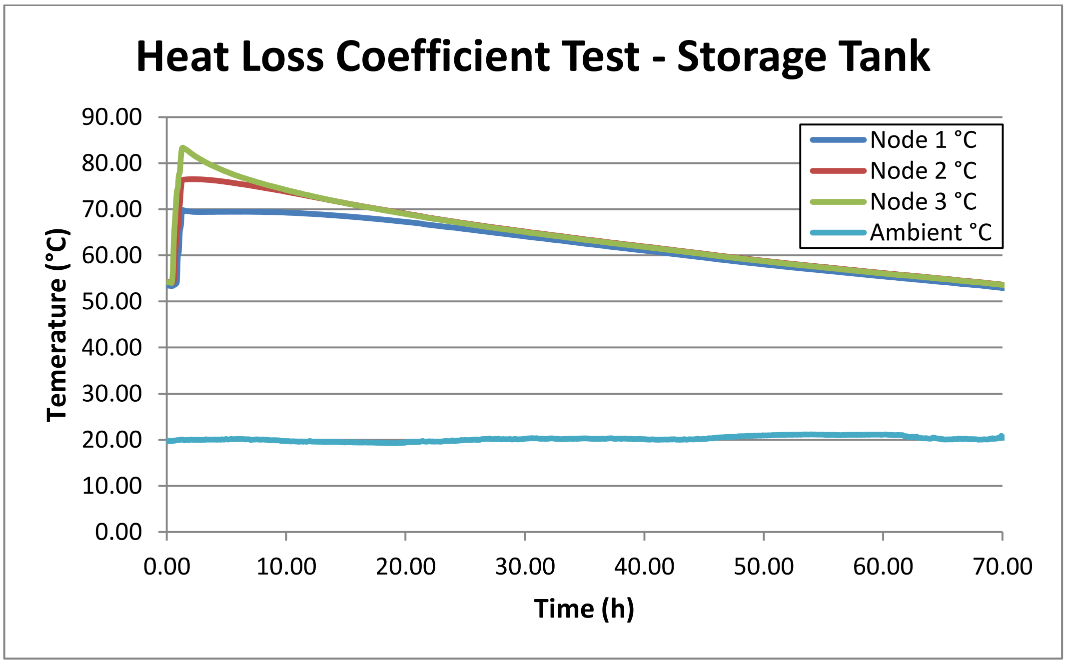

Figure 55: TEST1: Experimental results (Over 70 hours)

Time Minutes	Node 1 °C	Node 2 °C	Node 3 °C	Average °C	Ambient °C
0	53.45	54.21	54.18	53.95	19.66
5	53.44	54.22	54.14	53.93	19.67
10	53.42	54.20	54.13	53.92	19.76
15	53.40	54.15	54.10	53.88	19.74
20	53.37	54.13	54.07	53.86	19.69
25	53.35	54.10	54.06	53.84	19.72
30	53.40	54.10	56.46	54.65	19.80
35	53.53	54.56	63.46	57.18	19.78
40	53.67	58.88	67.04	59.86	19.82
45	53.80	62.31	70.56	62.22	19.87
50	54.18	64.96	73.80	64.31	19.90
55	59.82	65.83	74.68	66.78	19.93
60	60.78	69.51	77.37	69.22	19.93
65	65.30	70.97	78.06	71.44	19.97
70	66.34	74.23	81.03	73.87	20.02
75	69.24	76.04	83.10	76.13	20.06
80	69.78	76.34	83.37	76.50	20.03
85	69.75	76.42	83.22	76.46	19.91
90	69.69	76.44	83.09	76.41	19.88
95	69.64	76.46	82.99	76.36	19.95
100	69.60	76.48	82.87	76.32	19.95
105	69.56	76.49	82.69	76.25	19.97
110	69.54	76.50	82.53	76.19	19.93
115	69.52	76.51	82.37	76.13	19.95
120	**69.49**	**76.51**	**82.19**	**76.06**	**20.04**

Table 10: TEST1: Experimental logged results (First 2 hours interval)

Hours	**Duration**	**Ta**	**Ti**	**Tf**	**UA**	**U**
2-10	8 hours	20	76.06	72.42	0.99	0.64
10-20	10 hours	20	72.42	68.43	1.17	0.75
20-30	10 hours	20	68.43	64.78	1.16	0.74
30-40	10 hours	20	64.78	61.60	1.09	0.70
40-50	10 hours	20	61.60	58.54	1.13	0.72
50-60	10 hours	20	58.54	55.89	1.05	0.67
60-70	10 hours	20	55.89	53.39	1.06	0.68
Average Value		**U=**	**0.70**	**W/m^2**		

Table 11: TEST1: Experimental logged results calculations

Figure 56: TEST1 - Apparatus: Element (Top), Tank with stoppers (Middle) and Laptop logging data (Bottom)

5.2.2. TEST2: Heat Loss Coefficient of Vacuum Tubes (ID=42, L=1.8m)

As in TEST1 for the storage tank, the same method is applied to determine the heat loss coefficient for the tubes (Figure 57). Another important parameter that is calculated from this test, is the coefficients a and b that plays a vital role in determining the collector efficiency, see equations below.

$$U = \frac{mC_p}{A_a}\frac{T_i - T_f}{T_m - T_a} \qquad (5.210)$$

Where m, C_p and A_a represents the mass of the water inside the tube, the specific heat of the water and area of the inner tube respectively. The subscripts of the temperatures indicate i-initial, f-final, m-mean and a-ambient temperatures.

$$\eta = \eta_o - a\left(\frac{T_c - T_a}{G}\right) - b\left(\frac{T_c - T_a}{G}\right)^2 \qquad (5.3)$$

Where η , η_o and G represents the collector efficiency, optical efficiency and total solar radiation on tilted collector respectively. The temperatures with subscripts c and a represents the average water temperature inside the collector tubes and ambient temperature respectively. In order to determine a and b linear regression (Figure 58) is applied to a series of tube heat loss tests with the same environmental conditions, see.

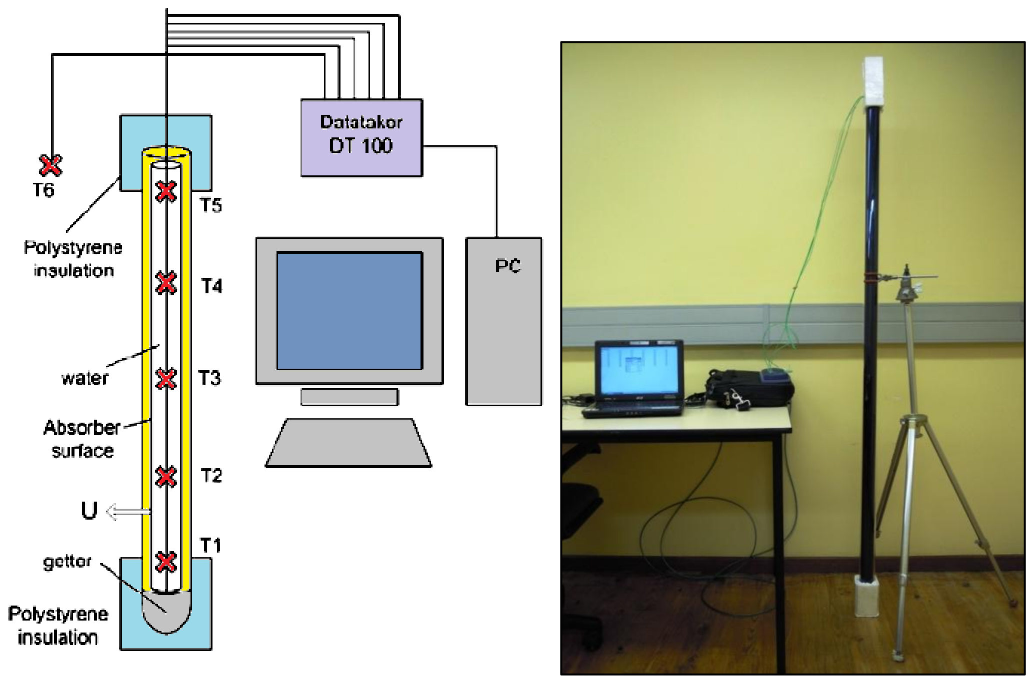

Figure 57: TEST2: LEFT: Experimental setup schematic (Budihardjo, 2005)
RIGHT: Experimental setup - Clearly showing end caps insulated

The apparatus should be set up as in Figure 57. Attach five thermocouples equally spaced on the rod. Insert the rod in the tube which is vertically mounted with a stand. Ensure that the end and opening of the tube is well insulated with the polystyrene end caps. When the apparatus is set up, fill the tube with boiling water and start logging the temperatures. The duration of the test is 17 hours.

The test results of each day is saved in an excel spread sheet format. Calculations are done on these results to obtain explanatory graphs and values on the tube. The following graph (Figure 58), shows the average temperature of the water in the tube during the test duration.

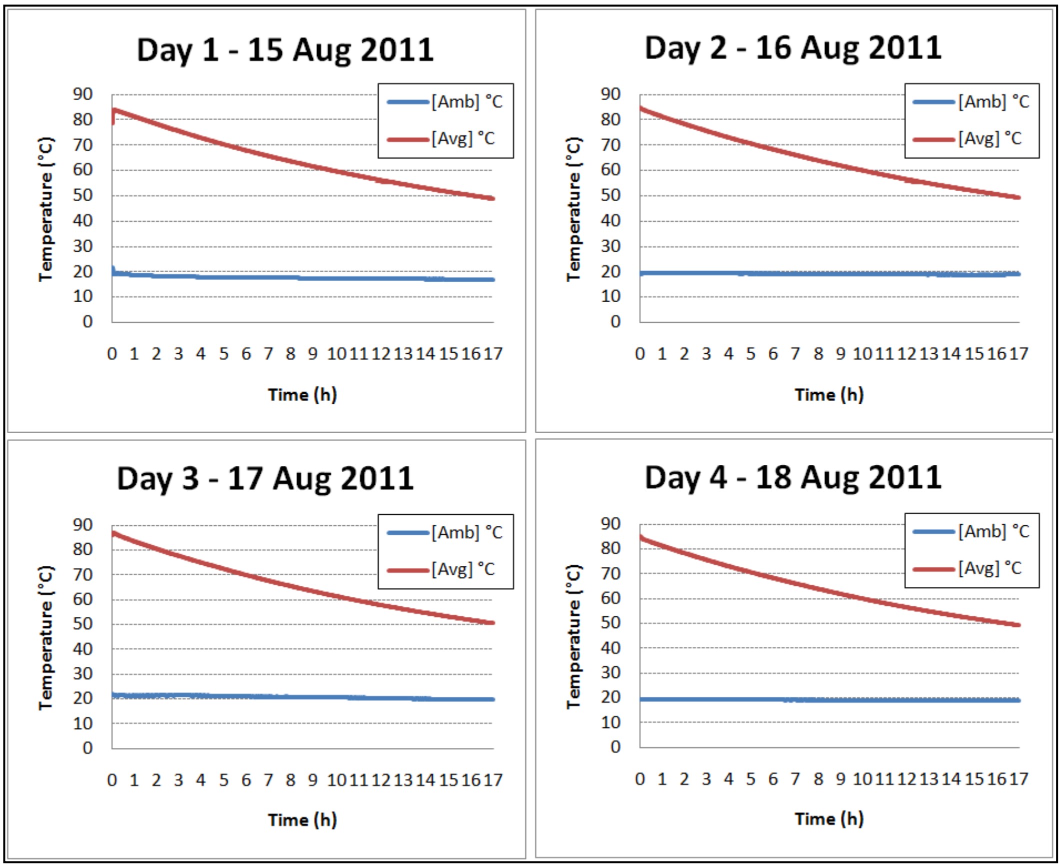

Figure 58: Average water temperature in tube (1 day = 1 test)

A series of six tests were conducted including a repeatability test to check for continuity. The results of the six tests were used in the linear regression to determine the coefficients (*a* and *b*) in the efficiency formula. The following section includes the test results (Appendix A) as well as the values that were obtained from calculations, shown in Figures. Tests conducted on tubes with 42mm inner diameter, length of 1.8m and center distance between adjacent tubes are 90mm.

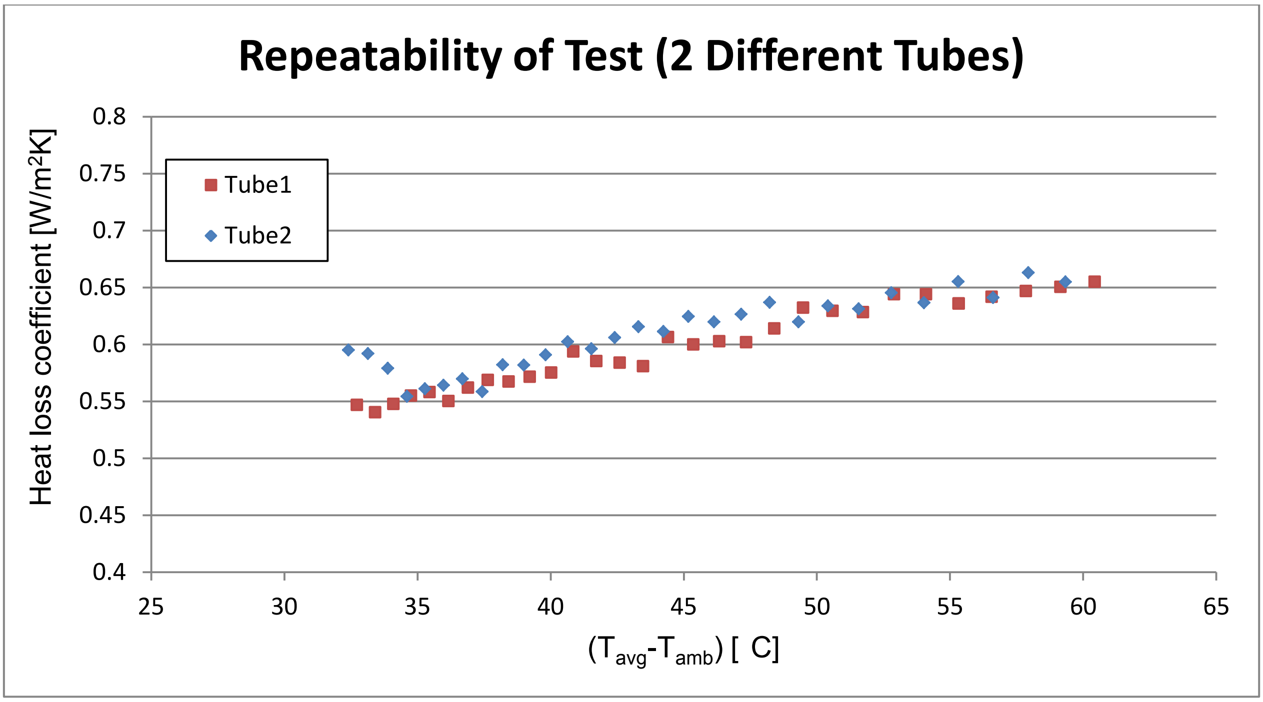

Figure 59: Repeatability test of TEST2 - Two different tubes

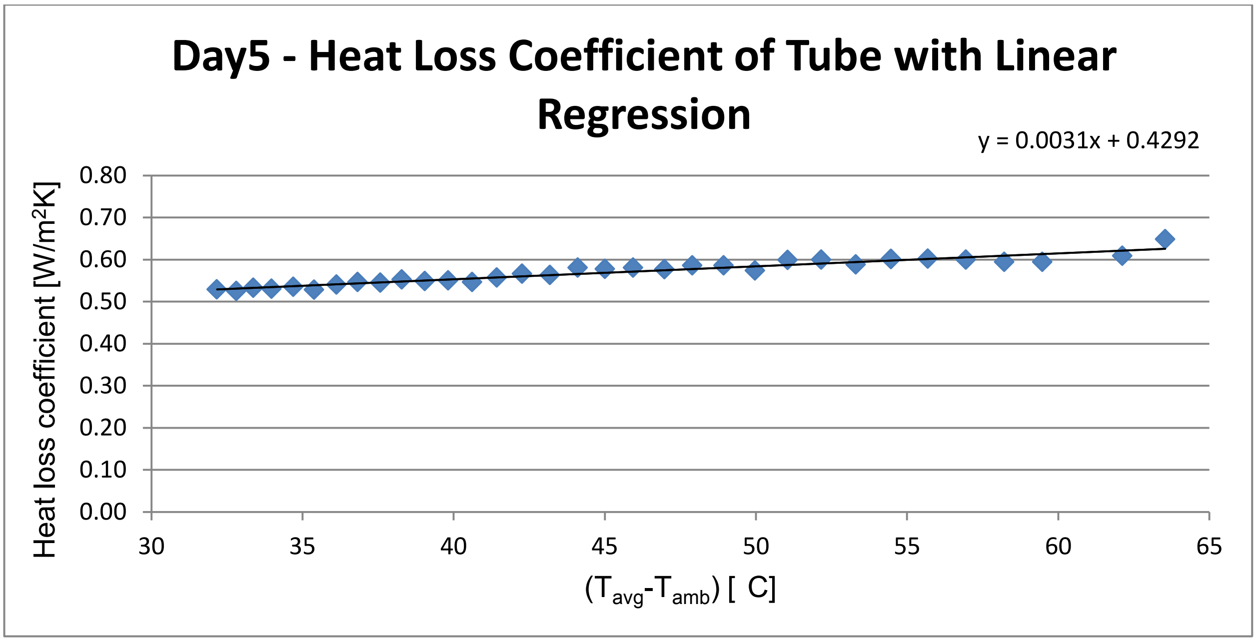

Figure 60: TEST2: Day5 - Linear regression (a=0.6292, b=0.0045)

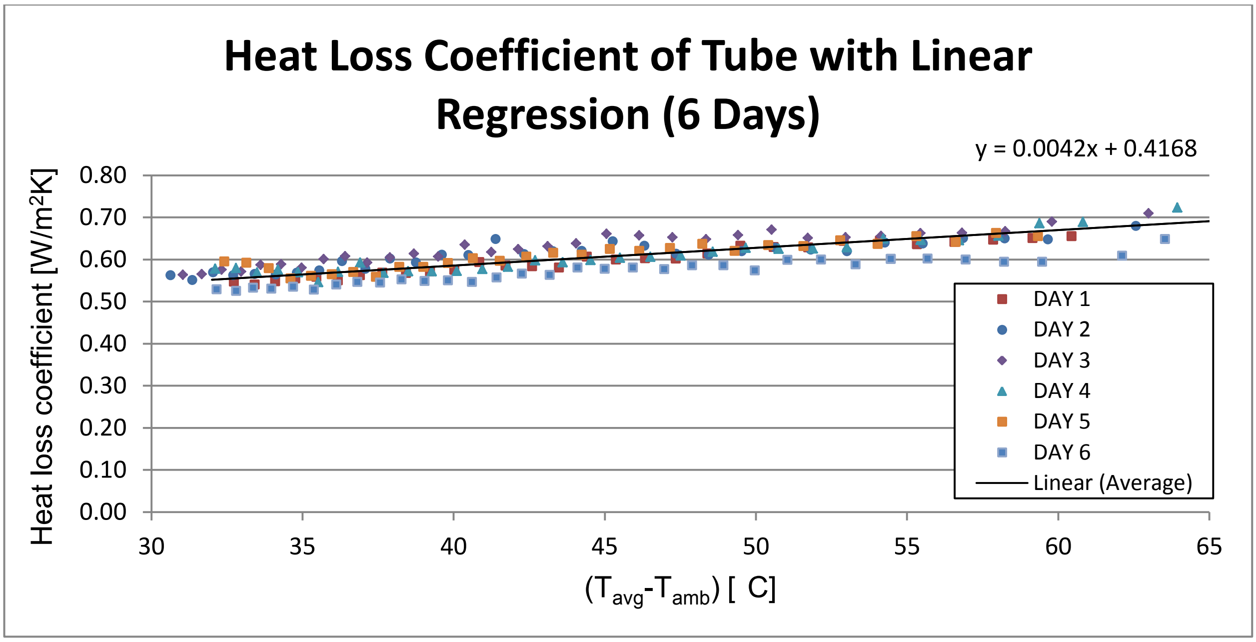

Figure 61: TEST2: Linear regression of 6 Tests (a=0.6110, b=0.0062)

$$a = 0.4168 \frac{\pi.42}{90} = 0.6110 \tag{5.4}$$

$$b = 0.0042 \frac{\pi.42}{90} = 0.0062 \tag{5.5}$$

5.2.3. TEST3: Optical Efficiency of Collector

The optical efficiency of the collector is determined by an outdoor test. The test is over a period of 30min during solar noon. The total solar radiation and initial and final tank temperature is measured during this period. The results from TEST1, tank heat loss coefficient, are used in the following equation together with the measured results.

$$\eta_o = \frac{Q_u}{GA} = \frac{mC_p\ T_2 - T_1\ + {}_{t1}^{t2} U_{loss-tank} A_{tank}\ T - T_a}{GA} \tag{5.6}$$

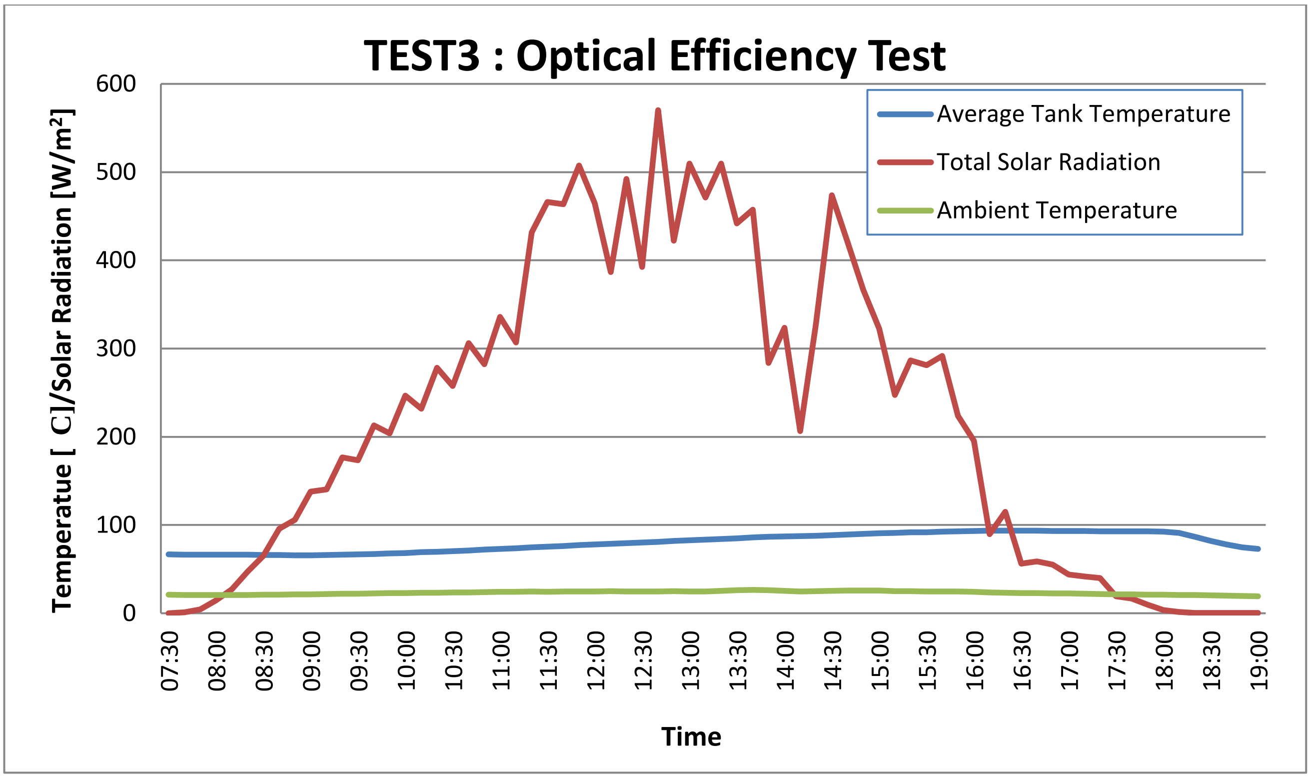

Figure 62: TEST3: Optical efficiency data set (19 July 2012 - Cape Town)

TIME	T1	T2	T3	T4	T5	T_Avg	Solar (G)	T_Amb
11:30	38.53	35.76	38.37	44.66	36.39	38.742	136.78	14.32
11:40	38.86	36.04	38.78	45.44	36.87	39.198	358.35	14.73
11:50	39.27	36.43	39.21	45.62	37.36	39.578	326.93	15.40
12:00	39.86	37.00	39.86	45.64	37.82	40.036	410.29	16.06

Table 12: TEST3: Solar noon data set (2 July 2012 - Cape Town) $\eta_o = 0.5410$

TIME	T1	T2	T3	T4	T5	T_Avg	Solar (G)	T_Amb
11:30	57.46	54.73	57.50	62.48	54.59	57.352	445.10	15.13
11:40	58.28	55.57	58.39	63.22	55.42	58.176	453.10	15.17
11:50	59.15	56.29	59.11	64.19	56.14	58.976	460.05	15.32
12:00	60.01	57.22	59.93	65.03	56.9	59.818	467.20	15.45

Table 13: TEST3: Solar noon data set (5 July 2012 - Cape Town) $\eta_o = 0.5437$

TIME	T1	T2	T3	T4	T5	T_Avg	Solar (G)	T_Amb
11:30	71.51	73.70	76.15	81.69	73.71	75.352	466.00	24.50
11:40	72.33	74.55	77.16	82.44	74.64	76.224	463.50	24.72
11:50	72.96	75.46	78.12	83.64	75.62	77.160	507.33	24.74
12:00	73.84	76.42	78.84	84.79	76.68	78.114	464.68	24.84

Table 14: TEST3: Solar noon data set (19 July 2012 - Cape Town) $\eta_o = 0.5504$

5.2.4. TEST4: Thermal Performance of System

This test indicates how well the system performs at a given geographical location, under various weather conditions, for a specific time of the year (winter/summer) with a given amount of solar radiation received. The location for this test was on a roof at the University of Cape Town (GPS coordinates 33°57’27°S 18°27’38°E). Two different tests were conducted to determine the thermal performance of the system. The first test results were not ideal, thus a second test with improvements were conducted. The following section explains the methodology followed for conducting the experiments, lessons learnt and improvements made.

The thermal performance of the system is measured by placing thermocouples inside the storage tank at various height levels. The temperatures are then logged together with a total solar radiation reading. To ensure continuous results, the ideal test conditions would be to have the water temperature of the tank at ambient temperature at the beginning of each day, before energy is collected from the collector. Thus the total energy collected by the system can be determined from incorporating results from TEST1-3, the daily solar radiation profile and thermocouple readings.

Test results from TEST1 indicate that the storage tank is well insulated and that the energy gained throughout the day from the collector, will not be lost throughout the night purely by convection/radiation loss. Due to constraints the hot water could not be recycled back into the tank to ensure that enough thermal energy is removed from the system. The heat loss was thus induced by circulating the hot water through a heat exchanger at night time.

The induced circulation was achieved by a circulating pump and control system. A PV panel is used to charge a battery during the day (powering the circulation pump by night). A control system measures the voltage over the PV panel during the day and when the voltage drop to a certain set value, a timer is activated, activating the circulation pump for a set time. Water is circulated through the heat exchanger and cold water return to the storage tank.

- **TEST4-A: October 2011**

The heat exchanger used for this test was a copper tube creating a loop by leaving the bottom of the tank and entering the side top of the tank (Figure 63). The tubing is 22mm in diameter. The control system was made from typical power electronic components (Figure 64) such as op-amps, relays, capacitors and resistors. The control system built on a circuit board was tested in a lab before putting it in the field to ensure all components where functioning correctly. The data logged for this period was in October 2011. Test results and interpretation is showed and discussed in the following paragraph. Although the results from TEST4-A were undesirable, it is included as valuable conclusions were made that inspired improvements amended on the system and more desirable data results were achieved TEST4-B.

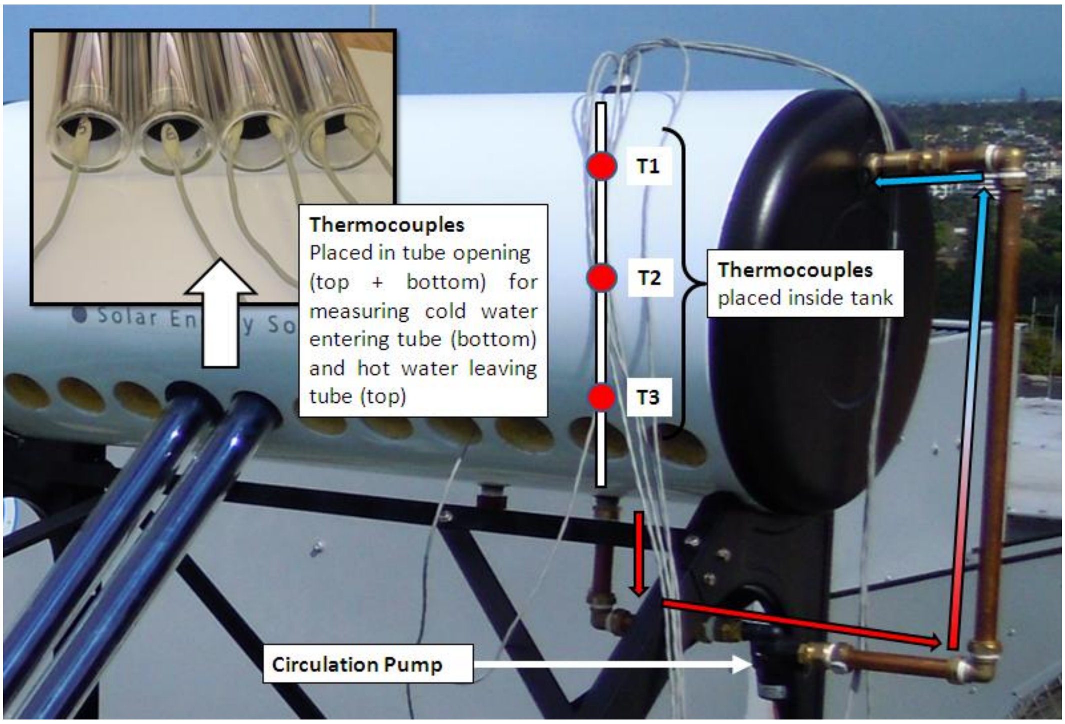

Figure 63: Heat exchanger and thermocouple positions for TEST4-A

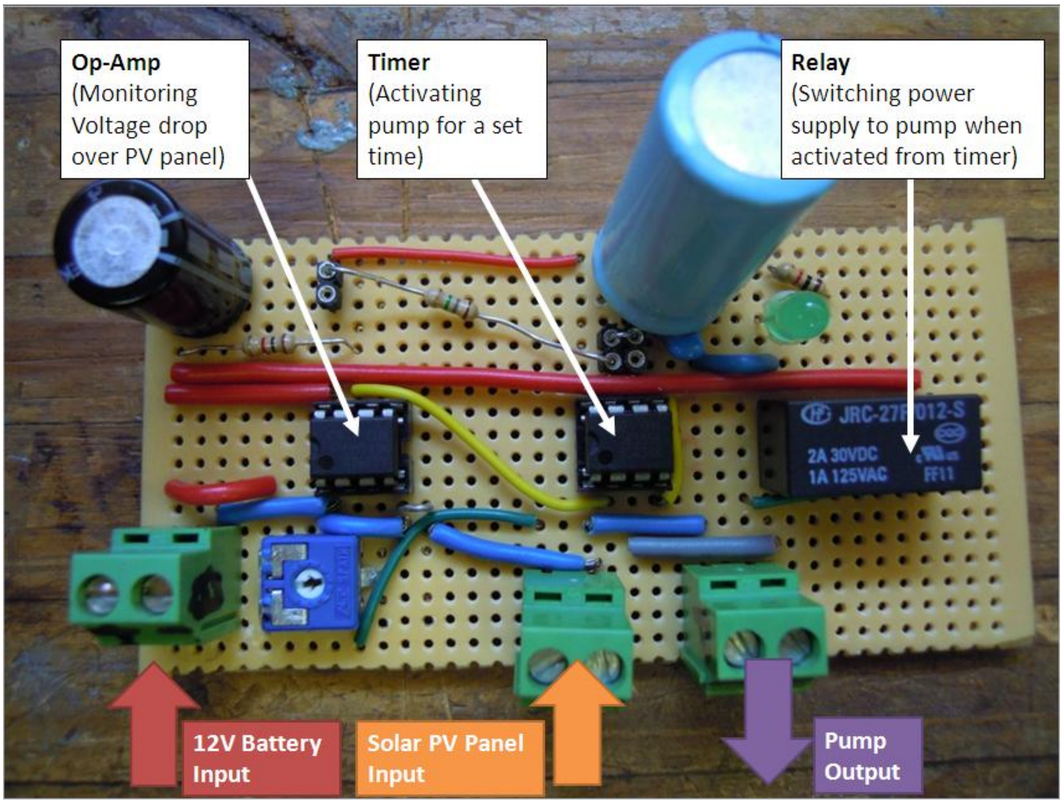

Figure 64: Control system for TEST4-A

A total of nine thermocouples were placed inside the LP SWH system. Three thermocouples were placed in the tank at three elevated levels, at the bottom of the tank, the middle and in the top of the tank. An average of these three thermocouple readings would indicate the thermal energy gain or loss of the system in the appropriate formula. The other six thermocouples were placed inside the tubes as indicated in Figure 63 to measure the cold water entering the tubes, and hot water leaving the tubes. During installation five of the thermocouples were lost due to poor quality. The following figure shows the results obtained from the first attempt. Two thermocouples at the tube openings (hot water leaving – top) and two tank thermocouples (top and middle) were working. These thermocouple readings supplied enough information to make valuable interpretations and improvements on the system.

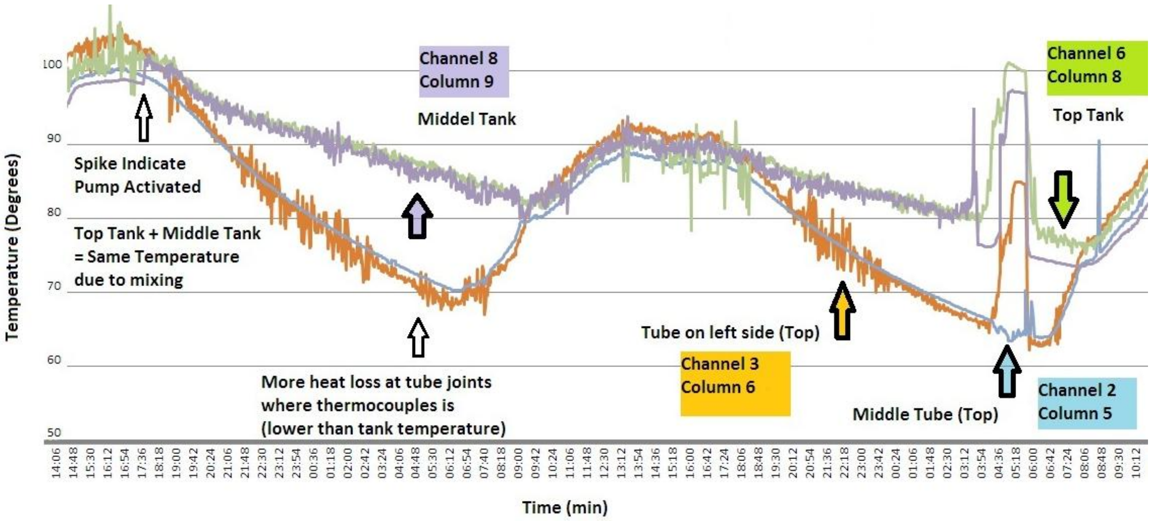

Figure 65: Thermocouple reading analysis TEST4-A

From the above figure, it is clear that the sampling time was set at an interval too high, thus creating irregularity/spiking in the graph. The second observation is that the amount of cooling from the circulation pump and heat exchanger (seen in Figure 63) is not sufficient. The pump was activated at about 17:15 (when the voltage dropped over the PV panel), and almost no cooling is observed, just mixing inside the tank. Furthermore, the overall amount heat loss is not sufficient for the next day to ensure that the system will not reach high temperatures (boiling) which cause turbulence and promote energy loss. It would be ideal to operate the system in temperatures ranging from ambient to 60-70 degrees, allowing heating to reach 80 degrees maximum, thus having a cooling temperature drop of about 20 degrees.

Conclusion:

The sampling rate should be changed to a lower sampling rate. The heat exchanger has to be improved to ensure for better cooling. No thermocouples are required in the tubes; increase the number of thermocouples in the tank for better variation in readings. Improve the control system for better reliability.

- **TEST4-B: July 2012**

In this test, the results of TEST4-A have been considered and improvements on the system were made. All the thermocouples and electrical interface components have been replaced with off-the-shelve components. Thus no components have been used to build the desired control system on a circuit board. The schematic of the wiring system can be seen in Appendix-B, and implementation in Figure 66 below. Thus clearly showing the improvements on the electrical interface made. Furthermore the heat exchanger has been improved by using the radiator of an automobile, the improved surface area with fins and tubes allow for better heat loss. The radiator has been placed in such a way that the extraction fan of the building blow on the radiator, inducing forced convection and thus improving the efficiency of the radiator. The five thermocouples have been placed inside the tank at various levels, equally spaced. The following figure shows the schematic of the improved system. The test results are showed and discussed in the following paragraph.

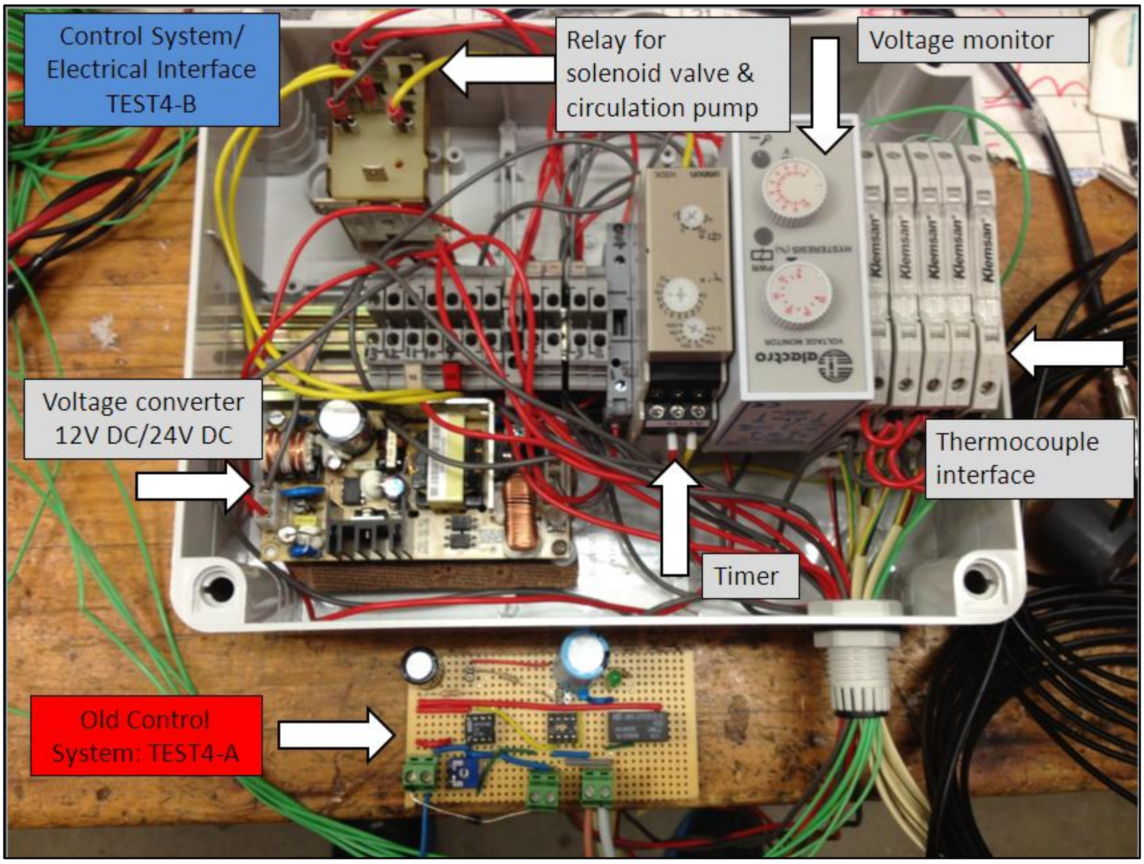

Figure 66: Electrical interface and control system TEST4-B

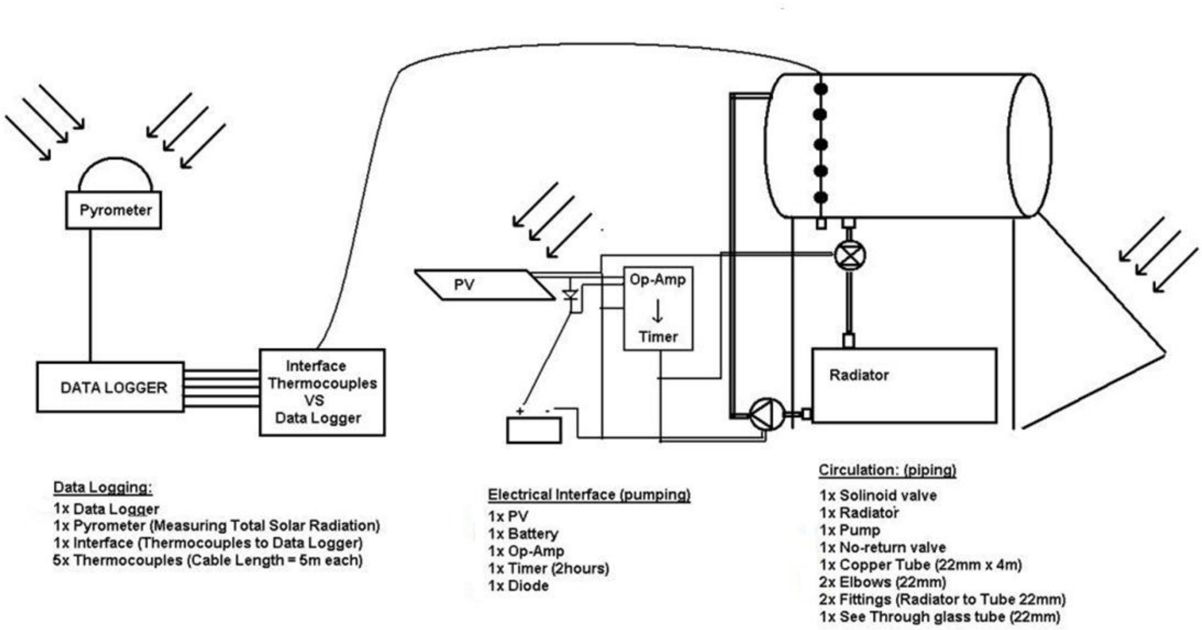

Figure 67: Improved system with radiator and electrical interface TEST4-B

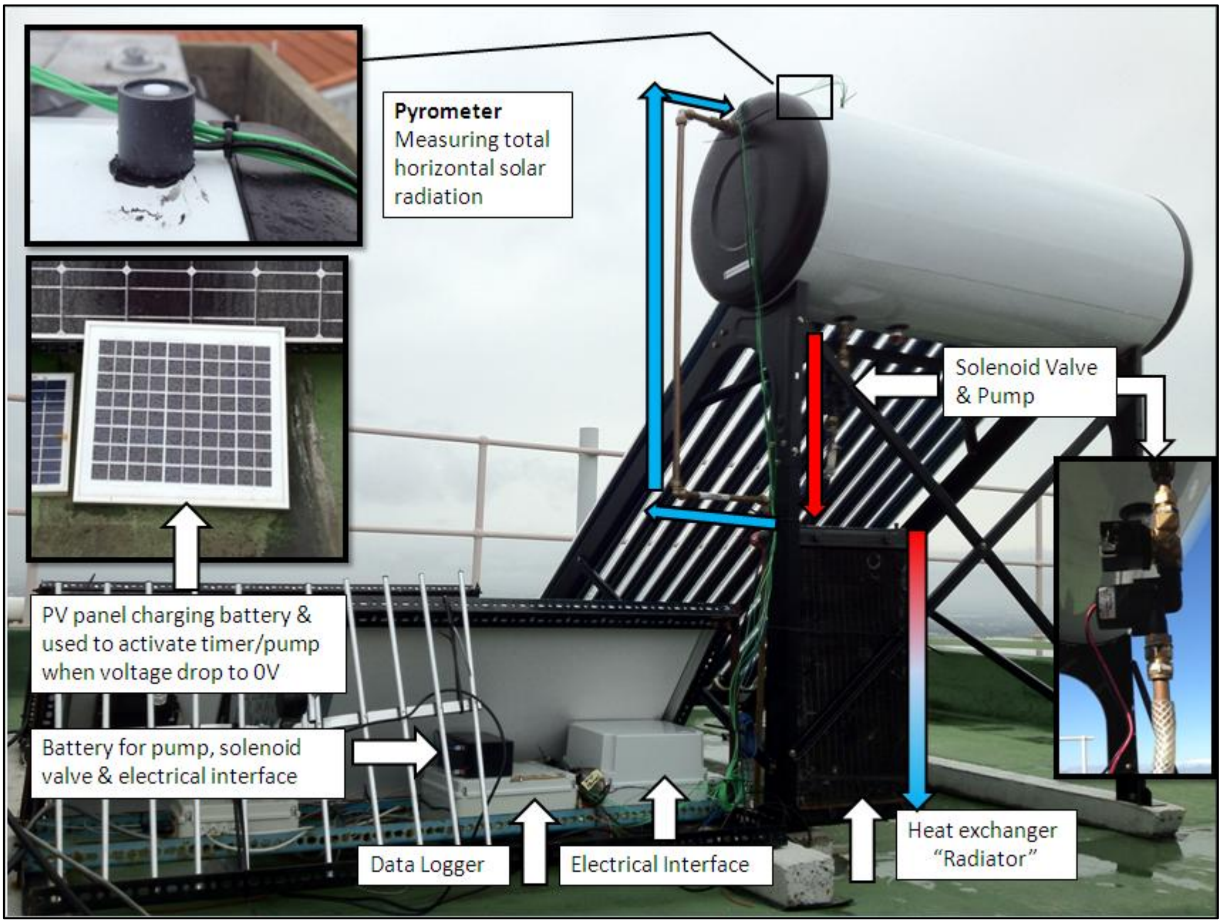

Figure 68: TEST4-B Experimental setup

Due to the improvements made on the system, more desirable results were obtained. The electrical interface and control system delivered results that were accurate and reliable, the control system operated in an effective manner to ensure for efficient cooling. An average cooling of 20 degrees per cooling cycle was observed. The circulating pump was activated for 60 minutes for one cooling cycle. A further 5 degree drop in temperature was observed overnight. A complete set of experimental data for the month of July 2012 was obtained. Calculations and a comparison between the system performance and simulation model will be based on these results. See the Appendix for more experimental results and Section 7 for interpretation of these results.

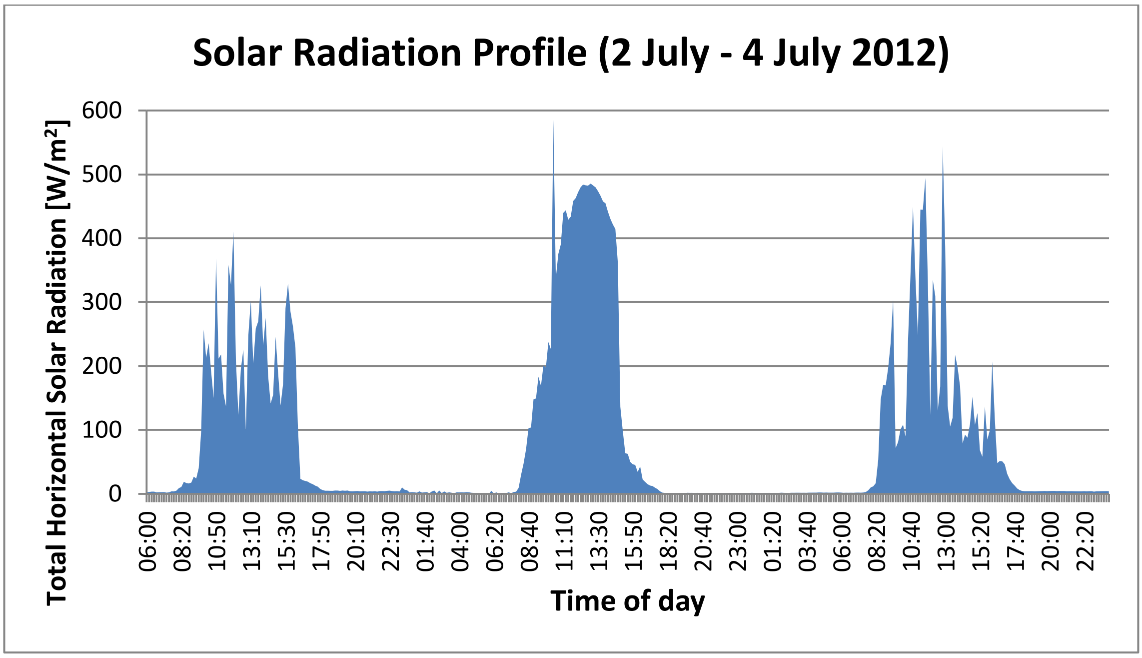

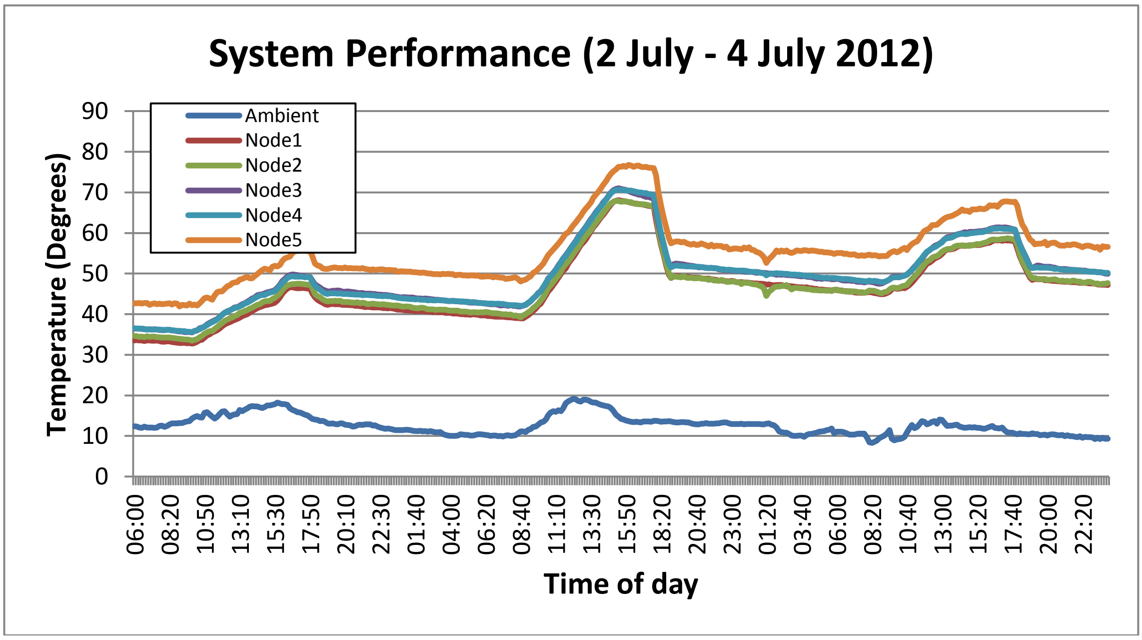

Figure 69: Solar radiation profile (Top) and system performance (Bottom)

6. SIMULATIONS

A simulation model has been developed for LP SWHs. This simulation model is used to simulate the effects of various tilt angles, length-radius ratios, effect of water temperature and solar radiation received. The simulation model is based on the theory covered in the above sections and results obtained are valuable for practical considerations for LP SWH design and installations. The flow patterns in a thermosiphoning tube has been investigated by Budihardjo in 2005 and results obtained indicate that a tube with uniform top heating induce flow as a single stream to the bottom of the tube and back to the top in a loop. Larger heat fluxes flow may induce transitional or turbulent flow, but the counter-flowing stream characteristics still hold (Schmid *et al.*, 1986).

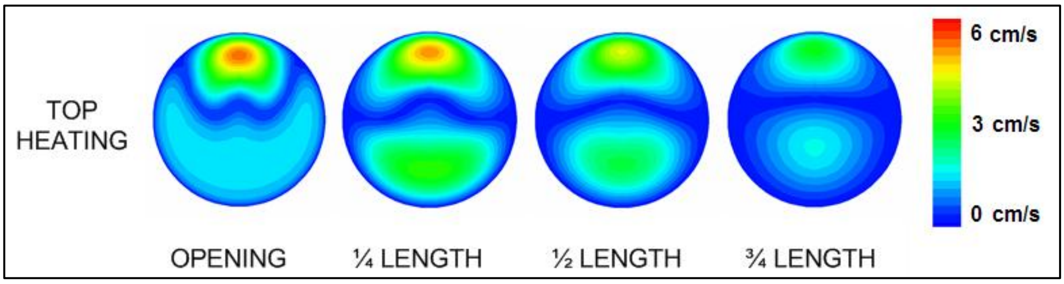

Figure 70: Velocity contours at various axial locations, Tube length = 1420 mm, diameter = 34 mm, tilt angle = 45°, heat input 75 W (Budihardjo, 2005)

- **Tilt Angle**

The tilt angle of a collector plays a very important role in solar collectors. Literature shows that extensive research has been done to determine the optimal tilt angle for solar collectors such as flat-plate collectors. However, collectors such as the LP SWH systems consists out of tubes, tracking the sun passively due to the tube geometry, thus having a higher peak solar window. It is favorable for any collector to intercept the direct radiation of the sun perpendicular to the absorber surface of the collector; this reduces the amount of rays being deflected away from the surface, losing in effect useable energy from the sun. A transverse and longitudinal incidence angle modification is thus desired for the tube geometry of the LP SWH collector (Zambolin *et al* 2010). A simulation model was created in TRNSYS to determine the optimal tilt angles for a collector. It was found that the tilt angle of 45° was indeed not the optimal tilt angle to use throughout South Africa. Four geographical locations where chosen for the simulation for comparison. These cities include Cape Town, Johannesburg, Durban and Upington. The tilt angle that provides maximum energy collected (Figure 71) on a tilted surface throughout the year is a tilt angle equal to the site latitude.

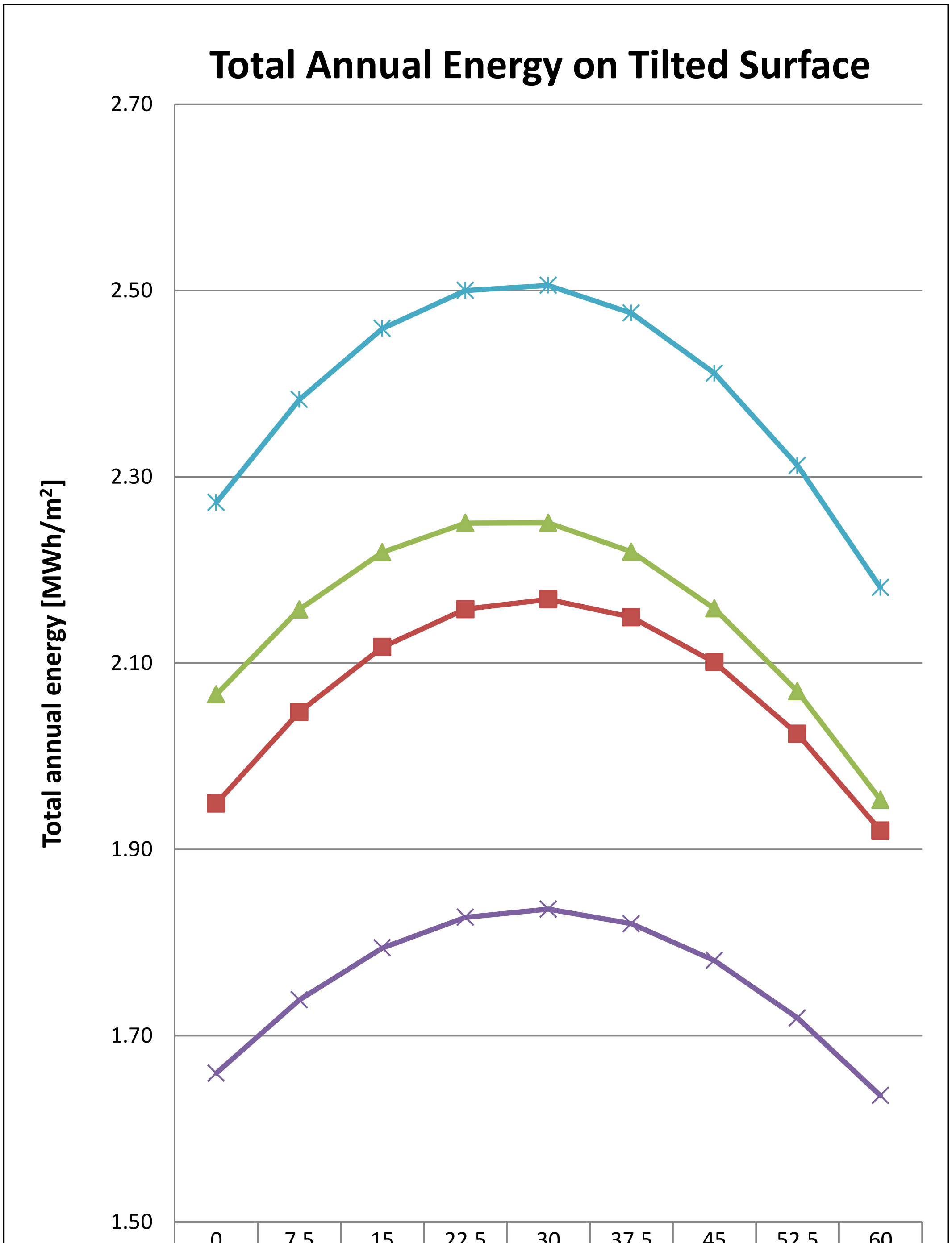

	0	7.5	15	22.5	30	37.5	45	52.5	60
CT	1.95	2.05	2.12	2.16	2.17	2.15	2.10	2.02	1.92
JHB	2.07	2.16	2.22	2.25	2.25	2.22	2.16	2.07	1.95
DBN	1.66	1.74	1.79	1.83	1.84	1.82	1.78	1.72	1.64
UPT	2.27	2.38	2.46	2.50	2.51	2.48	2.41	2.31	2.18

Figure 71: Total annual energy on a tilted surface

This theory is a well-known fact in the solar industry and considered by many solar collector installers and manufactures. However the consumer might not benefit as much from this tilt angle in the winter seasons when the demand for hot water increase. Thus the tilt angle is adjusted to accommodate the need of the consumer for winter seasons, it is found that a tilt angle approximately 15-20^0 higher than the site latitude would be more beneficial, this corresponds with the sun path during winter seasons. It is clear that the tilt angle of the collector should be adjusted seasonally to maximized energy collection (Figure 72). To optimize the tilt angle for the system based on the maximum amount of solar energy it receives, at least two tilt angles are required for the system. It is clear that different tilt angles are required for both summer and winter seasons. The following table shows the increase in energy by adjusting the tilt angle to accommodate the sun.

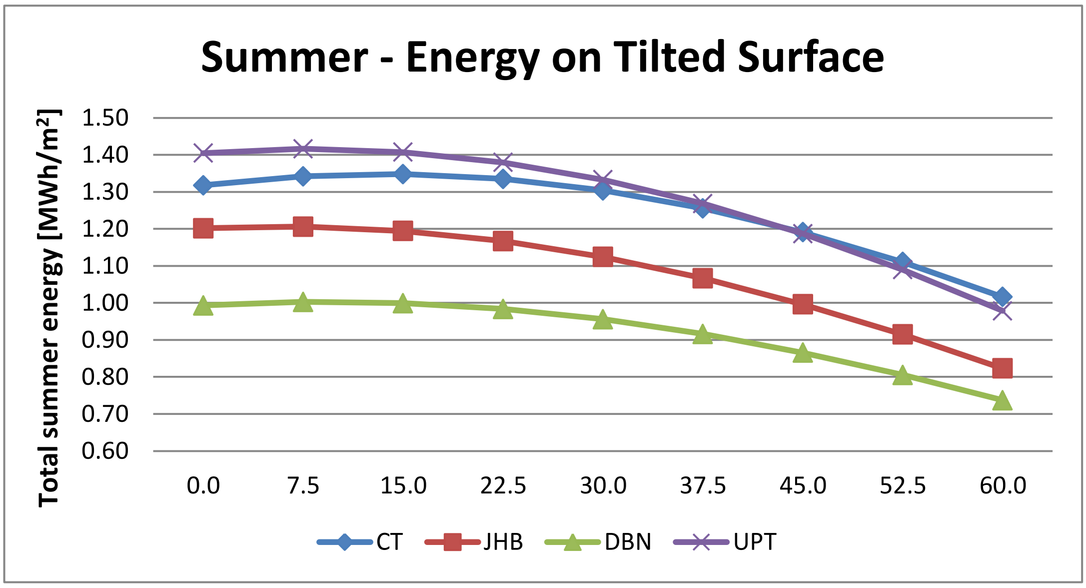

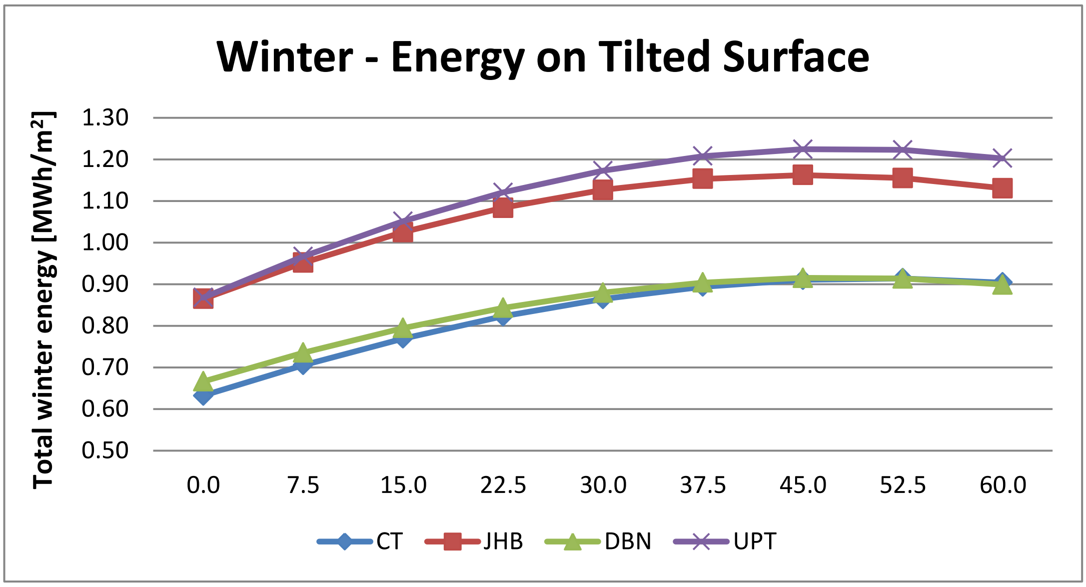

Figure 72: Summer (Top) and winter (Bottom) energy profiles for a tilted surface

Total annual energy on tilted surface per m^2: [MWh]	Cape Town 33.5' S	Johannesburg 26.28' S	Durban 29.53' S	Upington 28.26' S
Standardized Collector (45^o)	**2.02**	**2.07**	**1.72**	**2.31**
Maximise (Tilt at site latitude)	**2.17** *7.21* % ↑	**2.25** *8.72* % ↑	**1.84** *7.04* % ↑	**2.51** *8.56* % ↑
Optimise (Summer + Winter)	**2.26** *11.73* % ↑	**2.37** *14.44* % ↑	**1.92** *11.56* % ↑	**2.64** *14.21* % ↑
Tilt angle				
Summer	15	7.5	7.5	7.5
Winter	52.5	45	45	45

Table 15: Available energy increase by adjusting tilt angle

- **System Performance**

The following LP SWH system has been simulated in TRNSYS; 153 liter tank with 21 vacuum tubes with an inner tube diameter = 34 mm and tube length = 1.42 m. Detailed information on this system can be found in Budihardjo, 2005. The reasoning for using the system proposed in research conducted by Budihardjo was to validate the simulation results with Budihardjo's simulation and experimental results. The following graph shows an increase in tank temperature and the effect of the tank temperature on the mass flow rate within the tubes, the collector has a tilt angle of 45 degrees and energy collected by the collector and one tube is shown in the upper graph. Recalling Figure 46, in order to obtain the mass flow rate, the correlation developed by Budihardjo in 2005 was used in the simulation model. It is clear that an increase in tank temperature affect the mass flow rate, this is due to the effect of the Prandtl number. As the tank temperature increase, the Prandtl number decreases (the viscosity and specific heat decreases, and the thermal conductivity increases). A lower viscosity ensures less resistance in fluid flow and thus a larger mass flow. The high thermal conductivity ensure that heat conducts more efficiently throughout the fluid and the higher buoyance force results in the lower specific heat, requiring less heat to raise the temperature of the fluid by one degree (increasing the density difference within the fluid). On a clear sunny summer day in Cape Town, the collector will increase the tank temperature from 20 degrees to 50 degrees.

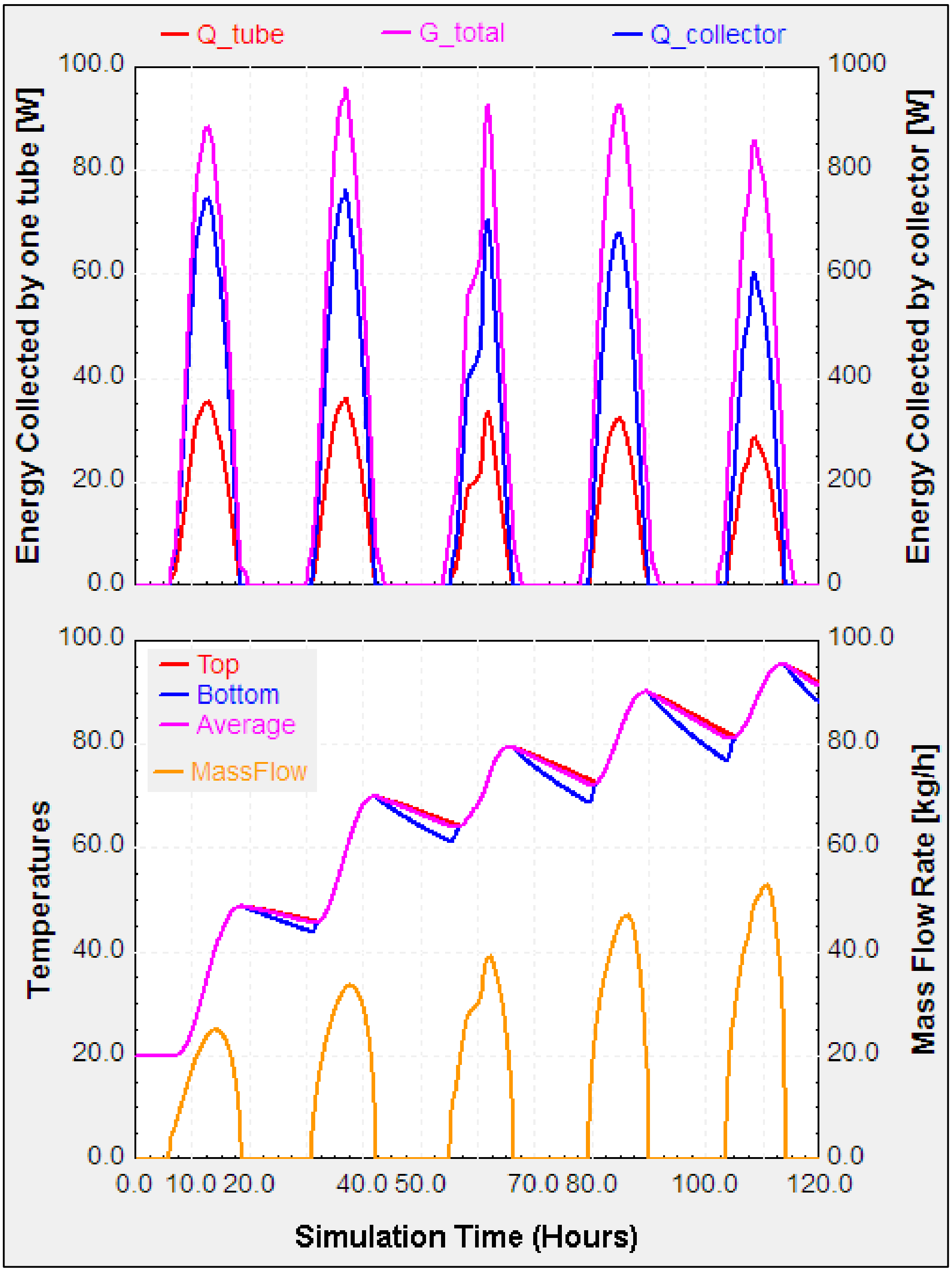

Figure 73: Effect of tank temperature on mass flow rate

Similarly the amount of solar radiation the collector utilizes affects the tank temperature and mass flow rate, shown in Figure 74, these simulation results are from a typical winter day in Cape Town.

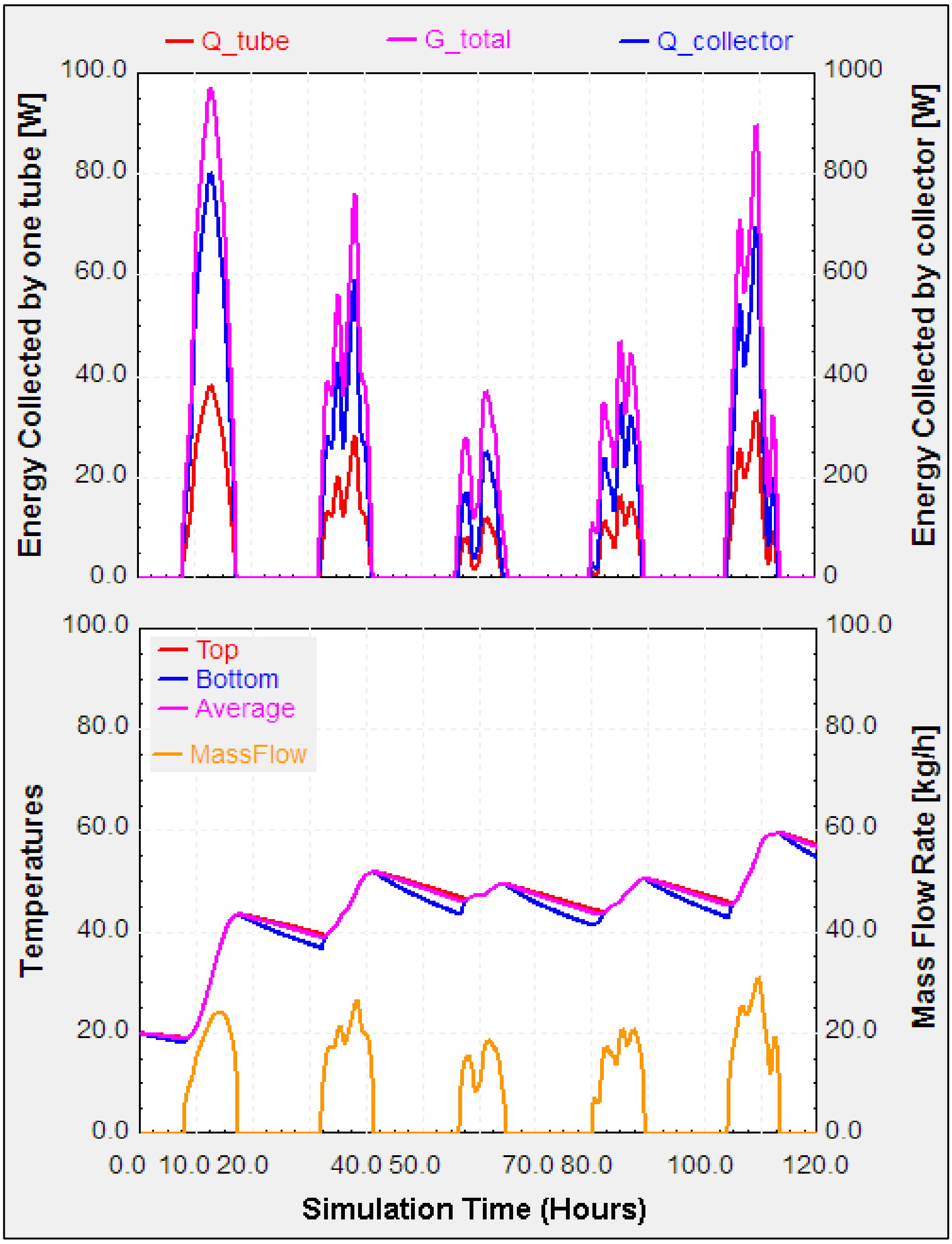

Figure 74: Effect of solar radiation on mass flow rate and tank temperature

The parameters (tube length, tube diameter and tank size) of the system have been changed to illustrate its effects on the system performance. It was found that if the 21 tubes are replaced with 12 tubes with a diameter of 47 mm and length of 1.8 m, similar results are found as in Figure 74. The energy collected by the collector is the same, but the power rating of each tube has increased from approximately 40 W to 70 W, this is due to the increase in diameter and length of the tube. This change greatly affected the mass flow rate within the tubes as represented in the following graph.

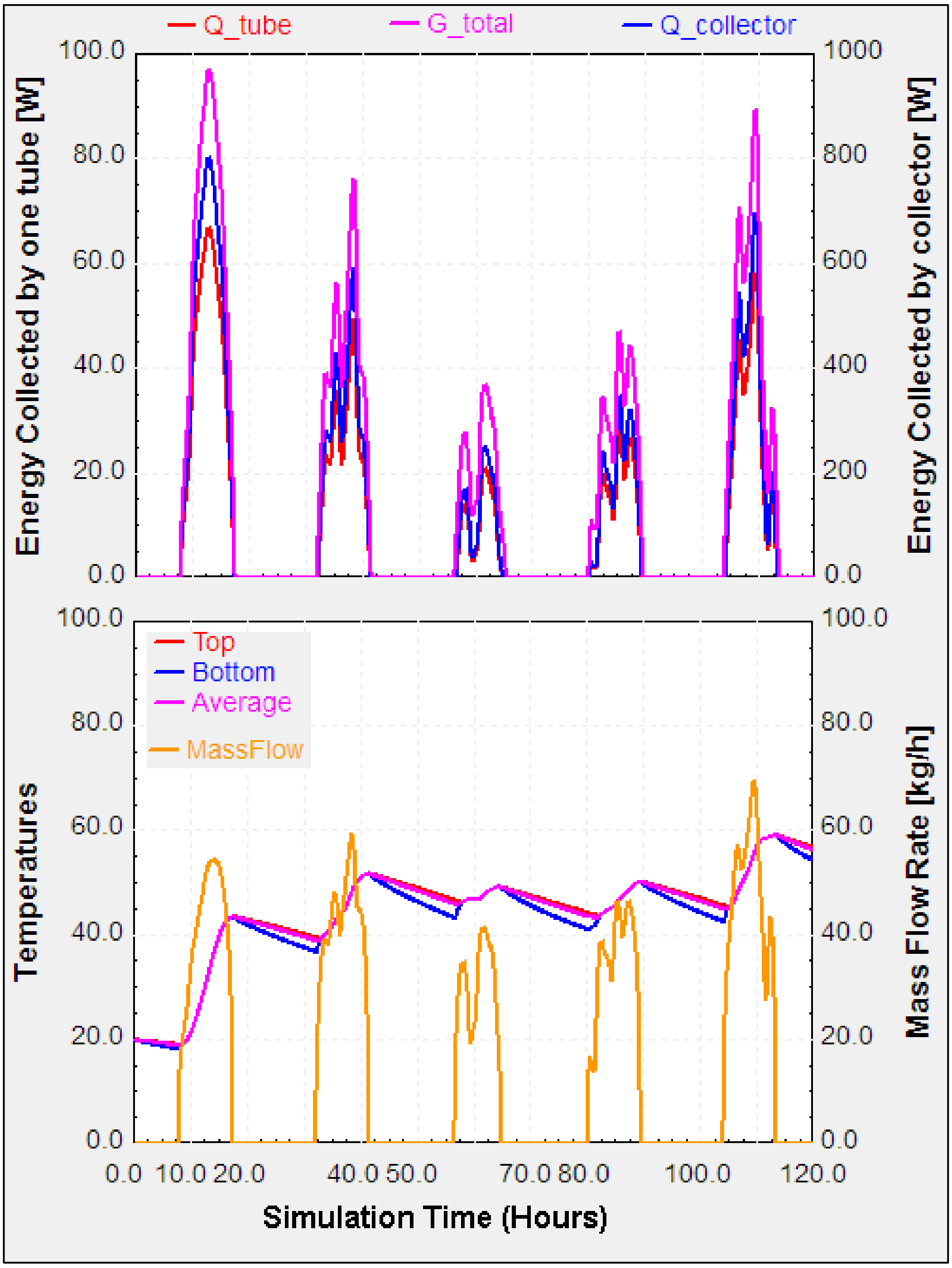

Figure 75: Effect of tube diameter and length on mass flow and tank temperature

The University of Cape Town investigated the performance of a LP SWH with the following specifications; tank size of 100 L with 12 tubes, tube inside diameter 42 mm and length 1.8 m. The collector's performance is monitored in Cape Town, on the roof at the University of Cape Town. Tests have been done on the system to determine the heat loss coefficient of the tank and tubes, and the optical efficiency of the collector. These results have been used in the TRNSYS simulation program. To obtain accurate results it is recommended that these tests are performed on the system components to implement it in a simulation program. Simulation results give a good approximation of the system performance when attributes of the system components are changed. These results can be used for design considerations and installations of LP SWHs to accommodate the consumer's needs and maximization of solar radiation received.

6.1. Simulation Model: System Performance – *TRNSYS*

The simulation model developed in TRNSYS simulates specifically the system performance for a given geographical location (Cape Town, Johannesburg, Durban or Upington). The simulation results from this model are used for comparison against the experimental results obtained in the previous section. The experimental results from TEST1-3 are used in this simulation model to obtain an accurate simulation of the system. Various other system attributes can also be monitored from this simulation such as the mass flow rate within the tubes, the Reynolds number (indicating if flow is laminar or turbulent) and water properties at simulated tank temperature. Results from this simulation model can be seen in Figure 73-Figure 75 as an example, more results are showed and discussed in Section 7.

6.2. Simulation Model: *MATLAB - Simulink*

The simulation model created in MATLAB – Simulink simulates various systems in order to observe the effects on the system with different system components and attributes such as tank volume, tube size, tank temperature and mass flow rate under the same solar radiation profile. These simulations are based on the theory covered in the previous sections and it is clear that the tube sizing and tank temperature affects the mass flow rate within the tube (thermosiphoning). Simulation results are used in the Section 7 where design considerations for LP SWH are discussed.

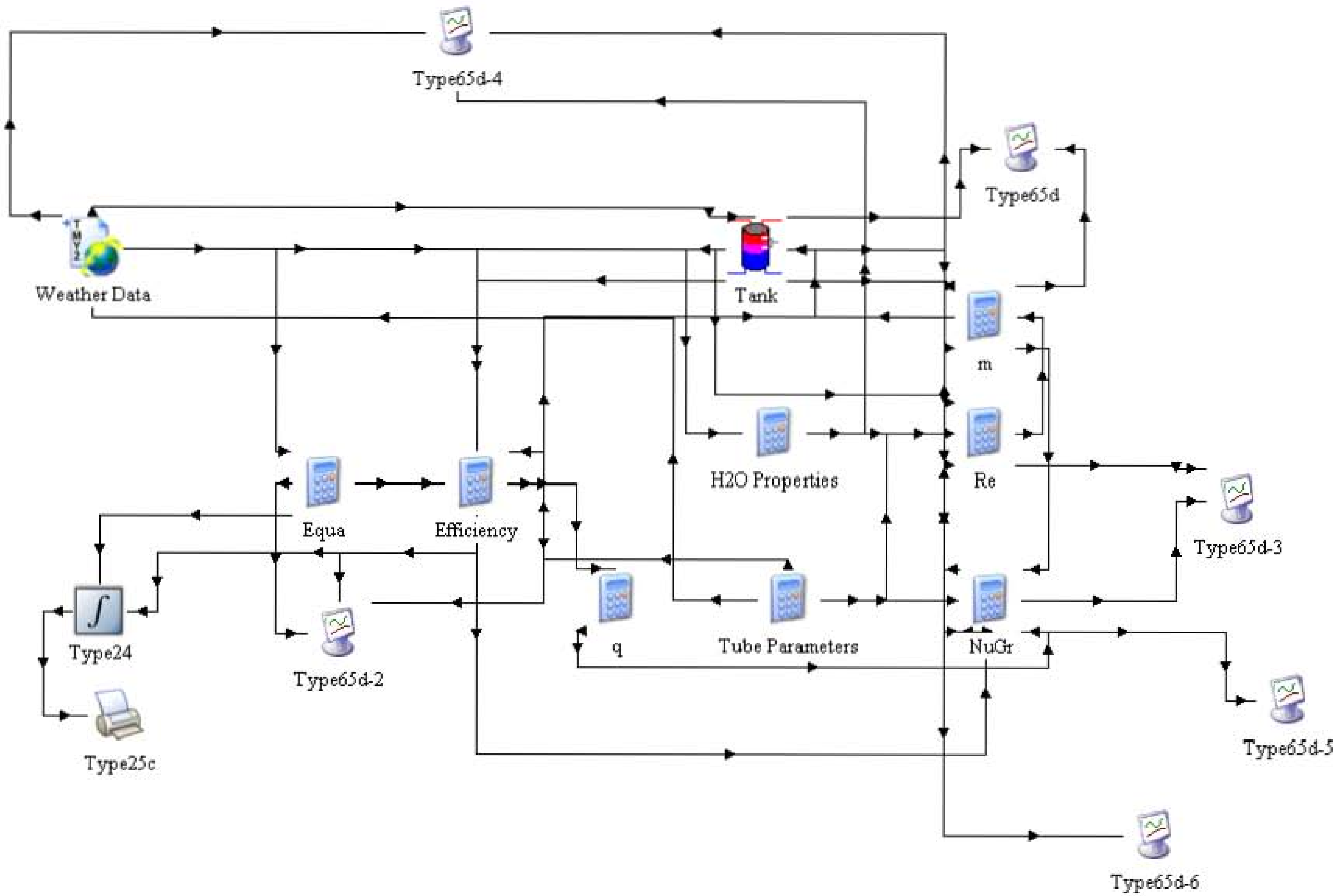

Figure 76: TRNSYS LP SWH Simulation Model

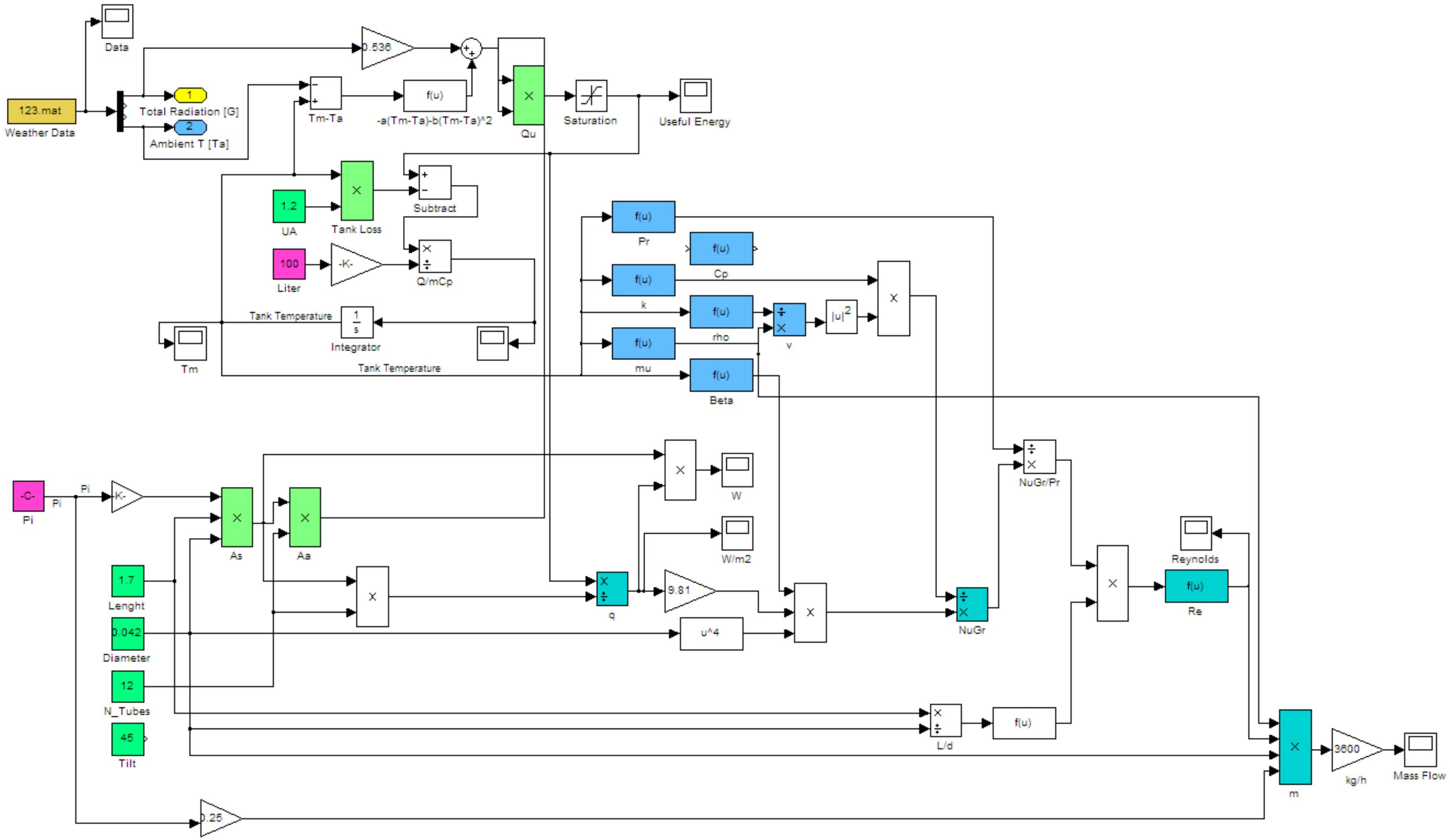

Figure 77: Simulink LP SWH Model (100L System, 12 Tubes, 1.8m lenght, 42mm diameter)

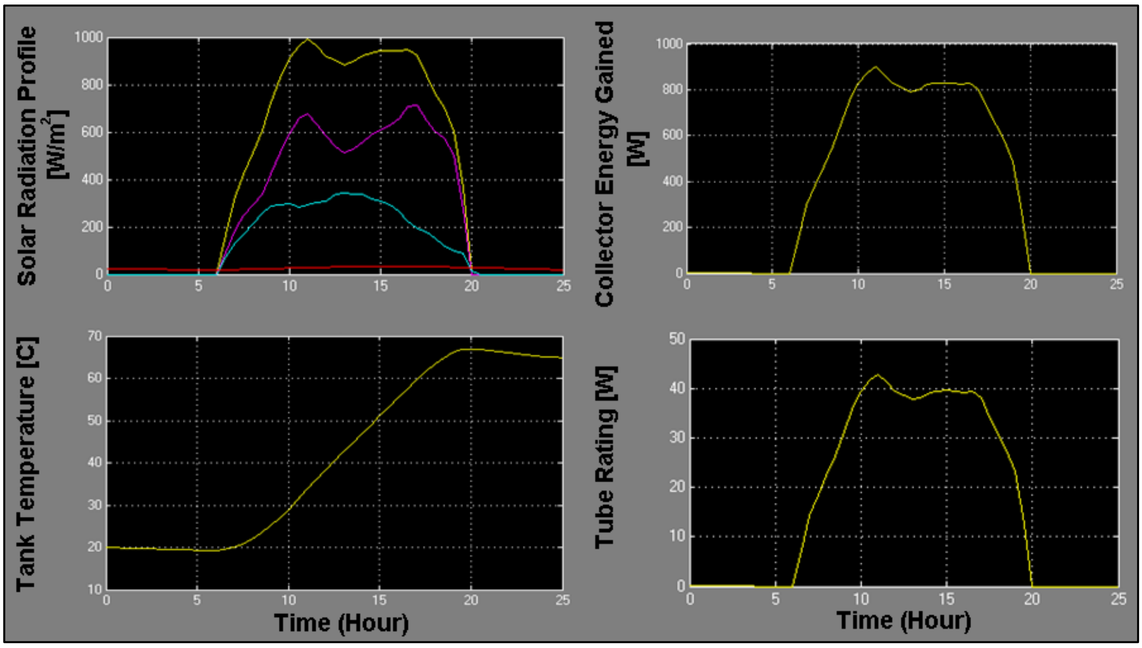

Figure 78: Simulink simulation (150L System, 21 Tubes, 1.4m length, 34mm diameter)

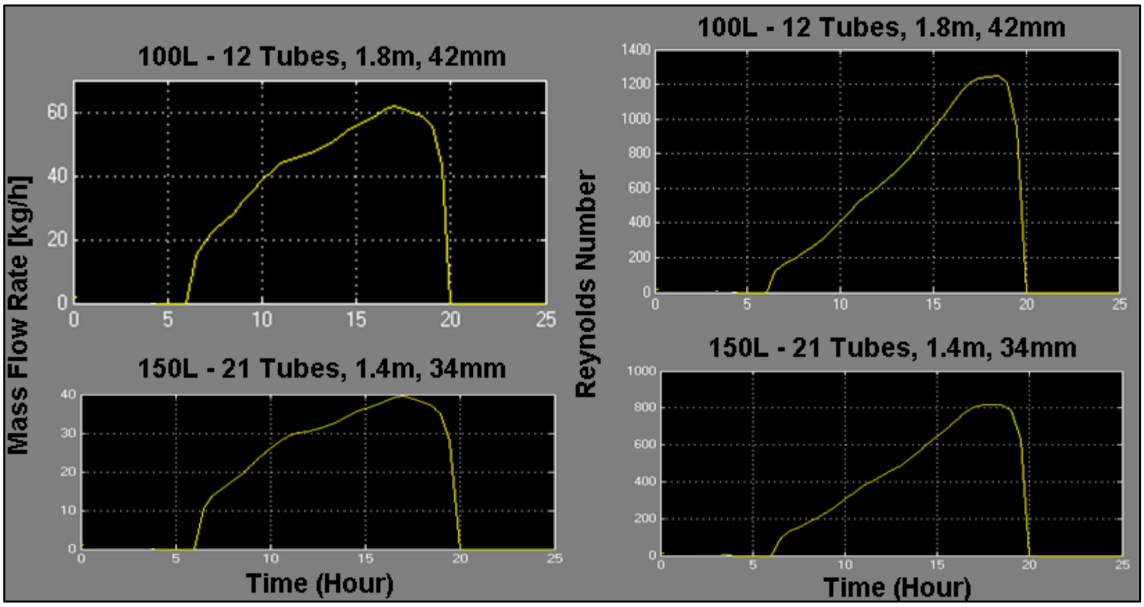

Figure 79: Comparisons between two systems (150L vs. 100L)

7. RESULTS

In this section the experimental and simulation results are compared and discussed. From this analysis the design consideration for LP SWH systems for South Africa is developed. The thermal performance of the system during July 2012 indicates how well the system performed during the winter season in the Cape Town.

7.1. Experimental Results

7.1.1. Thermal Energy Gained by System

The thermal performance of the system is shown in the graph below, where the green and red line represents the total horizontal radiation and the ambient temperature respectively. Tank temperatures are represented by the blue and black lines. The total amount of thermal energy gained per day is calculated, from Equation 4.4, and illustrated in Figure 81. The average thermal energy collected by the system range between 15 - 40 kW/day. On the 17 July, a total of 48 kW was collected; this was due to good solar radiation on that day, with the previous days being less ideal, allowing the system to be cooled down to a tank temperature of about 30 degrees on the morning of the 17 July. With good solar radiation on that day, the system collected enough energy to reach an average tank temperature of 70 degrees. The next day, 18 July, had a similar solar radiation profile, but the system only collected 41 kW, and the day after 30 kW. This is due to high initial tank temperatures at the beginning of each day. At high water temperatures it requires more energy to raise the temperature of the water with 1 degree, and this phenomenon is observed during these three days.

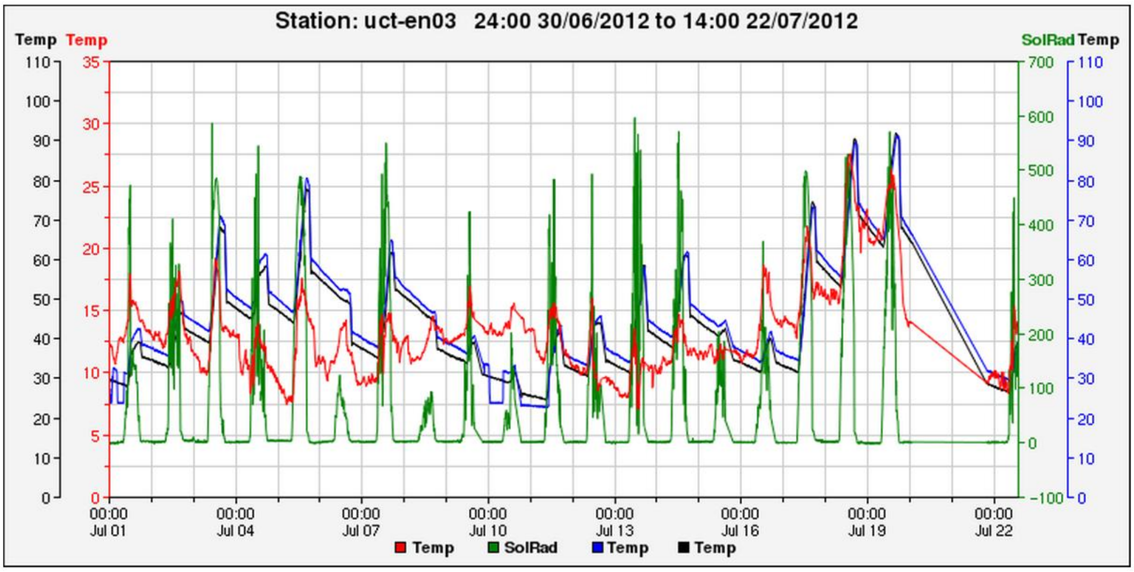

Figure 80: Experimental results - thermal performance of system in July 2012

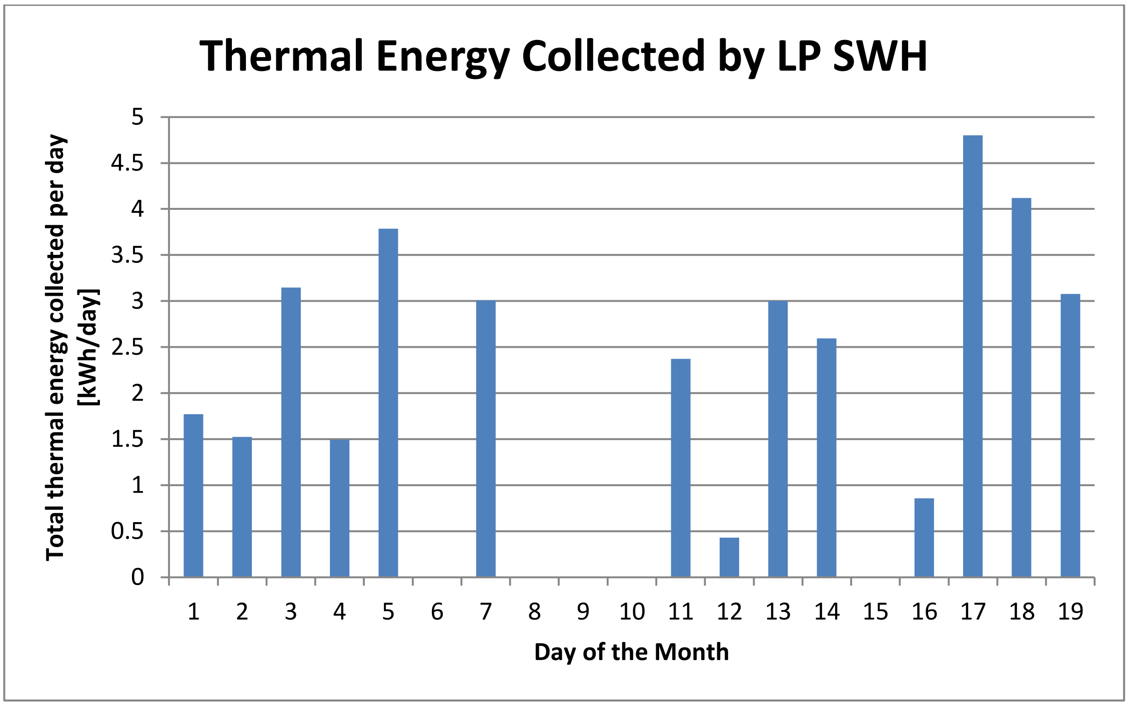

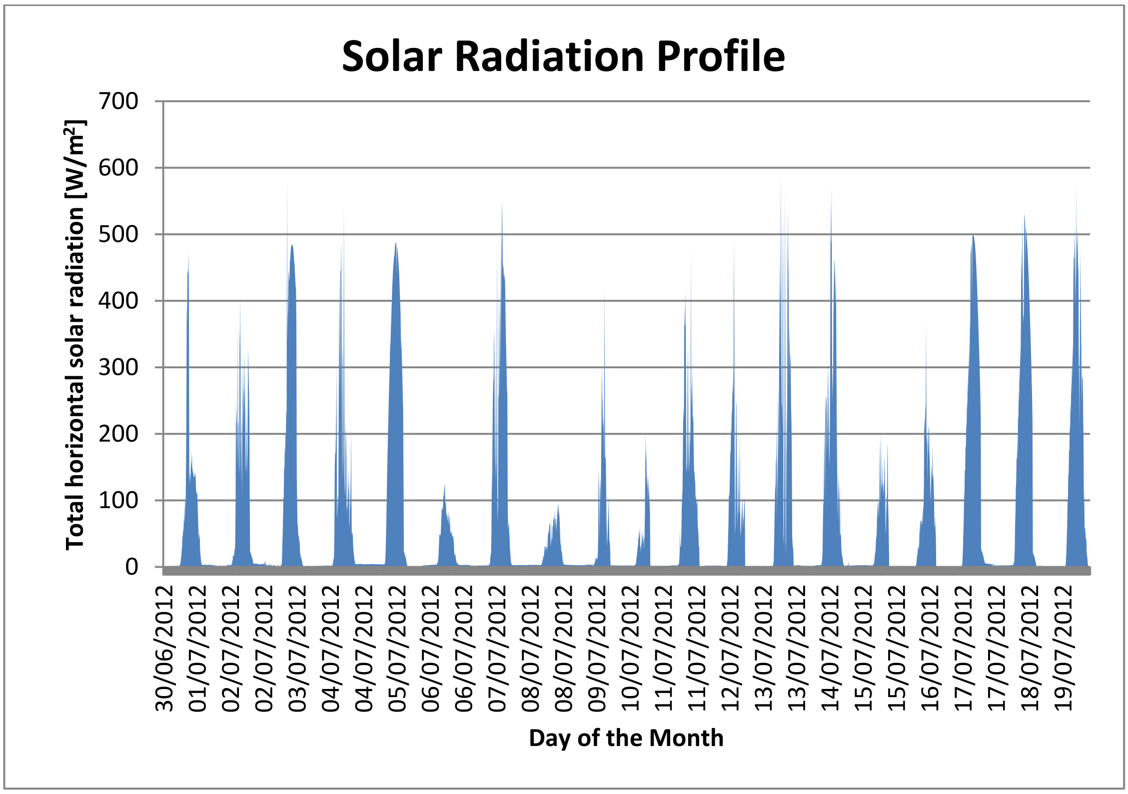

Figure 81: Total thermal energy gained by system (Top) with corresponding total horizontal radiation received (Bottom)

7.1.2. Environmental Impacts on Experimental Results

The environmental effects on the system can be seen in the experimental results. No solar radiation is observed (Figure 82) this was due to continuous heavy rainfall in the region over this period. The sudden drop in temperature within the tank is due to the cooling mechanism that is activated, the continuous temperature drop over the following days is due to the heat loss through the storage tank. This graph is similar to the test results conducted in TEST1, but with a higher thermal loss due to the low ambient temperatures and weather conditions.

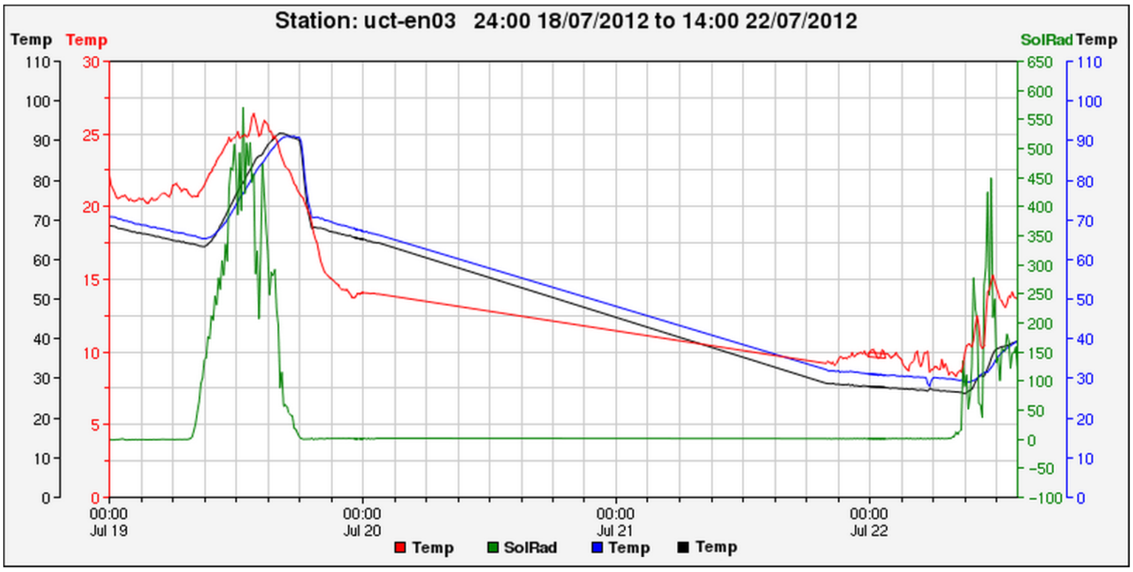

Figure 82: Heavily overcast and rain in Cape Town (20-22 July 2012)

7.2. Comparing Simulation and Experimental Results

The main aim of the simulation model is to optimize the LP SWH system for South Africa. To validate the simulation model, experiments have been conducted to obtain accurate system/component attributes for the simulation model, such as heat loss coefficient of the tank and tubes, optical efficiency of collector and efficiency constants a and b in the efficiency formula. These system/component attributes were obtained through experiments TEST1-3. In TEST4 the system performance was measured and is used in this section to compare against the simulation model's results. Experimental data used for comparison was chosen based only on the total horizontal solar radiation measured. A similar solar radiation profile is chosen in the simulation model in simulation month July (Figure 83). As observed from the experimental measured results, the simulation solar radiation profiles are similar, see Figure 83 and Figure 84, were the average peak solar radiation is in the range of 400-500 W/m^2.

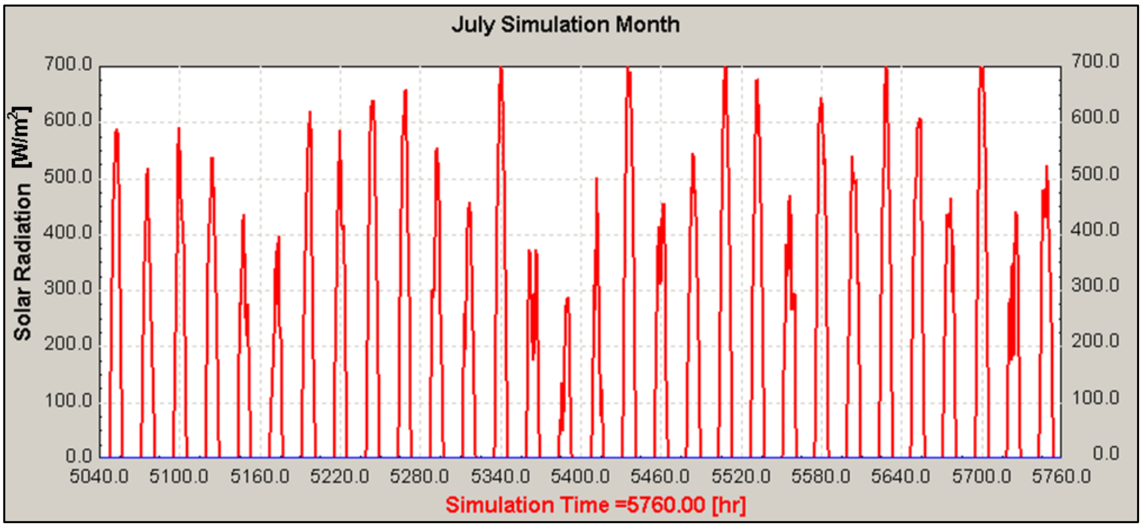

Figure 83: Simulation results - Total horizontal solar radiation in July (Cape Town)

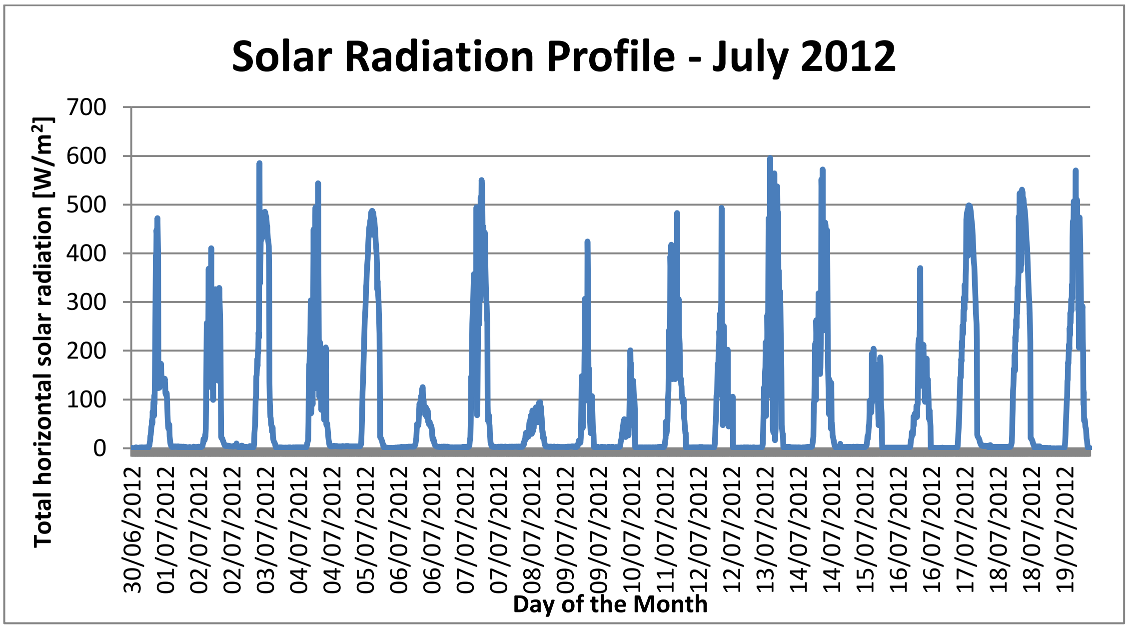

Figure 84: Experimental results - Total horizontal solar radiation in July (Cape Town)

The 3rd of July has been chosen to compare experimental and simulation results. On this day, the solar radiation profile is very close to a sine wave profile (Figure 85), a typical solar radiation profile to expect on a clear sunny day. The corresponding system performance is observed in Figure 86. The total horizontal solar radiation for this day is 14,692 kW/m^2. Thus a similar day has been chosen in the simulation model. The simulated day delivered the total horizontal solar radiation of about 14,600 kW/m^2.

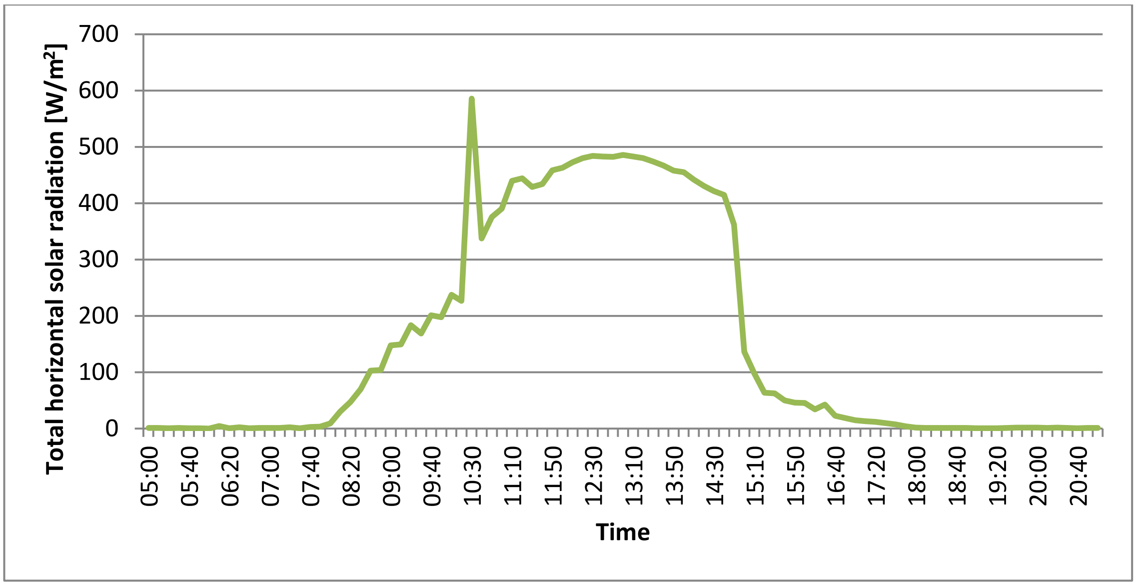

Figure 85: 3 July 2012 - Total horizontal solar radiation profile

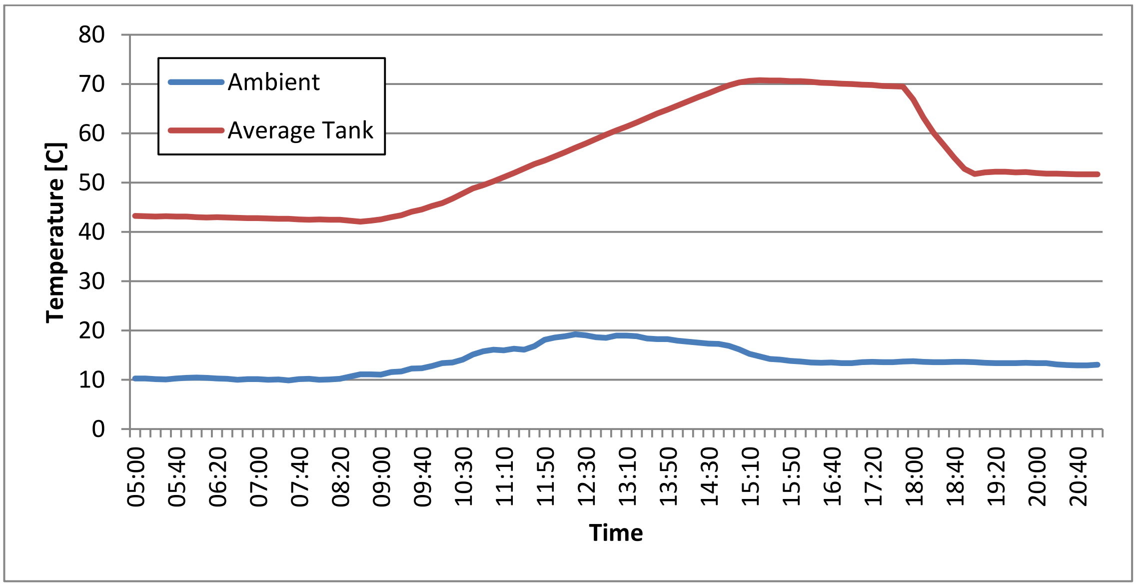

Figure 86: 3 July 2012 - System performance

In Figure 86 it is observed that the average tank temperature increased from 42 degrees to 71 degrees with an ambient temperature ranging between 10 to 20 degrees. In the simulation results, the average tank temperature increased from 40 degrees to 72 degrees with ambient temperatures ranging between 10 to 20 degrees during that time, (Figure 88). It is clear from this comparison that the simulation model is a good representative of the actual system. Thus the simulation model can represent the system accurately under any weather conditions for any geographical location. Results of the simulation model are presented in Section 6.

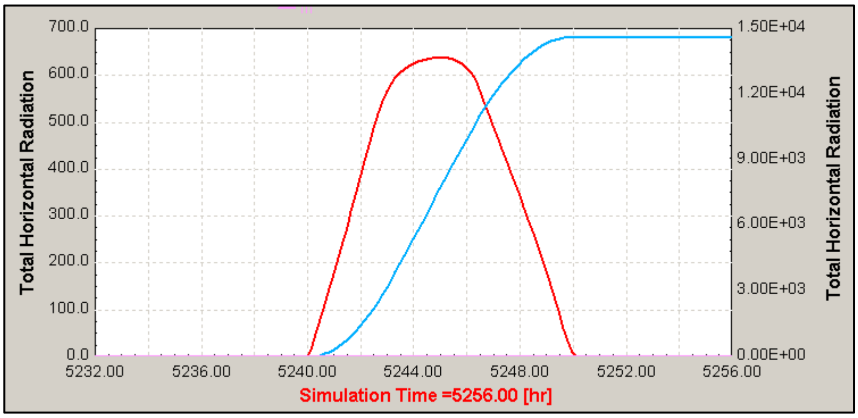

Figure 87: Solar radiation profile (Red) and total solar radiation received (Blue)

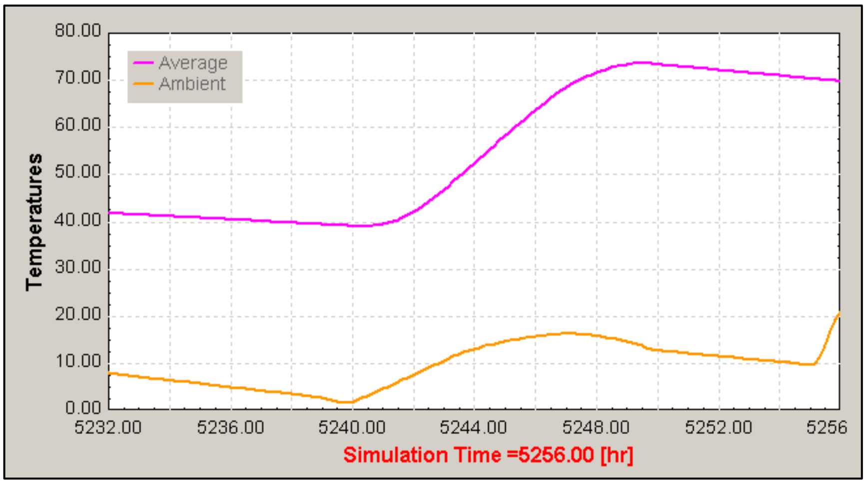

Figure 88: Average tank temperature increase during day

7.3. Validating Experimental Results

Budihardjo, 2005 conducted similar tests on a different LP SWH system in order to determine the mass flow rate correlation. This section demonstrates the difference and similarities between the two systems. The following table shows the comparison.

	Budihardjo, 2005 200L, 24 Tubes, 1.4m 34mm	**University of Cape Town 2012 100L, 12 Tubes, 1.8m, 42mm**
TEST1: Heat loss coefficient of tank	0.79 W/m^2	0.70 W/m^2
TEST2: Heat loss coefficient of tubes	$U_L = 0.0042(T_{avg} - T_{amb}) + 0.552$	$U_L = 0.0042(T_{avg} - T_{amb}) + 0.4168$
TEST2: a & b constants	a=0.8417, b=0.0063	a=0.6110, b=0.0062
TEST3: Optical efficiency	0.55	0.54

Table 16: Comparison between experimental results and literature

7.4. Design Considerations for LP SWH in South Africa

- **STEP 1: Choose Geographical Location**

The first and most important factor in designing a solar collector is the geographical location where it will be installed. Each location is unique in its weather conditions throughout the year, and the site latitude various from different sites. Thus this is an important factor to consider and an investigation in the weather conditions of the specific site should be undertaken. Various databases on the internet are available to obtain reliable information regarding weather conditions and annual solar radiation availability. Recalling Table 13, it is clear that various locations have different solar radiation availability and a solar collector system should be designed to accommodate the location. Harnessing solar radiation from the sun is discussed in Section 3.1. It is advisable to consider all aspects of the geographical location, such as weather behavior during summer and winter. In the Western Cape, during summer, less rainfall is observed with higher solar radiation readings. In rainfall season for Gauteng is in summer, thus more cloud cover is perceived but with a higher solar index. Thus a system designed for Gauteng, should take this into account that less solar radiation is available during this period, although a higher solar index is available. The same scenario could be applied for the Western Cape, having its rainfall season in winter, and having a lower solar index available. Thus a Western Cape system should accommodate the rainfall (cloud cover) and lower solar index.

Total annual energy on tilted surface per m^2: [MWh]	Cape Town 33.5' S	Johannesburg 26.28' S	Durban 29.53' S	Upington 28.26' S
Standardized Collector (45°)	**2.02**	**2.07**	**1.72**	**2.31**
Maximise (Tilt at site latitude)	**2.17** *7.21* %↑	**2.25** *8.72* %↑	**1.84** *7.04* %↑	**2.51** *8.56* %↑
Optimise (Summer + Winter)	**2.26** *11.73* %↑	**2.37** *14.44* %↑	**1.92** *11.56* %↑	**2.64** *14.21* %↑
Tilt angle				
Summer	15	7.5	7.5	7.5
Winter	52.5	45	45	45

Table 13: Available energy increase by adjusting tilt angle

- **STEP 2: Adjust Tilt Angle According to Geographical Location**

As seen from the simulation results, the tilt angle of a collector should be adjusted to accommodate the winter and summer seasons. If a fixed tilt angle is preferred throughout the year, a tilt angle is recommended to accommodate winter seasons when the demand for hot water is higher.

- **STEP 3: Determine Hot Water Demand**

The third factor considered in the design considerations is the consumer's requirements (hot water demand). It is evident that a large family would need a large system to accommodate their hot water demand. The following table could be used as a guide to determine the size of the solar tank.

Application	Volume water used	Temperature required
1 x hand wash	3 Liter	40 °C
1 x shower	35 Liter	40 °C
1 x bath	120 Liter	40 °C
1 x dish washing	5 Liter	40 °C
1 x dish washer	20 Liter	50 °C
1 x washing machine	30 Liter	50 °C
cleaning/cooking	3 Liter	40 °C
Average consumption values per person per day:		
Low consumption	20-30 Liter	40 - 45°C
Average consumption	30-50 Liter	40 - 45°C
High consumption	50-70 Liter	40 - 45°C

Table 17: Water consumption per person

The following equation determines the tank and collector size for a family. For example, if a family consists out of 4 people, the volume of the tank can be determined as follow:

$$V = \text{4 persons x } 50\,L\ @45℃ = 200\,L\ @\ 45℃\ per\ day \tag{7.1}$$

- **STEP 4: Determine Collector Size**

In Step 3 the hot water demand is calculated and the energy required to heat up the water from ambient temperature or colder water (15°C to 45°C) every day is:

$$Q = mC_p\Delta T = \ 200 \quad 4200 \quad 45 - 15 \ = 25.2\text{ MJ} = 7\text{kWh} \tag{7.2}$$

A 7 kWh collector can provide the family with hot water.

- **STEP 5: Determine Tube Size**

Power ratings of the tubes can be determined from the tube dimensions. For a given tube with an inner tube diameter of 47 mm and tube length of 1.8 m has a power rating of approximately 450 Wh/day in the summer and 380 Wh/day in the winter for weather conditions relevant to Cape Town. Thus 16 tubes (16x450=7.2kWh) will be necessary in the summer and 19 tubes (19x380=7.22kWh) in the winter. This scenario has been used in the simulation model and results are presented in Figure 89, supporting the calculations. If the location is prone to more cloudy weather conditions, where solar radiation is limited (Durban), more tubes will be required to deliver the same system performance of a collector of the same size situated in a more favorable location (Upington), thus increasing the collector size.

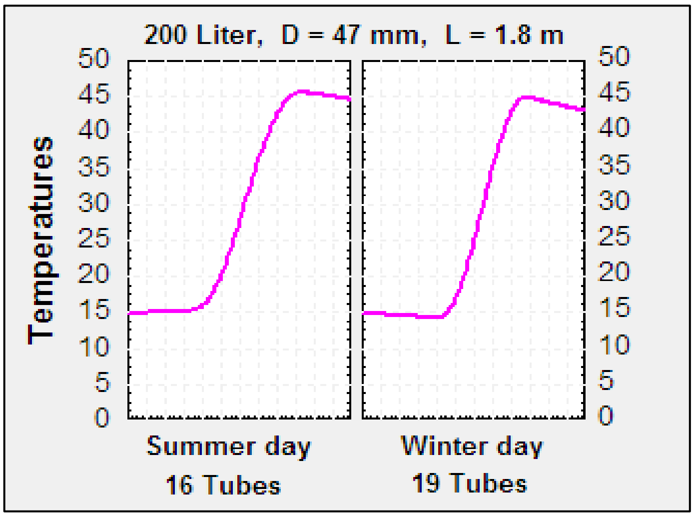

Figure 89: Collector size for summer and winter seasons (Cape Town)

The flow rate within the tubes can be altered by changing the tube dimensions. This was illustrated in Figure 74 and Figure 75 with the smaller tubes delivering a lower mass flow rate than the larger tubes, a greater amount of smaller tubes are required to deliver the same amount of heat. This may increase system costs. A lower mass flow rate might be required by the consumer depending on the application. It is recommended that the tube dimensions are changed, rather than the tilt angle of the collector due to the chance of losing available solar radiation.

- **STEP 6: Simulate System Performance**

In order to analyze if the system would perform according to the consumer's needs, the simulation model developed should be used. It is recommended that standardized system components should be used when designing a system as manufacturing costs of non-standardized components would be more expensive. Standardized components properties such as heat loss coefficients are normally available and could be incorporated into the simulation model.

The following section will demonstrate the 6-Step Design Guide developed for Design Consideration for LP SWH systems in South Africa. Three different scenarios have been created, each with its unique set of parameters, such as geographical locations and size of the family. In this demonstration the costs of the systems are not taken into account and could be investigated in future work.

- ***Scenario A: Single male living in Sandton***

This young male is 24 years old and would like to invest in a LP SWH system for his apartment in Sandton, Johannesburg - Gauteng. He is working from 8h00 to 17h00 during the week, and requires hot water for showering, cooking and other domestic usage when he returns from work.

› STEP1: Choosing Geographical Location – Solar Radiation Profile

From the simulation results (Figure 90), a LP SWH system should be designed to accommodate a summer season ranging between 700-800 W/m^2, and a winter season ranging between 400-600 W/m^2. It is also clear from this simulation results that there is a lot of cloud cover in the summer season, indicated by the large amount of gaps in the profile, especially in the beginning (January) and in the end of the year (October & November).

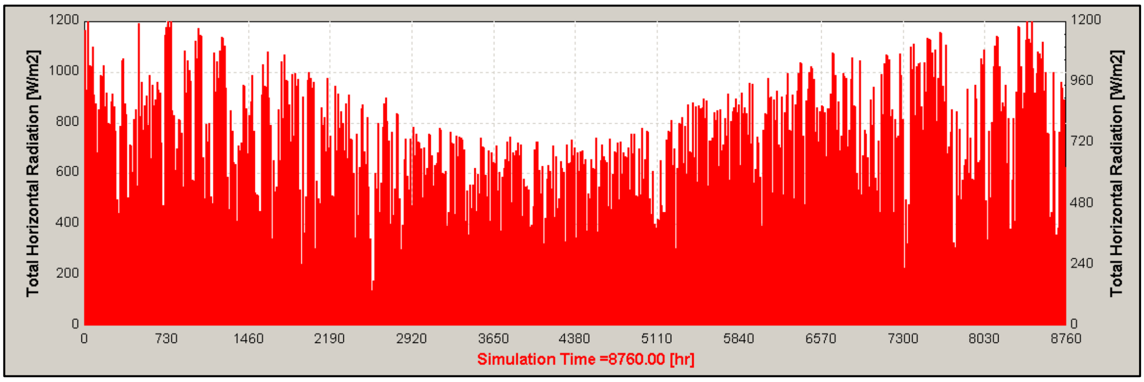

Figure 90: Total Horizontal solar radiation profile for Sandton (Jan-Dec)

› STEP 2: Adjust Tilt Angle According to Geographical Location

It is clear from Figure 90 that at least two tilt angles are required for this system. Thus various tilt angels have been simulated from the simulation model in order to choose the most beneficial tilt angle for summer and winter seasons. From the simulation results a tilt angle of 7.5-30 degrees would be most beneficial for summer and a tilt angle of 45-60 degrees for winter. Due to the thermosiphoning effect in the tubes, gravity is required, thus a tilt angle of 7.5 degrees will affect the thermosiphoning effect, thus a tilt angle of 30 degrees would be more desirable to ensure better heat transfer.

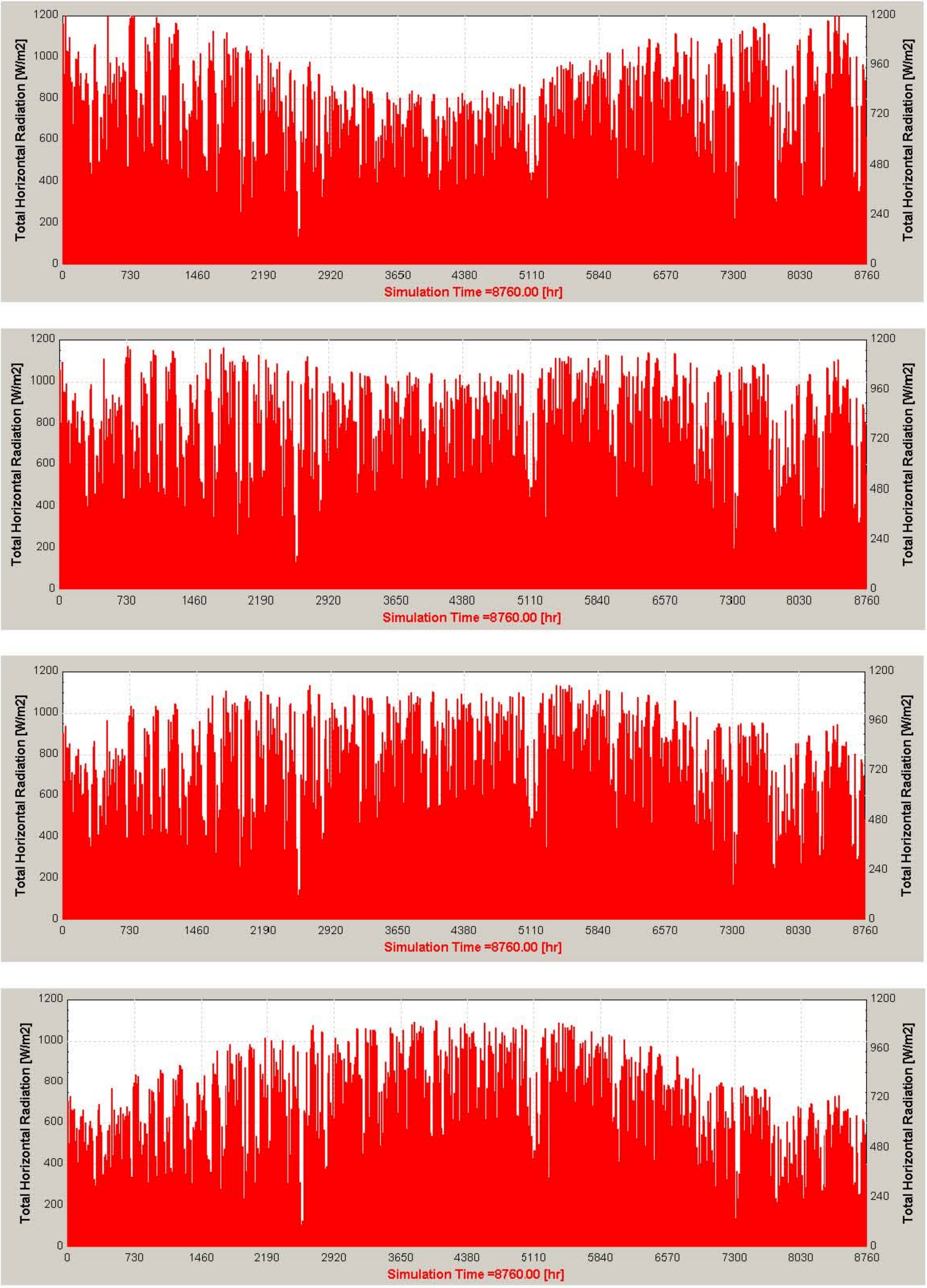

Figure 91: Annual solar radiation on various tilt angles (Top to Bottom = 7.5, 30, 45, 60 degrees)

› STEP 3: Determine Hot Water Demand

From Table 15, the hot water demand of this consumer would be more or less 50 liters at 45 degrees per day. Thus a 50 liter tank will suffice his needs, but due to standardization, it is preferred to offer him a 100 liter tank, as manufacturing costs would be higher for a non-standardized tank.

› STEP 4: Determine Collector Size

In Step 3 the hot water demand is calculated and the energy required to heat up the water from ambient temperature or colder water (15°C to 45°C) every day is:

$$Q = mC_p\Delta T = \quad 100 \quad 4200 \quad 45 - 15 \quad = 12.6\ \mathrm{MJ} = 3.5\mathrm{kWh} \tag{7.3}$$

A 3.5 kWh collector can provide the consumer with hot water.

› STEP 5: Determine Tube Size

It is recommended that standardized tubes are used when determining the tube sizing. The tubes will also have an impact on the total system cost, thus it is recommended to gather information on what is commercially available on the market. For the purpose of this demonstration, the tubes used in TEST2-3 are used as the component properties where obtained for the simulation model. Using the 1.8m length, 47mm diameter tubes, the power rating for a tube in summer is more or less 650 Wh/day with a collector tilt of 30 degrees. The power rating in winter is about 400 Wh/day with a collector tilt of 45 degrees. Thus in summer 6 tubes are required, and in winter 9 tubes.

› STEP 6: Simulate System Performance

The 6-Step design guide has been used as input for the simulation model. The simulation model simulated two days. The first day is in summer (1 January) with a collector consisting out of 6 tubes with a tilt angle of 30 degrees. The second day is winter (1 July) with a collector consisting out of 9 tubes with a tilt angle of 45 degrees. The collector's power rating for the simulation was calculated to be 3.3 kWh/day, thus could satisfy the requirement in Step4. As per Figure 92 it is clear that these two collector configurations will satisfy the consumer's need. More simulations can narrow down the design to optimize other weather conditions such as rainfall, and days with less solar radiation availability. The simulation results and the design guide is a good indication to the consumer and manufacturer in terms of cost and system performance. Higher tank temperatures can be achieved with adding more tubes to the system, but thus also increasing total system cost.

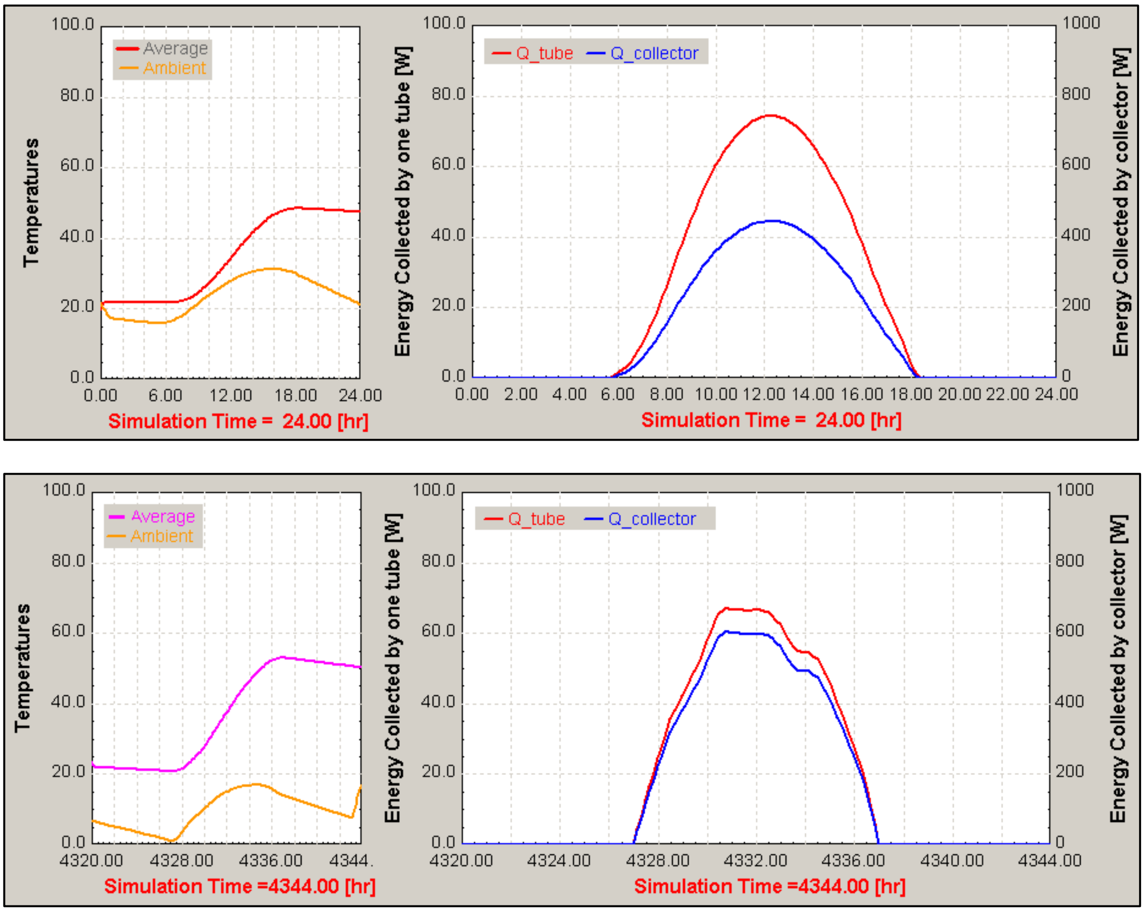

Figure 92: Summer (Top) and winter (Bottom) simulation for 100L system

- ***<u>Scenario B: Large family male living in Durban</u>***

A large family consisting out of a two parents, two children and two grandparents all live in a large house situated in Durban. The family is consider installing a LP SWH system in order to reduce their electricity bill. Due to the amount of people living in this house, a large quantity of hot water is used for cleaning, cooking, washing clothes and bathing.

› <u>STEP1: Choosing Geographical Location – Solar Radiation Profile</u>

The LP SWH system should be designed to accommodate the low radiation availability in Durban. From simulation it is clear that the system could utilize solar radiation in the summer season between 600-700 W/m^2, and a winter season between 400-600 W/m^2.

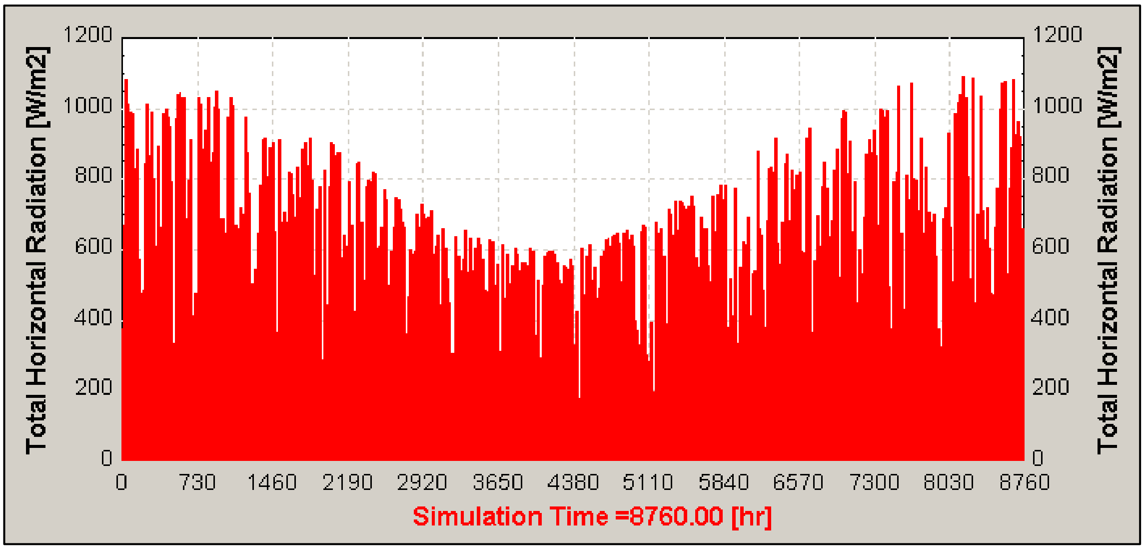

Figure 93: Total Horizontal solar radiation profile for Durban (Jan-Dec)

› STEP 2: Adjust Tilt Angle According to Geographical Location

It is clear from Figure 93 that at least two tilt angles are required for this system. Thus various tilt angels have been simulated from the simulation model in order to choose the most beneficial tilt angle for summer and winter seasons. From the simulation results a tilt angle of 7.5-30 degrees would be most beneficial for summer and a tilt angle of 45-60 degrees for winter. Due to the thermosiphoning effect in the tubes, gravity is required, thus a tilt angle of 7.5 degrees will affect the thermosiphoning effect, thus a tilt angle of 30 degrees would be more desirable to ensure better heat transfer. Looking at all the simulations at once, a 45 degree tilt angle could be used throughout the year.

› STEP 3: Determine Hot Water Demand

From Table 15, the hot water demand for a family of this size is high. The family would use more or less 320 liters at 45 degrees per day. Thus a 350 liter tank will suffice their needs

› STEP 4: Determine Collector Size

In Step 3 the hot water demand is calculated and the energy required to heat up the water from ambient temperature or colder water (15°C to 45°C) every day is:

$$Q = mC_p\Delta T = \quad 350 \quad 4200 \quad 45 - 15 \quad = 44.1\ \text{MJ} = 12.25\ \text{kWh} \qquad (7.3)$$

A 12.25 kWh collector can provide the consumer with hot water.

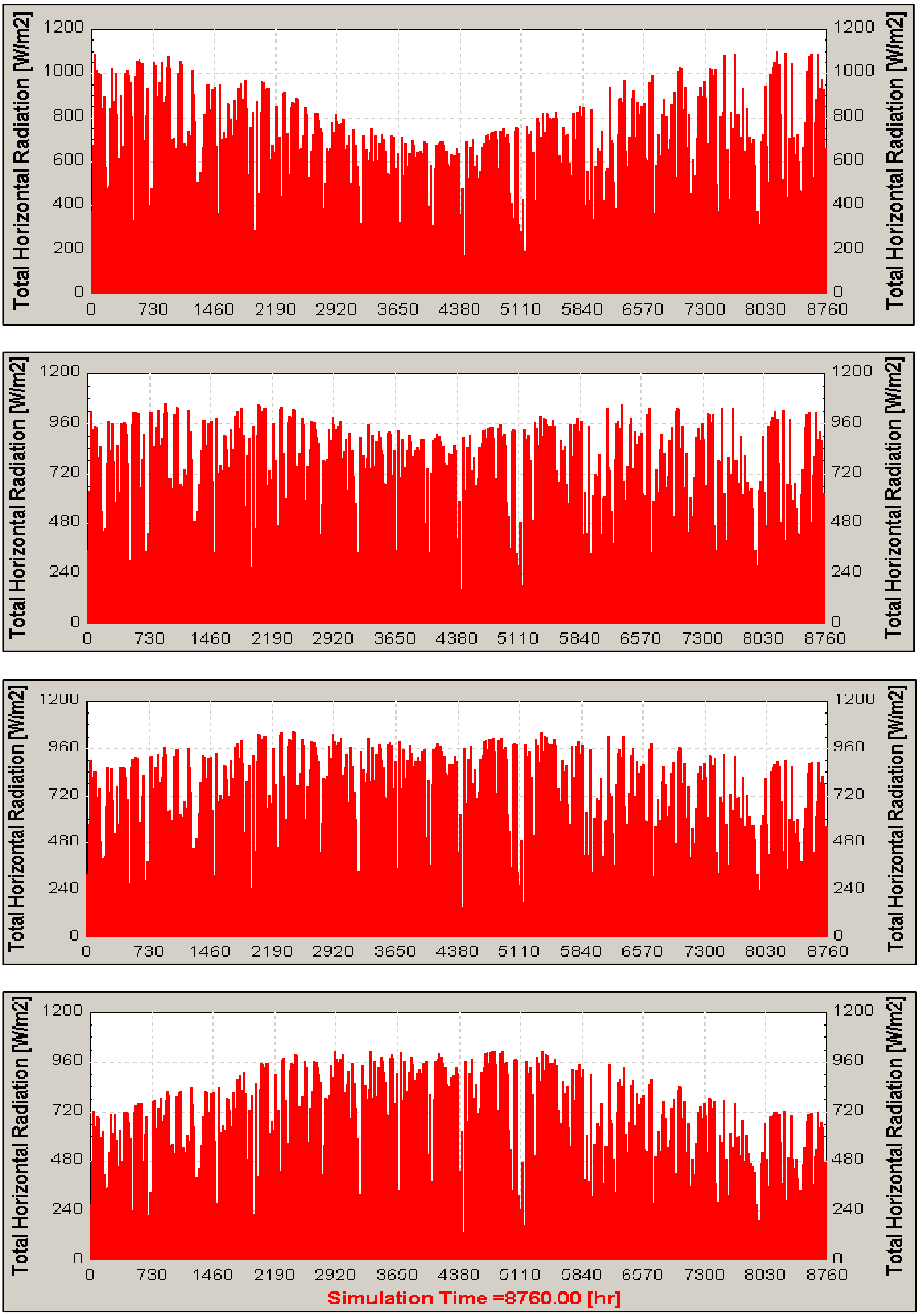

Figure 94: Simulation with various tilt angles Top to Bottom = 7.5, 30, 45, 60 degrees

› STEP 5: Determine Tube Size

Using the 1.8m length, 47mm diameter tubes, the power rating for a tube in summer is more or less 400 Wh/day with a collector tilt of 45 degrees. The power rating in winter is about 380 Wh/day with a collector tilt of 45 degrees. The tubes having similar power ratings are due to the tilt angle of the collector at 45 degrees, thus only a slight change in solar radiation availability is observed throughout the year (Figure 94). The collector would thus in summer need 31 tubes and in winter 33 tubes.

› STEP 6: Simulate System Performance

The 6-Step design guide has been used as input for the simulation model. The simulation model simulated two days. The first day is in summer (3 January) with a collector consisting out of 31 tubes with a tilt angle of 45 degrees. The second day is winter (1 July) with a collector consisting out of 33 tubes with a tilt angle of 45 degrees. The collector's power rating for the simulation was calculated to be 12 kWh/day, thus could satisfy the requirement in Step4. As per Figure 95 it is clear that these two collector configurations will satisfy the consumer's need. More simulations can narrow down the design to optimize other weather conditions such as rainfall, and days with less solar radiation availability. Higher tank temperatures can be achieved with adding more tubes to the system, but thus also increasing on total system cost.

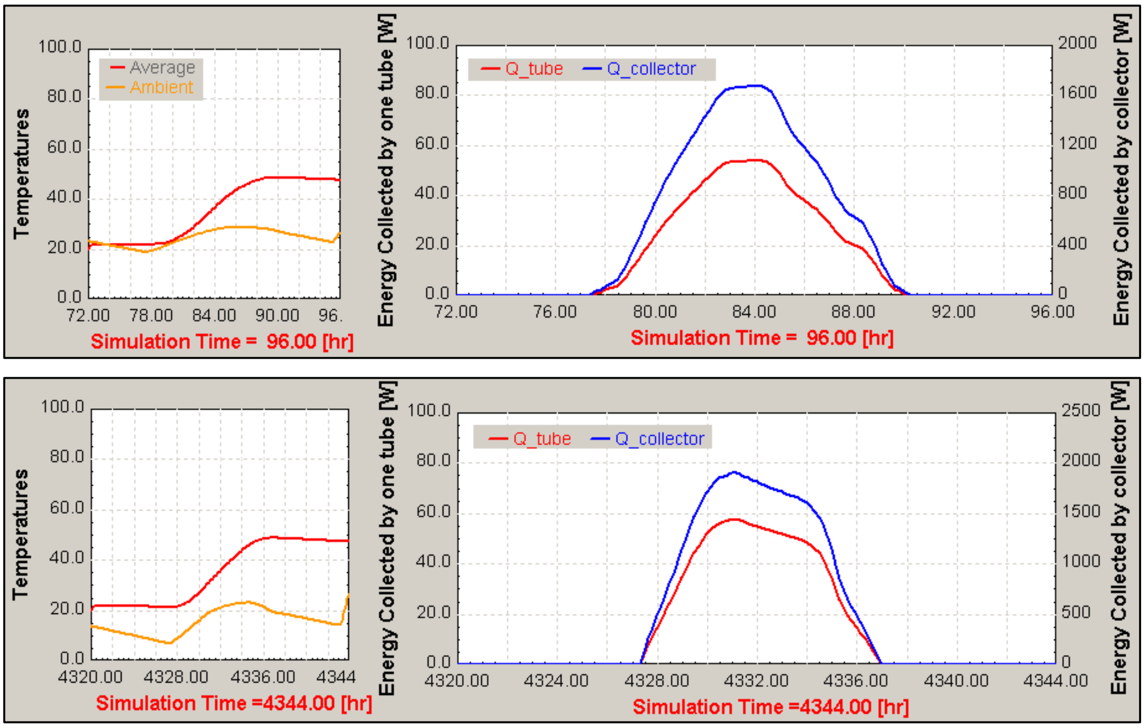

Figure 95: Summer (Top) and winter (Bottom) simulation for 350L system

8. CONCLUSIONS AND FUTURE WORK

8.1. Conclusions

This thesis investigated the application of solar water heating in South Africa. LP SWH systems are mainly imported from China and India, with a fixed tilt angle of 45 degrees. Due to the variation in the solar radiation distribution across South Africa, the need surfaced to investigate these systems for optimization. These systems work on the thermosiphoning effect or natural convection. Thus an extensive study has been undertaken to investigate this phenomena. Fluid flow plays an important role in the heat transfer process associated with natural convection. From theory, governing equations for natural convection were investigated and solved to obtain the velocity and temperature profiles. The three partial differential equations (governing equations) are non-dimensionalized and a similarity solution is applied to obtain two coupled non-linear ordinary differential equations which are solved in *MATLAB*. Two scenarios were considered for the simulation, a vertical wall with a constant wall temperature and a vertical wall with a constant heat flux. From the literature study, no comparison between the two scenarios have been found in the same source, thus this thesis covered both scenarios showing the similarities and differences. In LP SWHs vacuum tubes are used to absorb solar radiation and transfer it to the water, thus this method of heat transfer is similar to the vertical wall with a constant heat flux. From the literature study and simulation results, valuable insight in natural convection is obtained which can assist future designs and developments in any systems using natural convection as a method of heat transfer.

A simulation model based on the literature study has been developed for a LP SWH system. This simulation model is able to simulate the system performance for a given geographical location, where the user can specify the system attributes, such as the tilt angle of the collector, the volume of the tank, the number of tubes and the length and diameter of the tubes. To validate the simulation model, experiments on the system were conducted where the heat loss coefficient of the tank and tubes were determined, the optical efficiency of the collector and the system performance in real weather conditions. The results of the experiments were incorporated into the simulation model and the simulation results were compared against the experimental results. The results concurred and the simulation model was validated. Experimental results were compared against literature for validation and similarities were concluded. Thus the simulation model is a good representative for a LP SWH system and can be used for design considerations in future designs.

8.2. Future Work

A 6-Step Design Guide has been developed to assist the user to design a system which can satisfy the consumer's hot water demand. The only input required from the consumer is their geographical location and hot water demand. From this the user is able to predict with the 6-Step Design Guide the sizing of LP SWH system. The system performance can be simulated to validate if the proposed system could satisfy the consumer's need. Future work to consider is to expand the 6-Step Design Guide to incorporate a data base of standardized components, such as tank sizing and tube sizing (length and diameter). The heat loss coefficients of these components should also be available to the user to be able to incorporate it into the simulation model. The extended data base would give the user more freedom in developing a system which could satisfy the consumer's needs (financially, hot water demand and system response). Financial implications should also be investigated, such as the costing of individual components, manufacturing costs and payback periods. Currently South Africa does not have the technology to compete against the manufacturing capabilities in China to manufacture these systems on a competitive level, a techno-economic study should be undertaken to investigate the possibility of manufacturing these systems locally, creating jobs and manufacturing components more favorable for the climate and consumer's need in South Africa.

9. REFERENCES

Apricus, 2012, *"Solar Hot Water: Become part of the solution",* North America, Apricus Solar Co., Ltd 2010

Budihardjo I., Morrison G.L. and Behnia M., 2004, *"Development of correlation of natural circulation flow rate through single-ended evacuated tube solar collector*", Proceedings of 1st International Forum on Heat Transfer, Kyoto, Japan, 2004.

Budihardjo, I. 2005, *"Evacuated tubular solar water heaters"*, Phd thesis, University of NSW.

Cengel, Y.A. 2009, *Heat and Mass Transfer, A Practical Approach.* 3rd edition, McGraw Hill.

De Meyer, O.A.J. 2012, "*Renewable Energy",* Presentation at University of Cape Town

Duffie, J.A., Beckman, W.A., 1991. In: 2nd Edition. *Solar Engineering of Thermal Processes*. Wiley Interscience, New York

Emmert, J.T., Lean, J.L. and Picone J.M. 2012, *"Record-low thermospheric density during the 2008 solar minimum",* Geophys, Res. Lett., 37, L12102

Garfinkle, R. and Gardinkle, D. 2010, *"From the Sun to Black Holes to the Mystery of Dark Matter",* University of Chicago Press

Gebhart, B. 1988, *Transient Responses and Disturbance Growth in Buoyance-Driven Flows,* Journal of Heat Transfer, 110, 1166-1174

Goldstein, A.S. 2004, *A Computational Model for Teaching Free Convection,* Virginia Polytechnic Institute, Blacksburg, VA 24061-0211

Goldstein, B.R. 1997, "*Saving the phenomena: The background to Ptolemy's planetary theory",* Journal of the History of Astronomy (Cambridge (UK)) 28 (1): 1-12.

Jaluria, Y. 1980, *Natural Convection Heat and Mass Transfer,* Pergamon Press, Oxford.

Joyce, C. 2012, "*Power Plant Primer"*, Chapter 8, Power Engineering Magazine, PennWell Publishing Co., Eskom Library, Megawatt Park, Sunninghill Sandton

Kalogirou S.A. 2005, "*Solar Energy Engineering Processes and Systems",* Elsevier, British Library Cataloging-in-Publication Data

Kreith, F. and Goswami D.Y. 2007,*"Handbook of Energy Efficiency and Renewable Energy"*, Taylor & Francis Group, LLC

Lighthill, M.J. 1953, *"Theoretical considerations on free convection in tubes",* Quart. Journ. Mech. and Applied Math. 6(4), pp.398-439.

Lightle, K. 2011, *"Beyond Weather and the Water Cycle",* The Ohio State University, Phd Thesis

Morrison G.L., Budihardjo I. and Behnia M. 2002, "*Heat transfer in evacuated tubular solar collectors"*. Presented in 4th Pacific Rim Thermal Science and Energy Engineering Workshop, Kyoto, Japan.

Ostrach, S. 1953, "*An Analysis of Laminar Free-Convection Flow and Heat Transfer About a Flat Plate Parallel to the Direction of the Generating Body Force"*, NACA Report 1111.

Pohlhausen E. 1911, *"Der Warmeaustausch Zwischen Festen Korpen und Flussigkeiten mit kleiner Reiburg and kleiner warmeleitung"*, Z Angew Math Mech, Vol 1:115

Rabl, A. 1985, *"Active Solar Collectors and Their Applications",* Center of Energy and Environmental Studies, Princeton University

Schmid R., Pailthorpe B.A. and Collins R.E., 1986, "*Heat Transport in Liquid Filled Tubes",* Aust. J. Phys. 39, 919-43.

Schmidt, E. and Beckmann, W. 1930, *"Das Temperatur-und Geshwindigskeitsfel Von einer Warme Abgebenden Senkrechten Platte bei naturlicher Konvektion"*, Forsch-Ing_Wes Vol 1:391

Shahi, M. 2009, *"Numerical simulation of 3-Dimensional steady flow and heat transfer in single-ended tube"*, MSc thesis, The University of Semnan, Semnan, Iran.

Silberg, S. 2006, Chemistry, The Molecular Nature of Matter and Change, McGraw Hill

Sparrow, E.M. and Gregg, E.L. 1956, *'Laminar Free Convection from a Vertical Flat Plate with Uniform Surface Heat Flux",* Trans ASME, Vol 78: 435-440

Tang T., Gao W., Yu Y. and Chen Y., 2009, *"Optimal tilt-angles of all-glass evacuated tube solar collectors*", Energy 24, 1387-1395

Williams, J. 2012, *The astrophysical environment of the solar birthplace,* Contemporary Physics 51 (5): 381-396.

Window B., Cathro K.J., Chow S.P. and G.L. Harding 1983, *"Effect of collector components on the collection efficiency of tubular evacuated collectors with diffuse reflectors"*, Solar Energy, Vol 32, No. 2, pp251-262, 1984

Window, B. 1983, *"Heat extraction from single ended glass absorber tubes*", Solar Energy 31(2), pp.159-166

Wong, K.V. 2003, *Intermediate Heat Transfer,* Marcel Dekker Puplications

Young, K. 2005, *"Sun as Energy Source",* Sunshine State Standard 1[1].3

Zambolin E. and Del Col D., 2010, *"Experimental analysis of thermal performance of flat plate and evacuated tube solar collectors in stationary standard and daily conditions",* Solar Energy 84, 1382-1396

APPENDIX - A

	DAY 1		DAY 2		DAY 3		DAY 4		DAY 5		DAY 6		Average	
HOUR	Avg-Amb	U	Avg-Amb	U	Avg-Amb	U	Avg-Amb	U	Avg-Amb	U	Avg-Amb	U	Avg-Amb	U
0.5	64		64		65		66	0.78	63		64	0.65	65	0.78
1.0	63		63	0.68	63	0.71	64	0.72	62		62	0.61	64	0.69
1.5	60	0.65	60	0.65	60	0.69	61	0.69	59	0.65	59	0.59	63	0.69
2.0	59	0.65	58	0.65	58	0.67	59	0.69	58	0.66	58	0.59	62	0.64
2.5	58	0.65	57	0.65	57	0.66	58	0.66	57	0.64	57	0.60	61	0.69
3.0	57	0.64	56	0.64	55	0.66	57	0.65	55	0.66	56	0.60	60	0.66
3.5	55	0.64	54	0.64	54	0.66	55	0.65	54	0.64	54	0.60	59	0.65
4.0	55	0.64	54	0.64	54	0.66	55	0.65	54	0.64	54	0.60	58	0.65
4.5	54	0.64	53	0.62	53	0.65	54	0.65	53	0.65	53	0.59	57	0.64
5.0	53	0.64	52	0.62	52	0.65	53	0.63	52	0.63	52	0.60	56	0.63
5.5	52	0.63	51	0.63	51	0.67	52	0.63	50	0.63	51	0.60	55	0.65
6.0	51	0.63	50	0.62	49	0.66	51	0.63	49	0.62	50	0.57	54	0.64
6.5	49	0.63	48	0.61	48	0.65	50	0.63	48	0.64	49	0.59	53	0.63
7.0	48	0.61	47	0.61	47	0.65	49	0.62	47	0.63	48	0.59	52	0.63
7.5	47	0.60	46	0.63	46	0.66	48	0.61	46	0.62	47	0.58	51	0.63
8.0	46	0.60	45	0.64	45	0.66	47	0.61	45	0.62	46	0.58	50	0.62
8.5	45	0.60	44	0.62	44	0.64	46	0.60	44	0.61	45	0.58	49	0.62
9.0	44	0.61	43	0.62	43	0.63	45	0.60	43	0.62	44	0.58	48	0.62
9.5	43	0.58	42	0.61	42	0.62	44	0.59	42	0.61	43	0.56	47	0.61
10.0	43	0.58	41	0.65	41	0.62	43	0.60	42	0.60	42	0.57	46	0.62
10.5	42	0.59	40	0.61	40	0.64	42	0.58	41	0.60	41	0.56	45	0.62
11.0	41	0.59	40	0.61	39	0.61	41	0.58	40	0.59	41	0.55	44	0.61
11.5	40	0.58	39	0.59	39	0.61	40	0.57	39	0.58	40	0.55	43	0.60
12.0	39	0.57	38	0.60	38	0.60	39	0.57	38	0.58	39	0.55	42	0.59
12.5	38	0.57	37	0.58	37	0.59	38	0.57	37	0.56	38	0.55	41	0.60
13.0	38	0.57	36	0.60	36	0.61	38	0.57	37	0.57	38	0.54	40	0.59
13.5	37	0.56	36	0.57	36	0.60	37	0.59	36	0.56	37	0.55	39	0.58
14.0	36	0.55	35	0.57	35	0.58	36	0.57	35	0.56	36	0.54	38	0.58
14.5	35	0.56	34	0.56	34	0.59	36	0.55	35	0.55	35	0.53	37	0.57
15.0	35	0.55	33	0.57	34	0.59	35	0.57	34	0.58	35	0.54	36	0.57
15.5	34	0.55	33	0.56	33	0.57	34	0.58	33	0.59	34	0.53	35	0.56
16.0	33	0.54	32	0.57	32	0.58	34	0.57	32	0.60	33	0.53	34	0.56
16.5	33	0.55	31	0.55	32	0.57	33	0.58	32		33	0.53	33	0.56
17.0	32		31	0.56	31	0.56	32	0.58	31		32	0.53	32	0.56

Table 18: TEST2 - Experimental results: Heat loss coefficient U_{avg}=0.62 W/m^2

APPENDIX - B

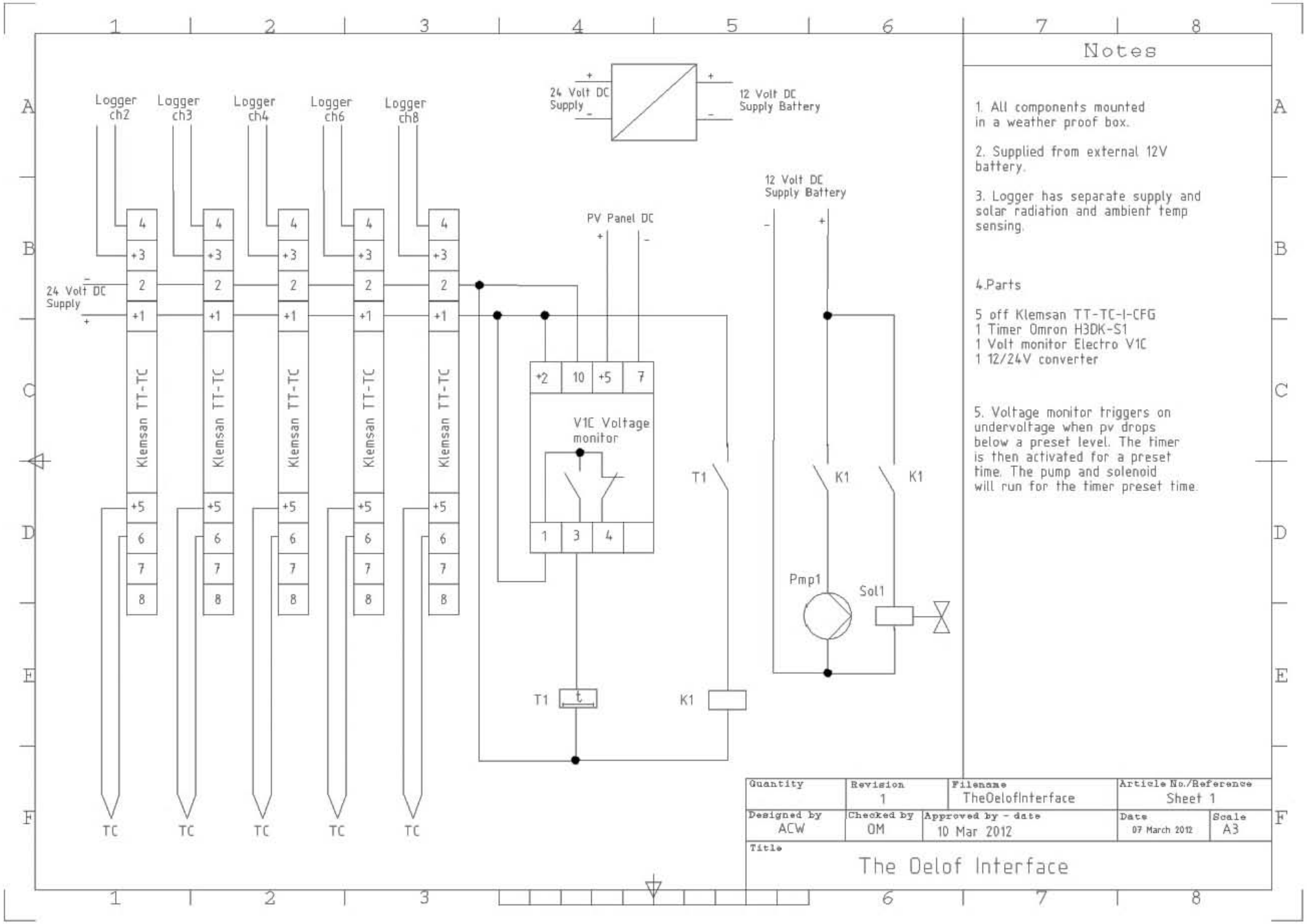

Figure 96: Electrical interface schematic for TEST4-B